รายงานวิจัยฉบับสมบูรณ์

โครงการ : การศึกษาฤทธิ์ของ Cyclin D1-CDK4 ในขบวนการตอบสนองหลังจากเกิดการทำลายของ DNA

โดย ดร.ศิวนนท์ จิรวัฒโนทัย

มีนาคม 2554

บทคัดย่อ

Cyclin D1 เป็นโปรตีนที่พบในปริมาณสูงผิดปกติในมะเร็งหลายชนิด ความผิดปกตินี้ส่วนใหญ่เกิดจากการกลายพันธุ์ของ Cyclin D1 ยีน ทำให้เป็นไปได้ว่า ความผิดปกติของระดับ Cyclin D1 นี้ไม่ใช่เรื่องบังเอิญ แต่น่าจะมีส่วนในการก่อมะเร็ง ดังนั้นการวิจัยหน้าที่ของโปรตีนชนิดนี้ในมะเร็ง จึงมีความสำคัญอย่างยิ่ง ต่อการหาหนทางรักษาผู้ป่วยโรคมะเร็งชนิดที่มี Cyclin D1 ในปริมาณสูง เช่น มะเร็งเต้านม และมะเร็งเยื่อบุผิว

ด้วยการใช้เทคนิควิเคราะห์ Immunoaffinity protein purification coupled with LC/MS/MS ในมะเร็งหลายชนิดพบว่า Cyclin D1 จับกับโปรตีนหลายชนิดที่ ไม่มีการรายงานมาก่อน ในจำนวนนี้ รวมถึงโปรตีนที่มีหน้าที่ซ่อมสารพันธุกรรม (DNA) ที่แตกหัก อาทิ โปรตีนชื่อ RAD5, และเมื่อกำจัด Cyclin D1 จากเซลล์มะเร็งโดยใช้ short-interfering RNA (siRNA) พบว่าเซลล์มะเร็งนั้น ๆ จะถูกฆ่าจากสารหรือรังสีที่ใช้ในการรักษามะเร็งได้ง่ายขึ้นเมื่อเทียบกับ control, เป็นข้อมูลที่ยืนยันว่า Cyclin D1 มีหน้าที่ในการปกป้อง DNA ของเซลล์มะเร็ง และอาจทำให้มะเร็งดื้อต่อรังสีและเคมีรักษา หน้าที่ใหม่ของ Cyclin D1นี้ไม่มีส่วนเกี่ยวข้องกับหน้าที่ทราบกันดีของ Cyclin D1 ในขบวนการควบคุมการแบ่งตัวของเซลล์ (cell cycle regulation) เนื่องจากหน้าที่ใหม่ของ Cyclin D1นี้ สามารถพบได้ในเซลล์ที่ไม่ต้องพึ่งพา Cyclin D1 ในการแบ่งตัว เช่น เซลล์ที่ไม่มี retinoblastoma protein (pRb-negative cell), และหน้าที่ใหม่ของ Cyclin D1 นี้ไม่เกี่ยวข้องกับฤทธิ์ของ CDK4 เนื่องจากการให้สารที่ยับยั้งฤทธิ์ของ CDK4, PD 0332991, ไม่มีผลใด ๆ กับการซ่อม DNA ที่แตกหัก นอกจากนี้ยังพบว่า Cyclin D1 จับกับ RAD51 โดยตรง และ Cyclin D1 ยังรวมตัวกันอยู่ในบริเวณที่ DNA เกิดความเสียหายโดยอาศัยโปรตีนอีกชนิดชื่อ BRCA2

RAD51เป็นโปรตีนหลักในการซ่อม DNA ในขบวนการ Homologous recombination, การลดระดับของ Cyclin D1 รบกวนการทำงานของ RAD51 โดยจะทำให้การรวมตัวของ RAD51ในบริเวณ DNA ลดลงส่งผลให้การซ่อม DNA บกพร่อง

การลดปริมาณของ Cyclin D1 ในเซลล์มะเร็งนี้ มีผลทำให้เซลล์มะเร็งมีความไวต่อการรักษาโดยใช้รังสีรักษาทั้งในระดับหลอดทดลอง (in vitro) และในสัตว์ทดลอง (in vivo) โครงการวิจัยนี้ช่วยค้นพบหน้าที่ใหม่ของโปรตีนที่สงสัยกันมานานว่ามีส่วนในการก่อมะเร็ง โดยเป็นหน้าที่ในการซ่อม DNA, จากความรู้นี้ทำให้ Cyclin D1 เป็นเป้าที่สำคัญในการรักษามะเร็ง, ทั้งชนิดที่มี และที่ปราศจาก retinoblastoma protein

Keyword: Cyclin D1, CDK4, RAD51, BRCA2, DNA damage, cell cycle, cancer

Abstract

Cyclin D1 is a cell cycle protein that often overexpresses in several type of human malignancy. A large fraction of overexpressing Cyclin D1 from human cancers is a result of genetic mutation such as translocation, or amplification of Cyclin D1 gene, suggesting that overexpression of Cyclin D1 is not merely a result of highly proliferative stage of cancer cells, but is a major contributor of tumor formation. However, the precise role of Cyclin D1 in cancer formation is still unclear.

Immunoaffinity-protein purification coupled with LC/MS/MS analysis has shown that Cyclin D1 purified from several types of human tumors interacts with several novel interacting proteins that work in the DNA-damage response (DDR), including RAD51. We found that depletion of Cyclin D1 by short-interfering RNA (siRNA) confers DNA damage hypersensitivity to cancer cells after treatment with DNA damage agents. This finding suggests that Cyclin D1 may contribute to the cancer formation by protecting the cancer cell from DNA damage agents. This finding was seen in cancer cells lacking the retinoblastoma protein, which do not require D-cyclins for proliferation and it was found to be independent of cyclin D1-CDK kinase activity, because treatment with a CDK4-specific inhibitor PD 0332991 has no effect on DNA damage sensitivity.

We found that cyclin D1 directly binds RAD51, and that cyclin D1-RAD51 interaction is induced by DNA damage. Like RAD51, cyclin D1 is recruited to DNA damage sites following radiation in a BRCA2-dependent fashion. Interfering with cyclin D1 function impairs recruitment of RAD51 to damaged DNA and impedes the homologous recombination-mediated DNA repair. Reduction of cyclin D1 levels in human cancer cells increased sensitivity to radiation *in vitro* and *in vivo*, in solid tumors. These findings reveal an unexpected function of a core cell cycle protein in DNA repair and suggest that targeting cyclin D1 may be beneficial also in retinoblastoma-negative cancers which are currently thought to be oblivious to cyclin D1 inhibition.

Keyword: Cyclin D1, CDK4, RAD51, BRCA2, DNA damage, cell cycle, cancer

Executive Summary

รายงานฉบับสมบูรณ์

ชื่อโครงการ : การศึกษาฤทธิ์ของ Cyclin D1-CDK4 ในขบวนการตอบสนองหลังจากเกิดการทำลายของ DNA
(Study of Cyclin D1-CDK4 kinase activity in DNA damage response**)**

ชื่อหัวหน้าโครงการ : นายศิวนนท์ จิรวัฒโนทัย
: Mr. Siwanon Jirawatnotai
ตำแหน่งทางวิชาการ : อาจารย์ ระดับ 5

ระยะเวลาดำเนินการ : 2 ปี
เวลาทำงานวิจัยในโครงการประมาณสัปดาห์ละ 20 ชั่วโมง (ไม่ต่ำกว่า 17.5 ชั่วโมง/สัปดาห์)

สถานที่ติดต่อ: สถาบันชีววิทยาศาสตร์โมเลกุล มหาวิทยาลัยมหิดล
สถาบันมะเร็งดานา-ฟาเบอร์ คณะแพทย์ศาสตร์ มหาวิทยาลัยฮาร์วาร์ด

ที่ทำงาน 1. สถาบันชีววิทยาศาสตร์โมเลกุล มหาวิทยาลัยมหิดล
ถนนพุทธมณฑลสาย 4 ต. ศาลายา
อ. พุทธมณฑล จ. นครปฐม 73170
โทรศัพท์ 02-441-9003-7 ต่อ 1244 โทรสาร 02-441-9906
2. สถาบันมะเร็งดานา-ฟาเบอร์ คณะแพทย์ศาสตร์ มหาวิทยาลัยฮาร์วาร์ด
44 Binney ST. DFCI SM914, Boston, MA USA 02115
โทรศัพท์ 1-617-632-4311 โทรสาร 1-617-632-5006
e-mails : siwanon_jirawatnotai@dfci.harvard.edu, mbsjr@mahidol.ac.th

นักวิจัยที่ปรึกษา : ศ.เกียรติคุณสกล พันธุ์ยิ้ม (Emeritus Prof. Sakol Panyim)
(ตำแหน่งทางวิชาการ) : Professor
สถานที่ติดต่อ : สถาบันชีววิทยาศาสตร์โมเลกุล มหาวิทยาลัยมหิดล
ถนนพุทธมณฑลสาย 4 ต. ศาลายา

อ. พุทธมณฑล จ. นครปฐม 73170
โทรศัพท์ 02-441-9003-7 ต่อ 1244 โทรสาร 02-441-9906
e-mail : scspy@mahidol.ac.th

นักวิจัยที่ปรึกษา : Professor Piotr (Peter) Sicinski
(ตำแหน่งทางวิชาการ) : Professor of Genetics
สถานที่ติดต่อ : Department of Cancer Biology, Dana-Farber Cancer Institute,
44 Binney Street, Boston, MA 02115
โทรศัพท์ 1-617-632-5005 โทรสาร 1-617-632-5006
e-mail: peter_sicinski@dfci.harvard.edu

1. Background and significance

Cyclin D1 is a well-known onco-protein that overexpresses in several type of human malignancy.

In "normal" cell division, role of Cyclin D1 is to inactivate a cell cycle inhibitor pRb and to permit cell cycle entry. However, role of Cyclin D1 in tumor formation is still unclear. A large fraction of overexpressing Cyclin D1 from human cancers is a result of genetic mutation such as translocation, or amplification of Cyclin D1 gene, suggesting that overexpression of Cyclin D1 is not merely a result of highly proliferative stage of cancer cells, but is a major contributor of tumor formation.

Preliminary experiment has shown that Cyclin D1 purified from several types of human tumors interacts with proteins in the DNA-damage response (DDR). A pRb-negative human cervical carcinoma cell line that Cyclin D1 has been reduced by short-hairpin RNA is also hypersensitive to the DNA damage induced by ionizing radiation (IR), (Jirawatnotai S., unpublished data). The findings implicated that Cyclin D1 may drive tumor formation by stimulating cell division and protecting the cancer cells from DNA damage agents.

Up to now, most of the Cyclin D1 functions depend on CDK4 kinase activity. However, Cyclin D1 is postulated by several authors to possess kinase-independent functions. Therefore, one of the most critical remaining questions is whether the molecular function of Cyclin D1 in DDR depends on Cyclin D1-CDK4 activity.

Determination if Cyclin D1 functions in DDR depend on CDK4 activity is a critical question. Currently, CDK inhibitors are being tested in several human cancers. One of the compounds which inhibit CDK4 potently and specifically is *Pfizer*'s PD 0332991. It

inhibits CDK4 activity in the range of nanoM. Several existing cancer regimens are based on DNA damaging agents. Combination of inhibitor of Cyclin D1-CDK4 and DNA damaging agents would be a very attractive regimen. In this proposal, I propose to investigate if CDK4 inhibitor PD 0332991 will sensitize human cancer cells to the DNA damage agents.

2. Objective

1. To investigate role of Cyclin D1-CDK4 complex in the DDR in human cancers
2. To investigate whether CDK4 inhibitor PD 0332991 sensitizes human cancer cells to the DNA damage agents *in vitro*

3. Method

I will use colony survival assay as standard assay to test the DNA damage response. For the cancer cell model I select a pRB-inactivated human cervical carcinoma, Hela cells as a model. To show that the observation is not merely a cell line-specific, I also select another pRB-inactivated human prostrate cancer cells DU-145 as a back up.
CDK4 inhibitor PD 0332991 compound is available from *Pfizer* on a collaboration basis.

- Currently, there is not data regarding dose of PD 0332991 in Hela cells, hence the titration of the inhibitor' dose in the cells is needed to be performed. Hela cells will be treated with the various doses of PD 0332991 from 0 nM to 1000 nM in culture medium (10% FBS DMEM) to find the highest dose that do not kill cells and show the highest CDK4 activity inhibition within 16 hrs. I do not expect to see the growth inhibition of Hela cells within reasonable doses of PD 0332991. Hela cells do not contain active pRB, thus inhibition of CDK4 activity might not arrest the cells. The efficiency of PD 0332991 can be assessed by *in vitro* kinase assay using CDK4 from the treated cells and using recombinant pRB as a substrate. The same test shall be done in the DU 145 cells.
- Colony survival assay will be performed using a standard protocol. The cancer cells is trypsinized and single cells will be seeded in a very low density :1000, 2,000, 6,000, 10,000 and 30,000 cells/ 6 cm culture dishes, in triplicate. Next day, cell will be treated with the optimum does of PD 0332991 for 16 hrs. Then, DNA damage agents will be used to create several levels of DNA damage. I will use ionizing irradiation (IR) to create DNA damage. Cells that survive the DNA damage will appear as colonies after at least 2-3 weeks in cultures. Number of colony will be counted and the survival efficiency will be evaluated in compared to control which is cells without PD 0332991 treatment. The effect of CDK4 kinase inhibitor PD 0332991 from the test will be compared to the effect of the shRNA against Cyclin

D1, and shRNA against CDK4. Comparison of the survival efficiencies between the CDK4 inhibitor PD 0332991, and the preliminary data from shRNA Cyclin D1 will allow an interpretation if CDK4 play any role in to support DDR. Comparison between PD 0332991, and shRNA CDK4 will specify if the activity or the whole molecule of CDK4 is needed in the DDR. Alternatively, DNA damage can be created by Etoposide, an anti-cancer drug. Etoposide creates DNA damage at low does within 4 hrs incubation.

- To show that inhibition of CDK4 kinase activity delays DDR in the cells with damaged DNA, the cancer cells will be treated with PD 0332991 for 16 hrs then with low dose of IR (1 Gy). Cells from 0 hrs (no IR), 15 min, 4 hrs, 8 hrs, 16 hrs after the IR treatment will be harvested and the efficiency of DNA repair will be evaluated using Comet assay according to the standard protocol. The results can also be confirmed by disappearing of γ-H2AX foci after DNA damage.

4. Outcome of the project

The research project "Study of Cyclin D1-CDK4 kinase activity in DNA damage response" has been accomplished within 2 years as originally proposed by researcher with several positive outcomes.

Researcher has completed all the experiments that were proposed with clear results. In addition, inspired by new leads that have been discovered from the results and encouraged by the scientific advisors, researcher has also extended the research project to a very comprehensive level (please see summary of the results below). Results from this project are being written up as a manuscript for a submission to a peer-reviewed scientific journal, Nature. Lastly, due to a unique opportunity from this project that allows collaboration between a laboratory at the Institute of Biosciences, Mahidol University, and that at Dana-Farber Cancer Institute/Harvard Medical School, along with scientific advisors from both sides, the project has helped researcher to develop his research skill and to build a firm platform for future collaboration in an international level.

Summary of the discovery from the research project

1. Cyclin D1 was found to be essential for repairing damaged DNA caused by IR and chemotherapeutic agents, such as camptothecin, and etoposide. Cyclin D1 depleted cells are hypersensitive to DNA damage caused by IR, camptothecin, and etoposide.
2. Cyclin D1 is required for Homologous recombination (HR) DNA repair. HR is compromised in cyclin D1-depleted cells.

3. Loading of RAD51, a recombinase that is a key protein in HR DNA repair, is deficient in Cyclin D1 depleted cells.
4. Cyclin D1 binds to RAD51 directly and this physical interaction is necessary for RAD51 function in repairing DNA.
5. Cyclin D1 relocalized to damaged DNA, an indication of functional relevant of Cyclin D1 in DNA repair
6. Localization of Cyclin D1 to damaged DNA is BRCA2-dependent. Knockdown of BRCA2 abolished Cyclin D1 recruitment to damaged DNA.
7. Cyclin D1-depleted tumors were more sensitive to radiation treatment in compared to control tumors.

For detail of the results, please refer to Appendix “manuscript”.

5. Output of the project

A manuscript for a peer-reviewed scientific journal, *Nature*, is currently under reviewed.

Supplementary Material

Supplementary Figure 1

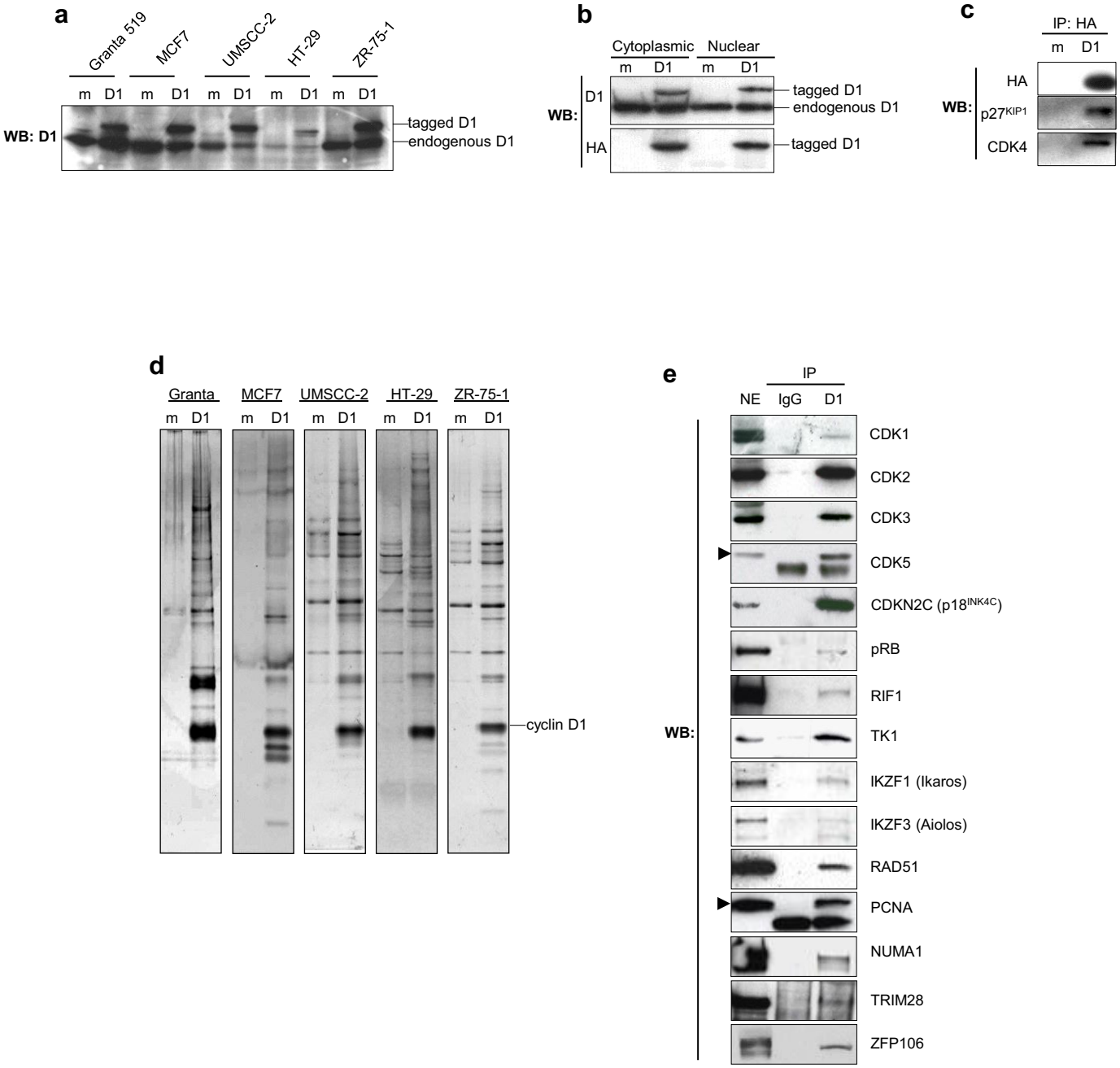

Supplementary Figure 1 I Expression of the tagged cyclin D1, immunopurification of cyclin D1-containing complexes, and verification of selected cyclin D1 interactors

a, Expression levels of tandemly (FLAG- and HA-) tagged cyclin D1 in the five indicated cancer cell lines, analyzed by western blotting (WB). Note approximately 1:1 ratio of the endogenous and the tagged cyclin D1.

b, Distribution of the tagged and the endogenous cyclin D1 in the cytoplasmic and nuclear fractions of Granta 519 cells. Anti-HA antibody was also used to detect tagged cyclin D1.

c, Physical interaction of the tagged cyclin D1 with two known cyclin D1-binding proteins, $p27^{KIP1}$ and CDK4, was verified by immunoprecipitation - western blot (WB) analysis using the indicated antibodies.

d, Silver-stained gels with cyclin D1-containing complexes purified from the indicated cancer cell lines. Bands corresponding to cyclin D1 are indicated.

In **a-d**, D1 denotes lysates prepared from cells expressing the tagged cyclin D1. m, "mock" lysates prepared from cells not expressing tagged cyclin D1.

e, Physical interaction of cyclin D1 with randomly selected fifteen high-confidence interactors, detected by mass spectrometry analyses in Granta 519 cells, was verified by immunoprecipitating (IP) cyclin D1, followed by western blotting (WB) with the indicated antibodies. For control, immunoprecipitations were performed with non-immune IgG (IgG). Nuclear extracts (NE) were also run and immunoblotted. In CDK5 and PCNA immunoblots, specific bands are marked by arrowheads.

Supplementary Figure 2

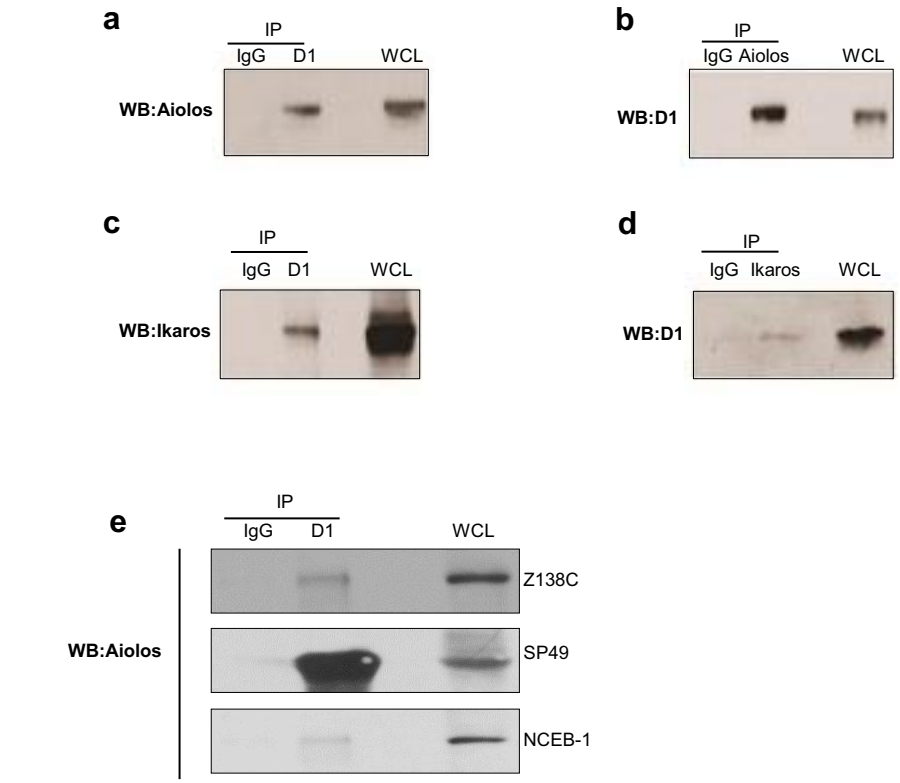

Supplementary Figure 2 I Cancer type-specific interactors of cyclin D1

(**a** and **b**) Physical interaction between cyclin D1 and Aiolos (IKZF3) and (**c** and **d**) between cyclin D1 and Ikaros (IKZF1) in Granta 519 cells was confirmed by immunoprecipitation (IP) followed by western blotting (WB) with the indicated antibodies. For control, immunoprecipitations were performed with non-immune IgG (IgG). Whole cell lysates (WCL) were also run and immunoblotted.

e, Interactions between cyclin D1 and Aiolos in additional mantle cell lymphoma cell lines, Z138C, SP49, and NCEB-1 were detected by cyclin D1 immunoprecipitation (IP), followed by western blotting (WB) with an anti-Aiolos antibody.

f, Expression of cancer type-specific interactors and ZFP106 (not type-specific interactor) in the five cell lines analyzed, detected by western blotting (WB) with the indicated antibodies. β-Actin was used as a loading control.

Supplementary Figure 3

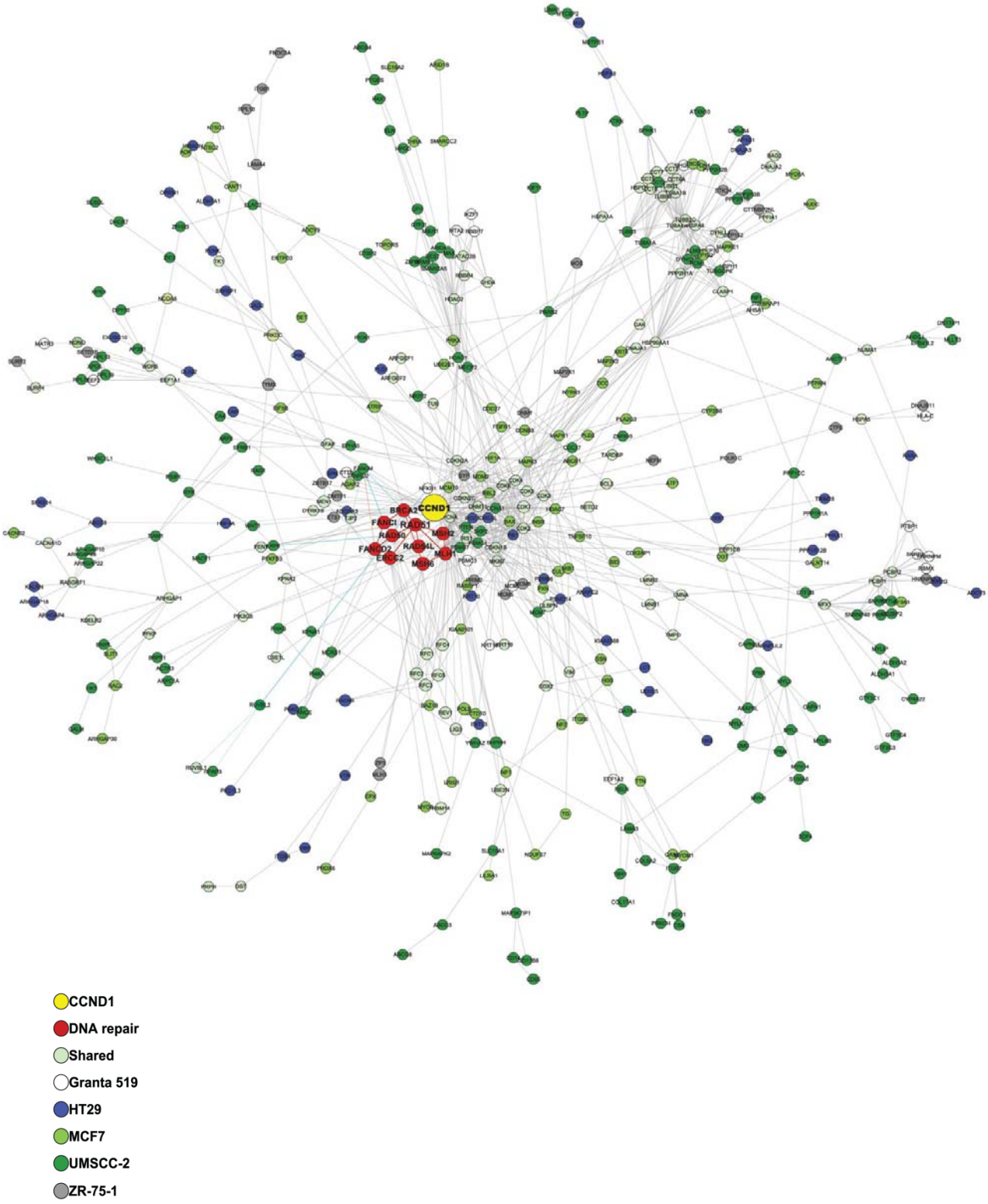

Supplementary Figure 3 I Physical network of cyclin D1 interactors

The network was constructed as described in Methods. Nodes represent proteins identified in LC-MS/MS analyses of particular cell lines as cyclin D1-interactors (using the cutoff of $p \leq 0.01$, Mann-Whitney U-test, Matlab). Lines between nodes indicate annotated interactions between proteins. Interactors found only in one cell line, or common to at least two cell lines (shared) are indicated. DNA repair network is highlighted in red.

Supplementary Figure 4

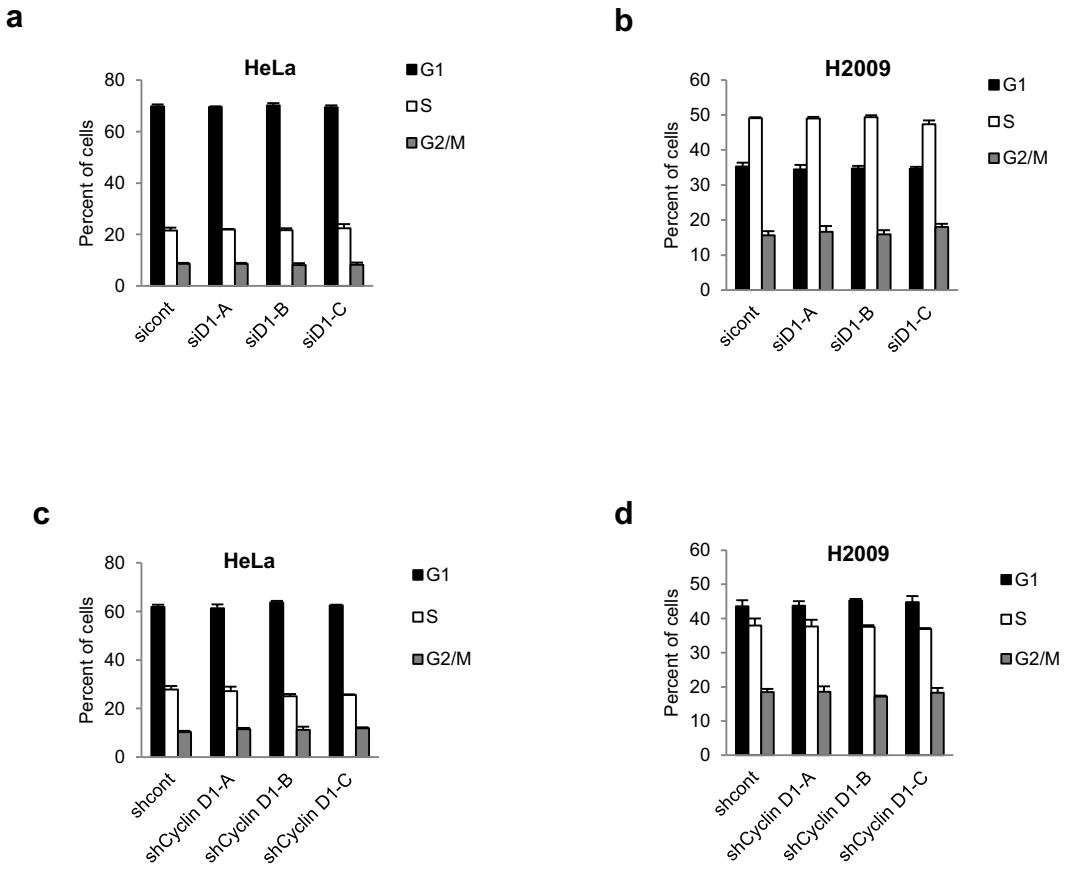

Supplementary Figure 4 l Unperturbed cell cycle progression of pRB-negative cancer cells following knock-down of cyclin D1

a, HeLa cells or **b,** H2009 cells were transfected with three different anti-cyclin D1 siRNAs, or with a control siRNA.

c, HeLa cells or **d**, H2009 cells were transduced with viruses encoding three different anti-cyclin D1 shRNAs or a control shRNA. In **a**-**d**, cells were pulse-labeled with BrdU and stained with anti-BrdU antibodies and with propidium iodide followed by FACS analysis. Shown are percentages of cells in particular cell cycle phases, error bars represent standard deviation, n= 3. As expected, knock-down of cyclin D1 had no impact on cell cycle progression of these pRB-negative cell lines.

Supplementary Figure 5

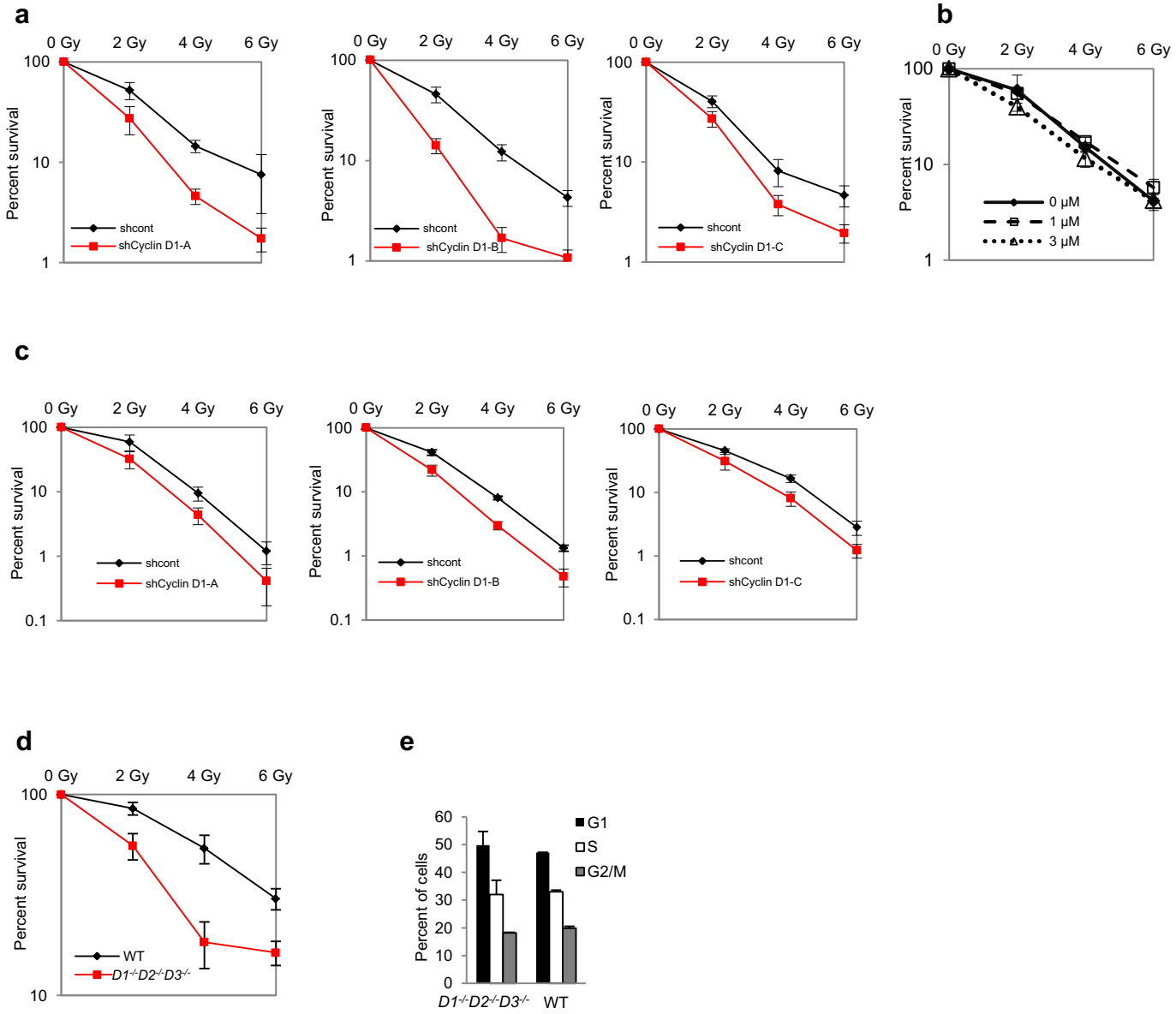

Supplementary Figure 5 l Increased sensitivity of cancer cells and MEFs to radiation following reduction of cyclin D levels

a, Colony survival assays of HeLa cells and **c**, H2009 cells expressing three different anti-cyclin D1 shRNAs (shCyclin D1) or a control shRNA (shcont). Cells were exposed to the indicated doses of radiation. Error bars represent standard deviation. SF_{50} values were: for HeLa cells: left panel, shcont = 2.15 Gy, shCyclin D1-A = 1.07 Gy; middle panel, shcont = 1.68 Gy, shCyclin D1-B = 0.73 Gy; right panel, shcont = 1.47 Gy, shCyclin D1-C = 1.06 Gy. For H2009 cells: left panel, shcont = 2.23 Gy, shCyclin D1-A = 0.96 Gy; middle panel, shcont = 1.45 Gy, shCyclin D1-B = 0.86 Gy; right panel, shcont = 1.75 Gy, shCyclin D1-C = 1.21 Gy. Left panel of Fig. 5a was also shown in the main text in Fig. 2a.

b, Colony survival assay of HeLa cells treated with the indicated doses of PD 0332991, a specific inhibitor of cyclin D-CDK4 and D-CDK6 kinase[1]. Error bars, standard deviation.

d, Colony survival assay of immortalized *cyclin* $D1^{-/-}D2^{-/-}D3^{-/-}$ and wild-type (WT) mouse embryonic fibroblasts[2]. Cells were exposed to the indicated doses of radiation. Error bars represent standard deviation. SF_{50} = 4.27 Gy for WT cells and 2.27 Gy for *cyclin* $D1^{-/-}D2^{-/-}D3^{-/-}$ cells.

e, Normal cell cycle distribution of *cyclin* $D1^{-/-}D2^{-/-}D3^{-/-}$ MEFs. Cells were stained with propidium iodide and analyzed by FACS. Shown are percentages of cells in particular cell cycle phases. Error bars represent standard deviation.

Supplementary Figure 6

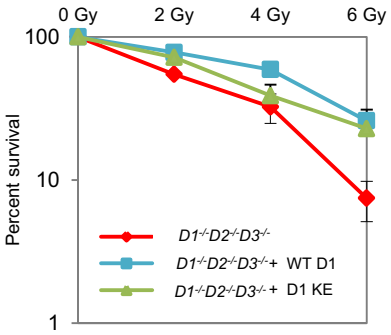

Supplementary Figure 6 l Increased radiation-resistance of *cyclin D1$^{-/-}$D2$^{-/-}$D3$^{-/-}$* MEFs following expression of wild-type cyclin D1 or 'kinase-inactive' cyclin D1 K112E mutant

Colony survival assays using immortalized *cyclin D1$^{-/-}$D2$^{-/-}$D3$^{-/-}$* MEFs expressing empty plasmid (*D1$^{-/-}$D2$^{-/-}$D3$^{-/-}$)*, wild-type human cyclin D1 (*D1$^{-/-}$D2$^{-/-}$D3$^{-/-}$* + WT D1), or cyclin D1 K112E "kinase-dead" point mutant[3] which is unable to activate the catalytic activity of CDKs (*D1$^{-/-}$D2$^{-/-}$D3$^{-/-}$* + D1 KE). Cells were exposed to the indicated doses of ionizing radiation. Error bars, standard deviation.

Supplementary Figure 7

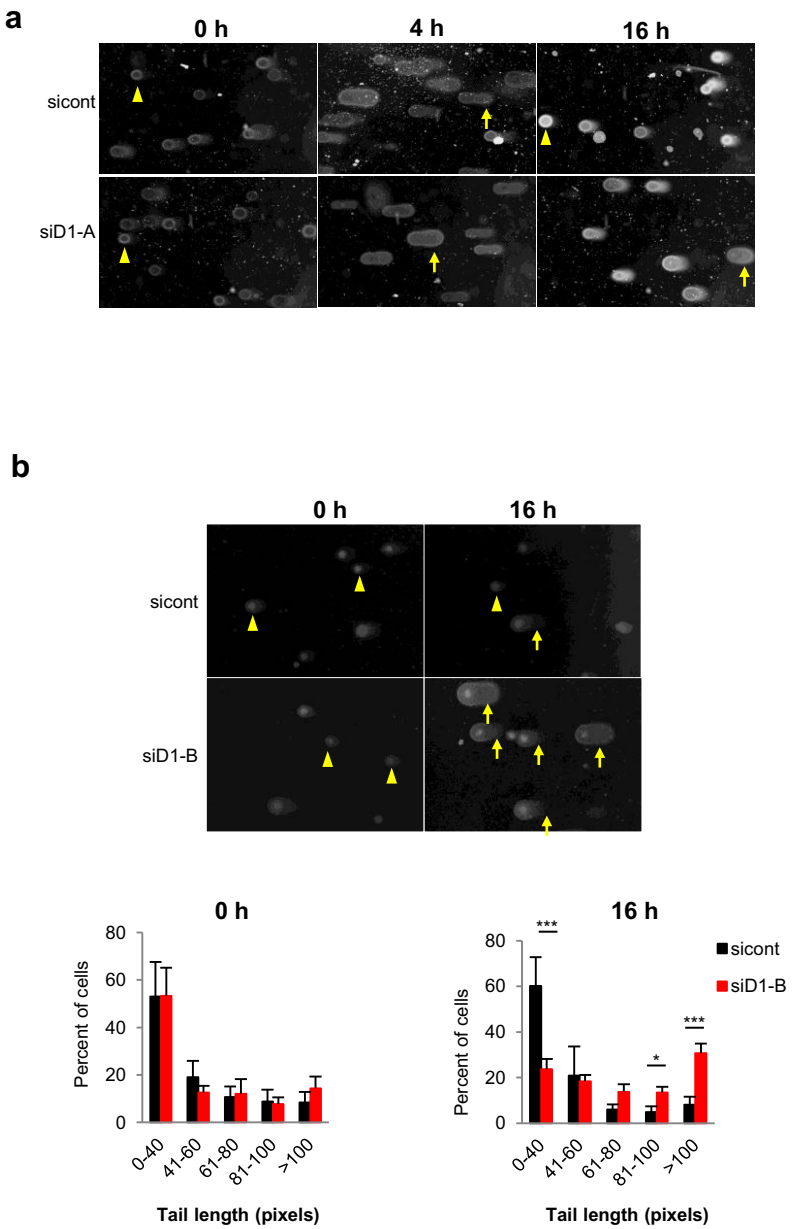

Supplementary Figure 7 I Impaired DNA repair upon reduction of cyclin D1 levels

a, Comet assay to measure DNA repair in HeLa cells transfected with anti-cyclin D1 siRNA-A (siD1-A) or control siRNA (sicont) before (0 hrs), at 4 hrs, or 16 hrs after ionizing radiation. Arrowheads point to cell nuclei, arrows point to damaged DNA "tails". Percentages of cells containing various comet tail length are shown in Fig. 2d.

b, Comet assay in HeLa cells treated with an independent anti-cyclin D1 siRNA-B (siD1-B). Arrowheads point to cell nuclei, arrows point to damaged DNA "tails". Percentages of cells containing various comet tail length before (0 hrs) or at 16 hrs after irradiation are shown in lower panel. Error bars denote standard deviation. ***, $p \leq 0.005$, *, $p < 0.05$.

In **a** and **b**, increased tail length is indicative of DNA damage.

Supplementary Figure 8

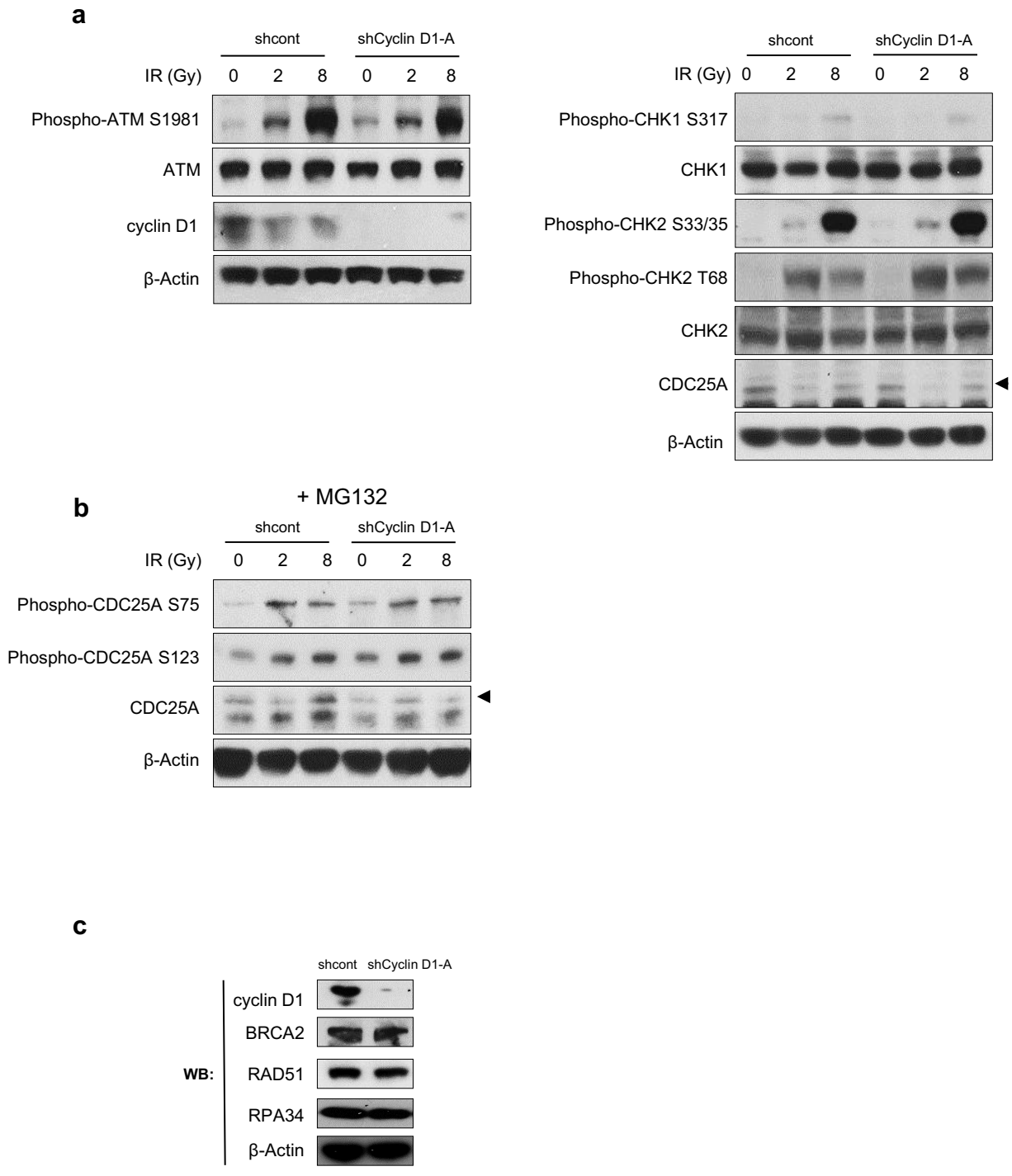

Supplementary Figure 8 I Analyses of DNA damage response proteins

a, Unaltered phosphorylation of DNA damage response proteins and normal levels of CDC25A after DNA damage in cells depleted of cyclin D1. HeLa cells expressing either control shRNA (shcont) or anti-cyclin D1 shRNA (shCyclin D1) were irradiated with the indicated doses of ionizing radiation (IR), harvested after 0.5 hrs and analyzed by western blotting. Note reduced cyclin D1 levels following IR, as reported[4]. β-Actin was used as a loading control. Arrowhead points to a CDC25A-specific band.

b, Unaltered phosphorylation of CDC25A in cyclin D1-depleted cells after DNA damage. HeLa cells were treated as in **a**, except that MG132 (a proteosomal inhibitor) was added to the culture medium 1 hr prior to the IR treatment to block degradation of CDC25A. Immunoblots were probed with phospho-specific antibodies against phospho-Ser75-CDC25A, or phospho-Ser123-CDC25A, or with an antibody against total CDC25A. Arrowhead points to a CDC25A-specific band.

c, Unaltered levels of DNA damage response proteins after cyclin D1 knock-down. Western blotting (WB) was performed with the indicated antibodies in HeLa cells expressing control shRNA (shcont) or anti-cyclin D1 shRNA (shCyclin D1). β-Actin was used as a loading control.

Supplementary Figure 9

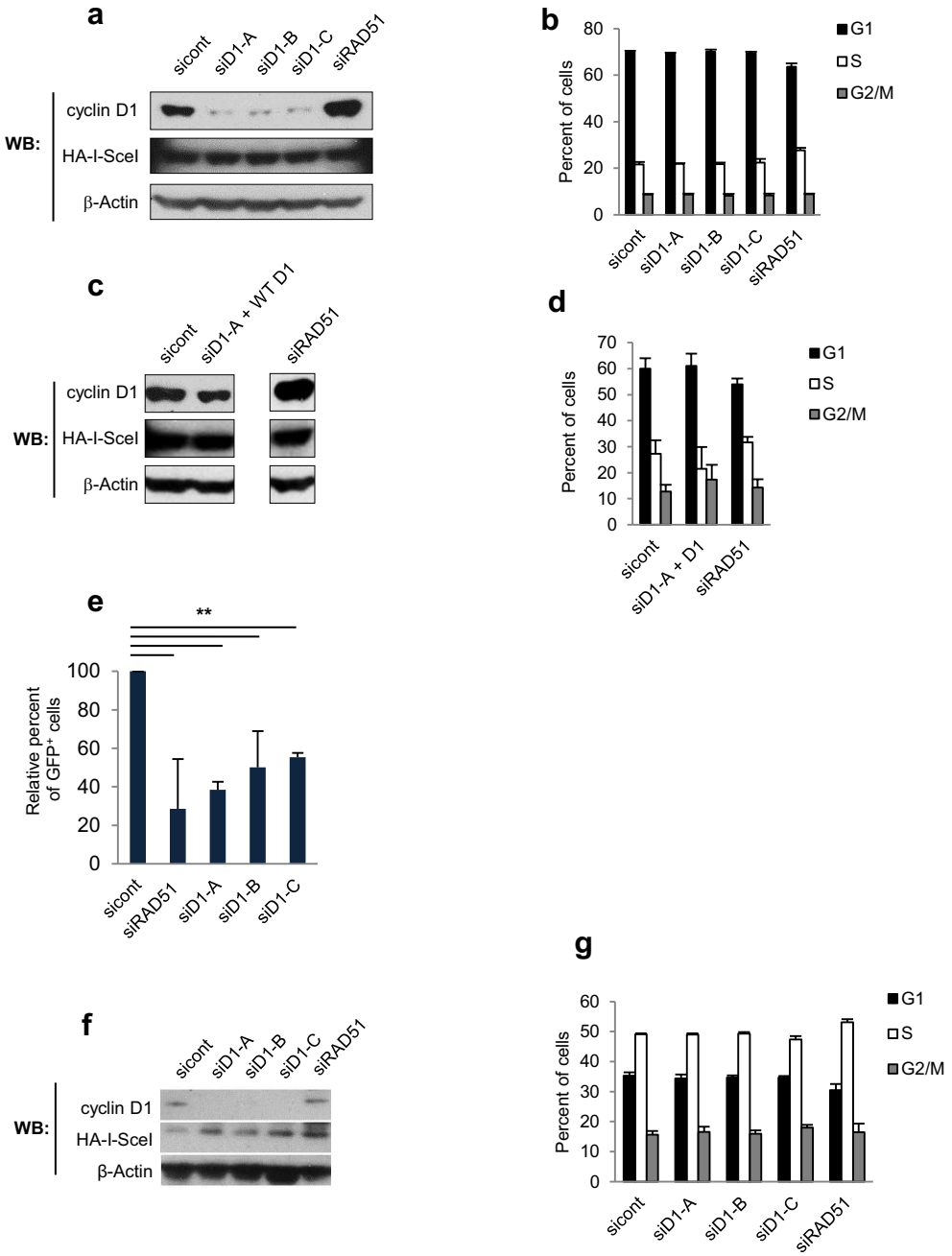

Supplementary Figure 9 I Homologous recombination assays in HeLa and in H2009 lung cancer cells

a-d, Cyclin D1 levels and cell cycle distribution of HeLa cells used for homologous recombination assays shown in the main text, Fig. 2e, f.

a, Western blot analysis (WB) of the levels of the indicated proteins in HeLa cells transfected with control siRNA (sicont), with three independent anti-cyclin D1 siRNAs (siD1-A, siD1-B, siD1-C) or anti-RAD51 siRNA (siRAD51). Immunoblotting with an anti-HA antibody was used to detect HA-tagged I-SceI endonuclease.

b, Cell cycle distribution of HeLa cells from **a**. Error bars, standard deviation.

c, Western blot analysis (WB) of the levels of the indicated proteins in HeLa cells stably expressing an siD1-A resistant cyclin D1(WT D1). Cells were transfected with control siRNA (sicont), cyclin D1 siRNA (siD1-A), or RAD51 siRNA (siRAD51). Immunoblotting with an anti-HA antibody was used to detect HA-tagged I-SceI endonuclease.

d, Cell cycle distribution of HeLa cells from **c**. Error bars, standard deviation.

e-g, Homologous recombination assays in H2009 lung cancer cells.

e, Homologous recombination rate in H2009 cells transfected with control siRNA (sicont), anti-RAD51 siRNA (siRAD51), or with three independent anti-cyclin D1 siRNAs (siD1-A, -B, -C). Error bars, standard deviation. **, $p \leq 0.01$.

f, Expression levels of the indicated proteins in H2009 cells transfected with different siRNAs were determined by western blotting (WB). Immunoblotting with anti-HA antibody was used to detect HA-tagged I-SceI endonuclease.

g, Cell cycle distribution of cells from **e**. Error bars, standard deviation.

(Cell cycle profiles of cyclin D1-depleted cells shown in Fig. 9b and 9g are the same as ones shown in Supplementary Fig. 4a, b).

Supplementary Figure 10

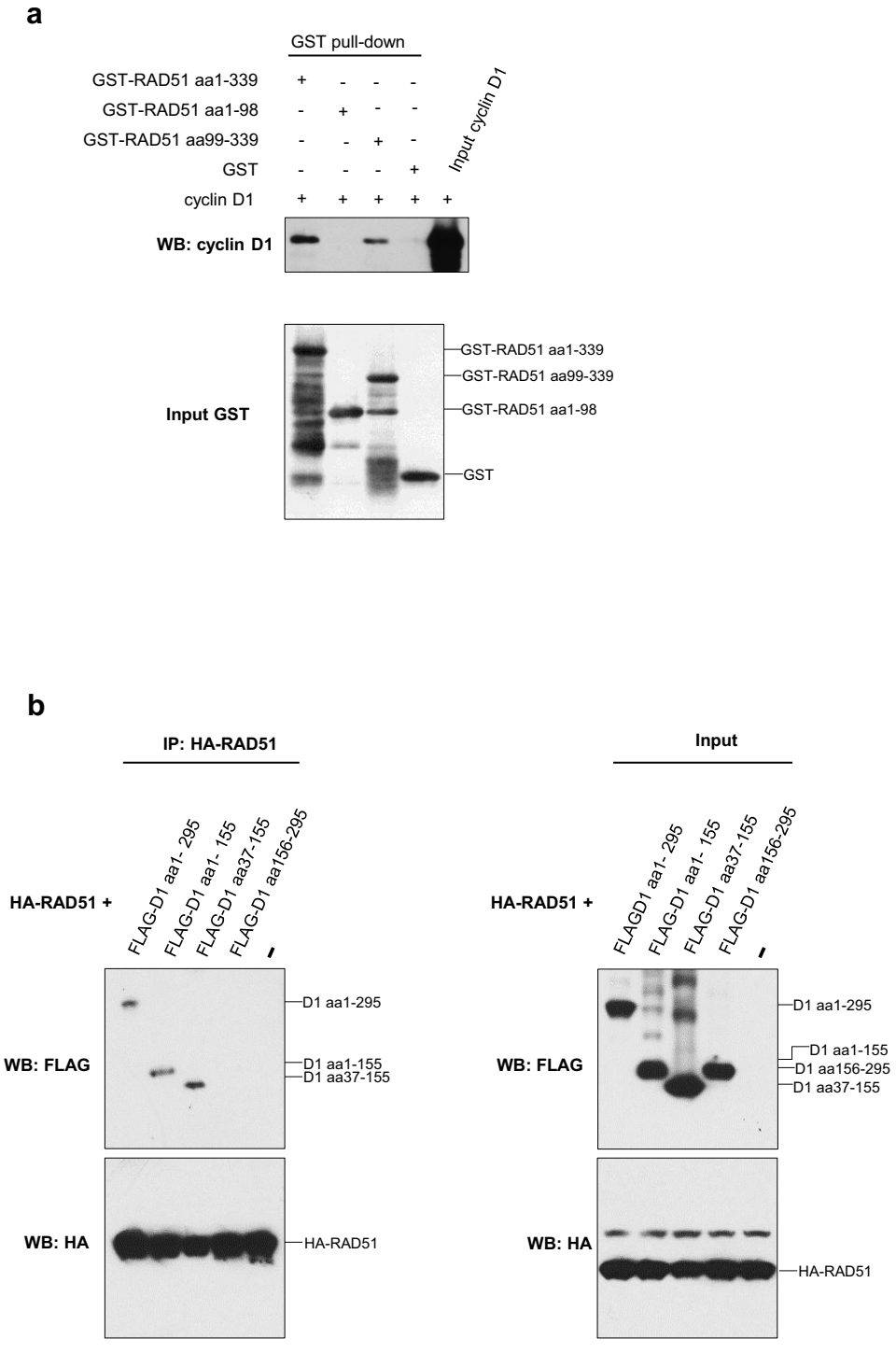

Supplementary Figure 10 l Analysis of cyclin D1 – RAD51 interaction

a, *In vitro* binding assays using GST-full length RAD51 (aa1-339) or the indicated GST-RAD51 deletion mutants, and purified recombinant cyclin D1. Upper panel: the indicated proteins were mixed, GST-containing proteins were precipitated using GSH Sepharose, resolved on a PAGE gel and immunoblotted (WB) with an anti-cyclin D1 antibody. Lower panel: GST-proteins used for binding reactions were resolved on a PAGE gel and probed with an anti-GST antibody.

b, *In vivo* binding assays**.** Left panel: FLAG-tagged full-length cyclin D1 (FLAG-D1 aa1-295) or the indicated cyclin D1 deletion mutants were expressed in 293 cells together with HA-tagged full-length RAD51. Complexes were immunoprecipitated with an anti-HA antibody, resolved on a PAGE gel and immunoblotted (WB) with an anti-FLAG antibody (to detect RAD51-bound cyclin D1). Re-probing with an anti-HA antibody was used to ensure equal immunoprecipitation efficiency. Right panel: the input lysates were resolved on a PAGE gel and immunoblots (WB) were probed with an anti-FLAG antibody (to detect transfected cyclin D1) or with an anti-HA antibody (to detect transfected RAD51).

Supplementary Figure 11

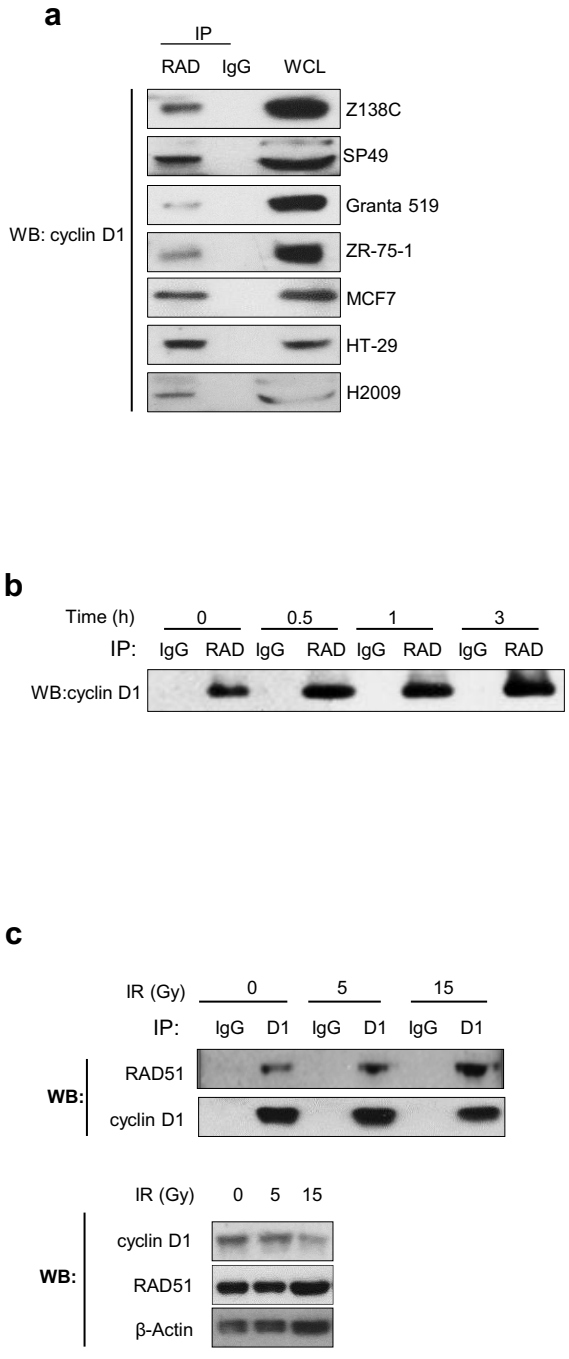

Supplementary Figure 11 I Analyses of the interaction between endogenous cyclin D1 and RAD51

a, Interaction between endogenous cyclin D1 and RAD51, detected in the indicated cell lines. RAD51 was immunoprecipitated (IP) and western blots (WB) were probed with anti-cyclin D1 antibody. WCL, whole cell lysate, IgG; non-immune IgG.

b, Increasing interaction between cyclin D1 and RAD51 over time, induced by radiation. HeLa cells were treated with 15 Gy of radiation, and harvested at the indicated time points. Anti-RAD51 antibody (RAD) or non-immune IgG (IgG) were used for immunoprecipitations (IP). Cyclin D1 was detected by western blotting (WB).

c, Upper panel: increased interaction between cyclin D1 and RAD51 in response to increasing doses of ionizing radiation (IR). HeLa cells were treated with the indicated doses of IR and harvested at 0.5 hrs after irradiation. Cyclin D1 was immunoprecipitated (IP) using anti-cyclin D1 antibody (D1). For control, we performed immunoprecipitations with non-immune IgG (IgG). RAD51 and cyclin D1 were then detected by western blotting (WB). Lower panel: levels of cyclin D1 and RAD51 proteins after treatment of HeLa cells with the indicated doses of radiation were determined in whole cell extracts using western blotting (WB). β-Actin served as loading control.

Supplementary Figure 12

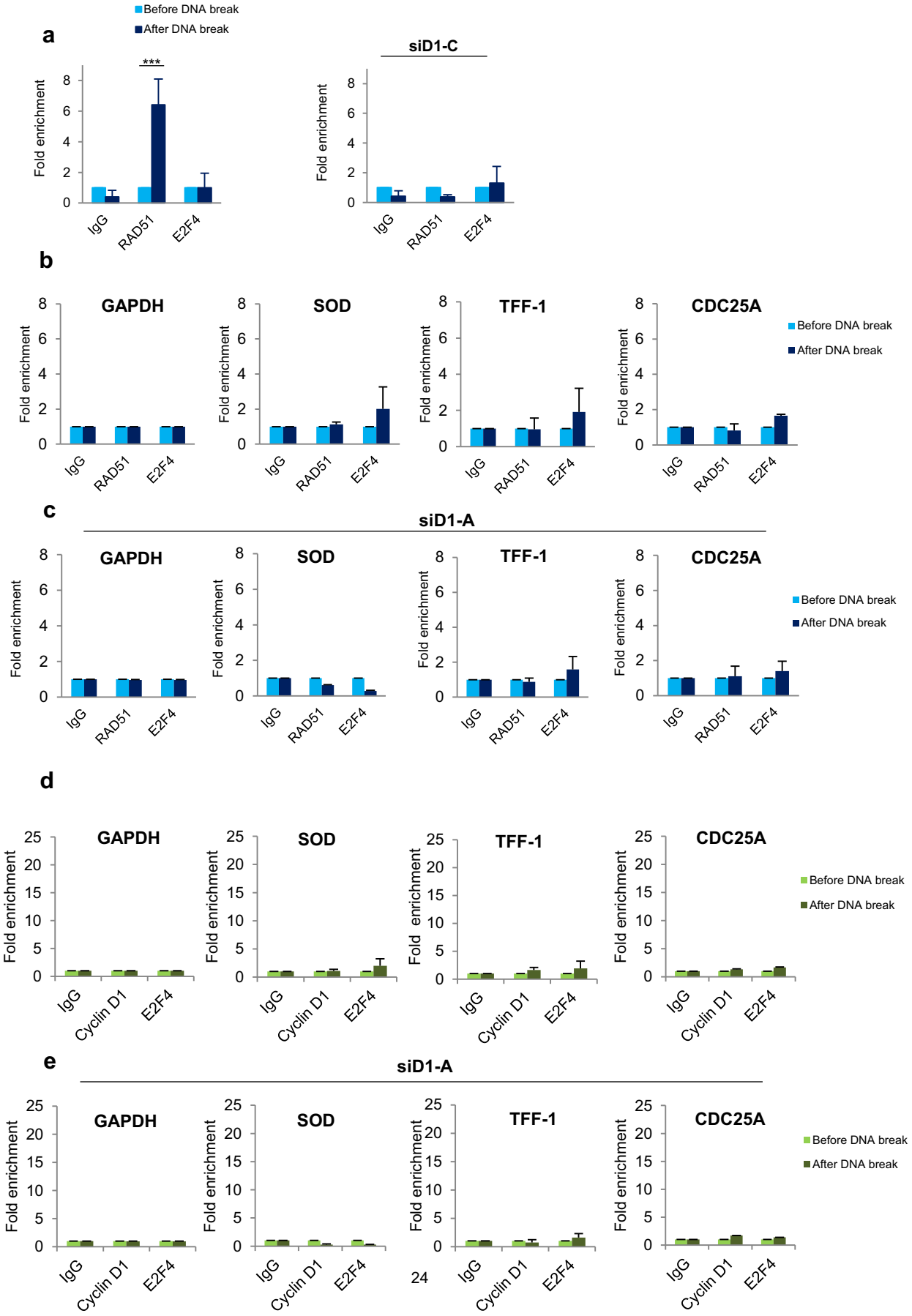

Supplementary Figure 12 I Targeted anti-RAD51 and anti-cyclin D1 chromatin immunoprecipitation

a-c, anti-RAD51 chromatin immunoprecipitation (ChIP).

a, Left panel: Recruitment of RAD51 to I-SceI - induced double-stranded DNA break was gauged by anti-RAD51 ChIP followed by PCR with primers adjacent to DNA damage site. Bars show enrichment around DNA damage site before (light blue) and after induction of a DNA break (dark blue). For control, we used anti-E2F4 and non-immune IgG (IgG) ChIP (followed by PCR with the same set of primers adjacent to DNA damage site) which did not show any enrichment after DNA damage. Right panel: the assay was repeated in cells transfected with anti-cyclin D1 siRNA. Note that cyclin D1 knock-down essentially abrogated RAD51 recruitment to DNA damage site. Error bars, standard deviation. ***, $p \leq 0.005$. This experiment is a repetition of analysis shown in Fig. 3h in the main text using another anti-cyclin D1 siRNA sequence.

b and **c**, Controls for targeted RAD51 chromatin immunoprecipitation. Anti-RAD51 ChIP followed by quantitative PCR was performed to gauge the recruitment of RAD51 to several control DNA segments (away from I-SceI-induced double-stranded DNA break) before and after induction of DNA break. In contrast to recruitment of RAD51 to the site of DNA break (panel **a**, and Fig. 3h in the main text), RAD51 was not recruited to control DNA segments. **b**, HeLa cells were transfected twice with control siRNA, or (**c**) with anti-cyclin D1 siRNA. Error bars, standard deviation.

d and **e,** Controls for targeted cyclin D1 chromatin immunoprecipitation (ChIP). Anti-cyclin D1 ChIP followed by quantitative PCR was performed to gauge the recruitment of

cyclin D1 to several control DNA segments (away from I-SceI-induced double-stranded DNA break) before and after induction of DNA break. In contrast to recruitment of cyclin D1 to the site of DNA break (Fig. 3i in the main text), cyclin D1 was not recruited to control DNA segments. **d**, HeLa cells were transfected twice with control siRNA or (**e**) with anti-cyclin D1 siRNA. Error bars, standard deviation.

Supplementary Figure 13

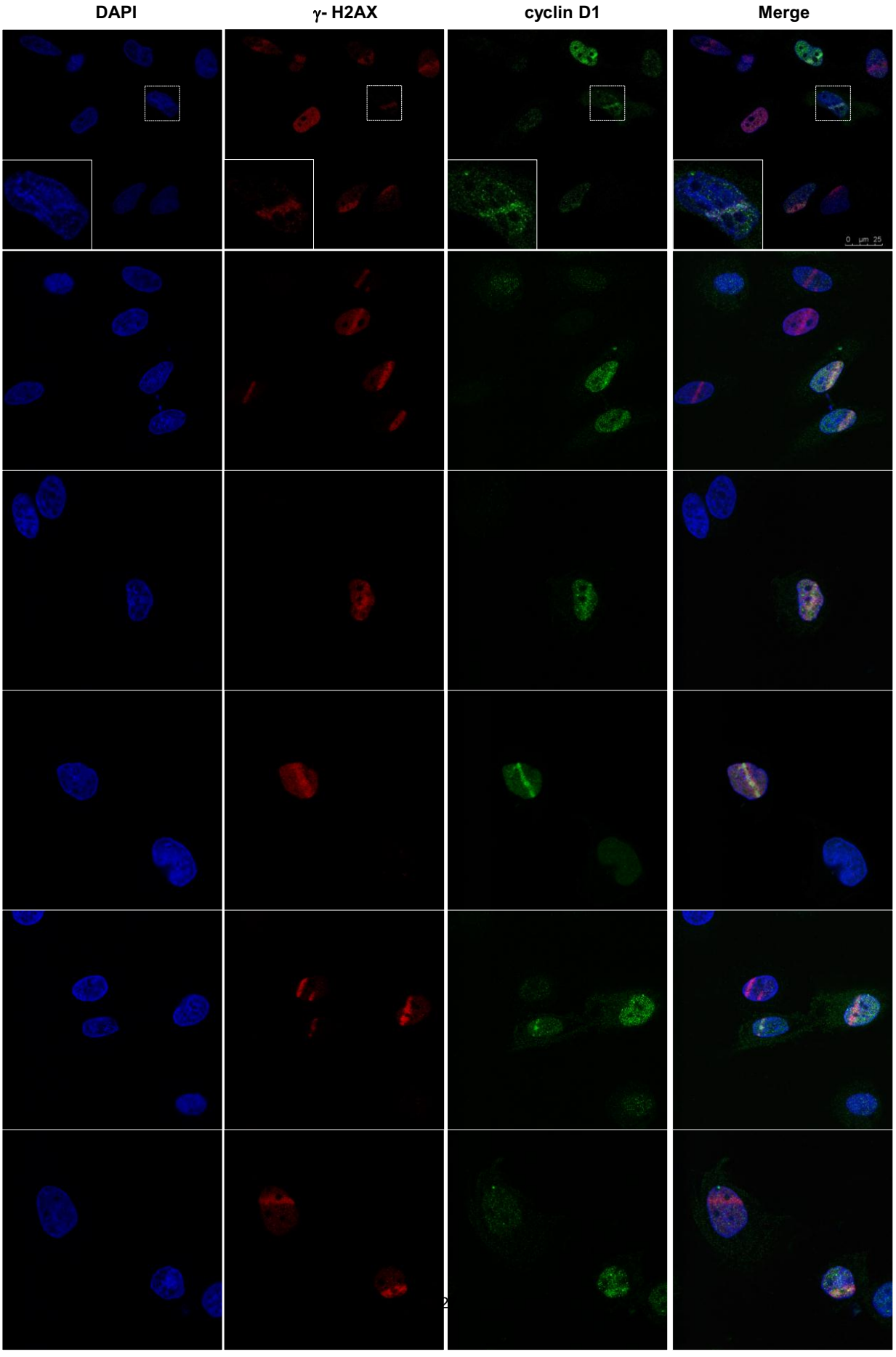

Supplementary Figure 13 | Recruitment of cyclin D1 to laser-induced DNA damage stripes

HeLa cells expressing HA-tagged cyclin D1 were co-stained for cyclin D1 (using an anti-HA antibody), γ-H2AX, and DAPI (to visualize nuclei). In the upper row of photographs, a selected nucleus is marked by a while box – its enlarged image is shown in the lower left corner.

Supplementary Figure 14

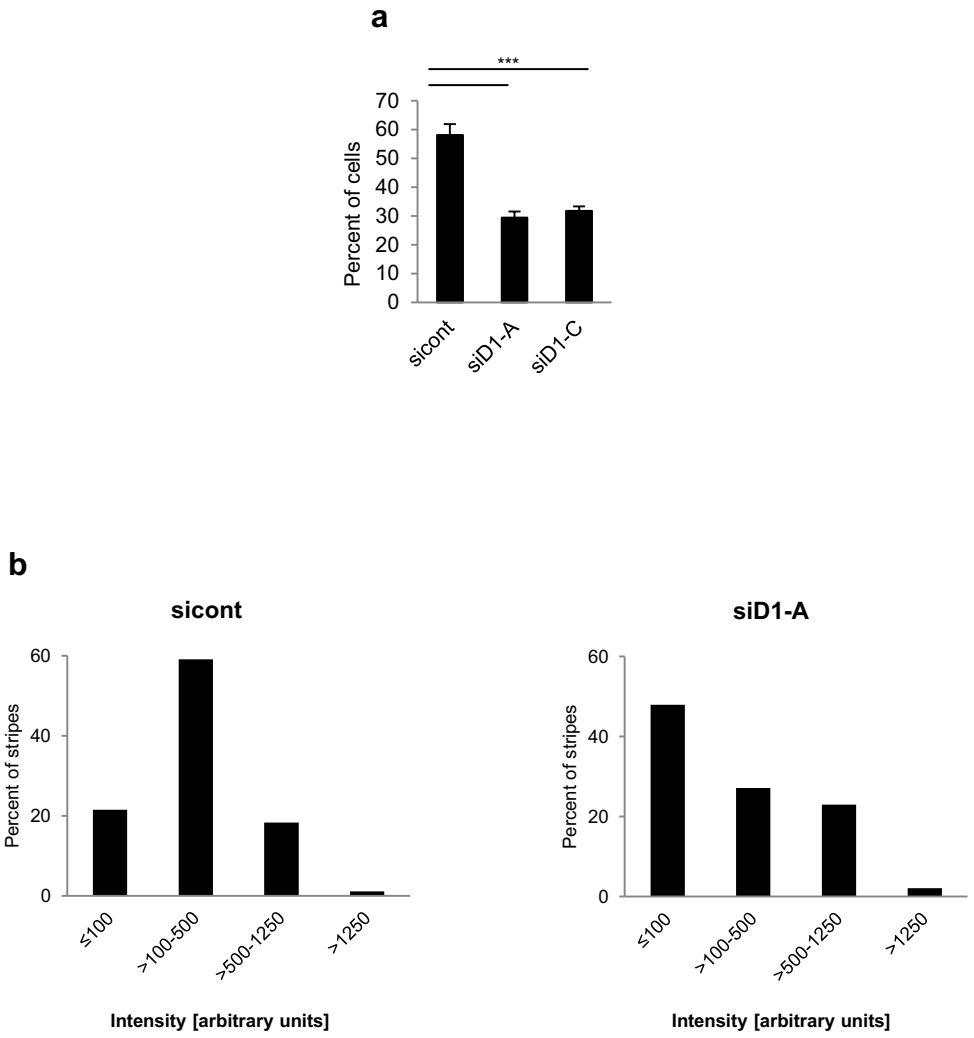

Supplementary Figure 14 l Reduced recruitment of RAD51 to laser-induced DNA damage stripes following depletion of cyclin D1

a, Decreased percentage of RAD51-positive stripes following cyclin D1 depletion. Laser-induced DNA damage was generated in HeLa cells, and cells were co-stained with anti-RAD51, and anti-γH2AX antibody. Shown is percent of γH2AX-positive cells displaying RAD51 stripes after laser-induced DNA damage, in cells transfected with control siRNA (sicont) or with anti-cyclin D1 siRNAs (siD1-A and -C). Error bars, standard deviation. ***, $p \leq 0.005$.

b, Decreased intensity of RAD51 stripes following depletion of cyclin D1 levels. Cells were treated as in **a**, and the intensity of RAD51 stripes was determined as described in Methods. Shown are histograms with percentages of RAD51 stripes displaying indicated staining intensities. Left panel, cells transfected with control siRNA (sicont). Right panel, cells transfected with anti-cyclin D1 siRNA (siD1-A).

Supplementary Figure 15

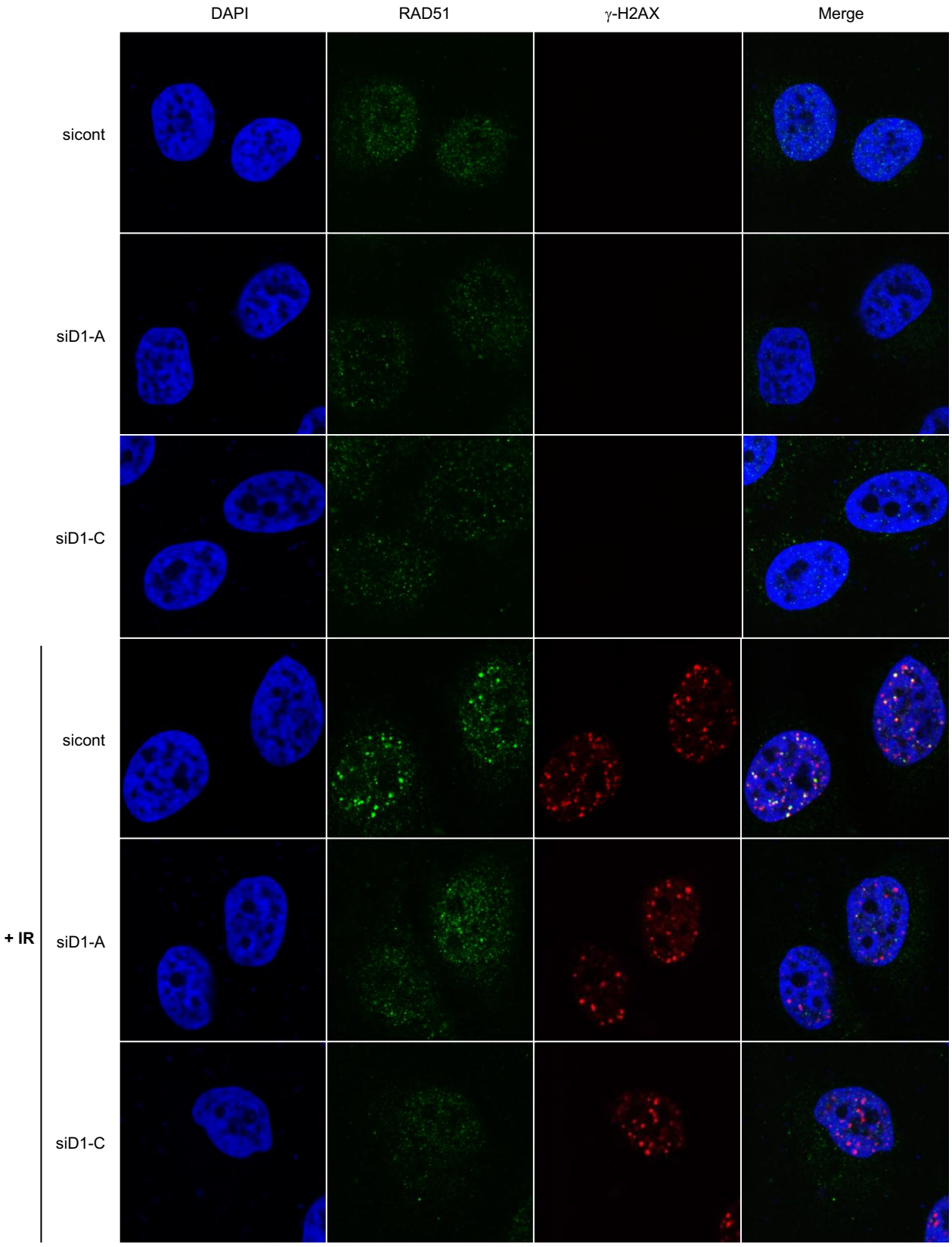

Supplementary Figure 15 l Decreased recruitment of RAD51 to DNA damage foci following depletion of cyclin D1

HeLa cells were transfected with control siRNA (sicont), or with two independent anti-cyclin D1 siRNAs (siD1-A and siD1-C). DNA damage was induced by 5 Gy of radiation (+IR), and cells were stained with antibodies against RAD51, γ-H2AX (a marker of DNA damage foci) or with DAPI. For quantification of foci, please see main text, Fig. 3k.

Supplementary Figure 16

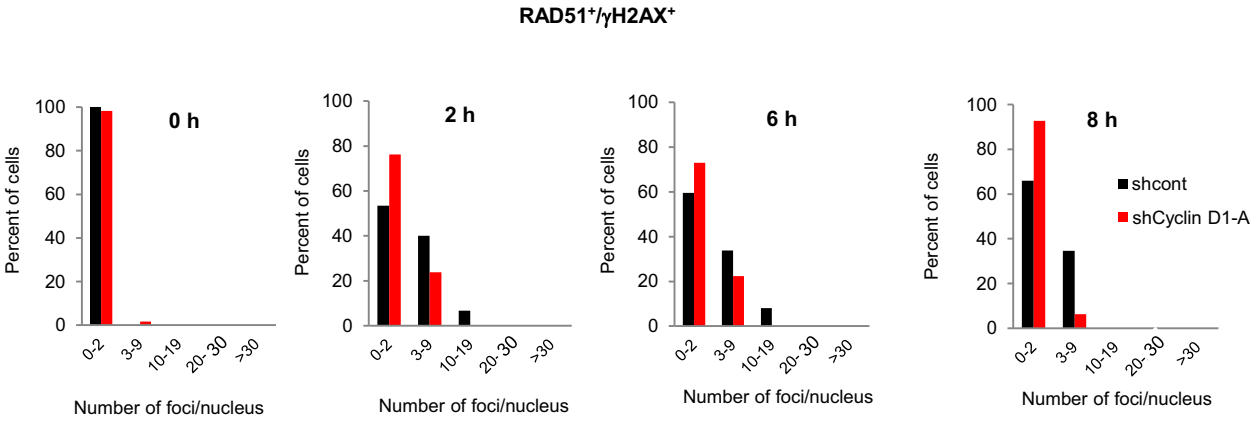

Supplementary Figure 16 l Reduced recruitment of RAD51 to DNA damage foci in H2009 lung cancer cells following cyclin D1 depletion

H2009 cells expressing either control shRNA (shcont) or an anti-cyclin D1 shRNA (shCyclin D1-A) were irradiated and analyzed at the indicated time-points. Shown is the percentage of cells displaying a given number of RAD51 foci per cell. The figure depicts results of a representative experiment from total n = 6.

Supplementary Figure 17

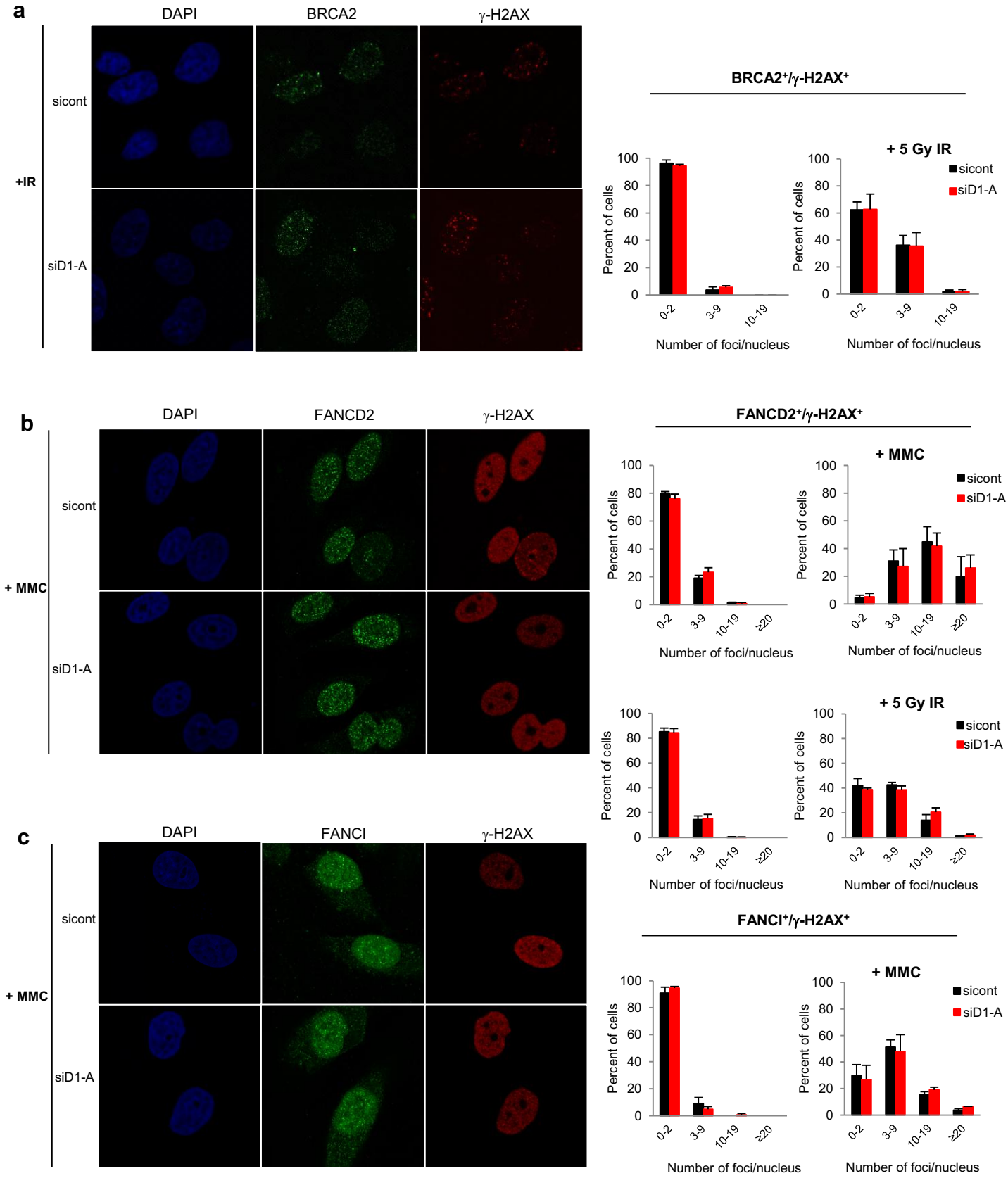

Supplementary Figure 17 (continued)

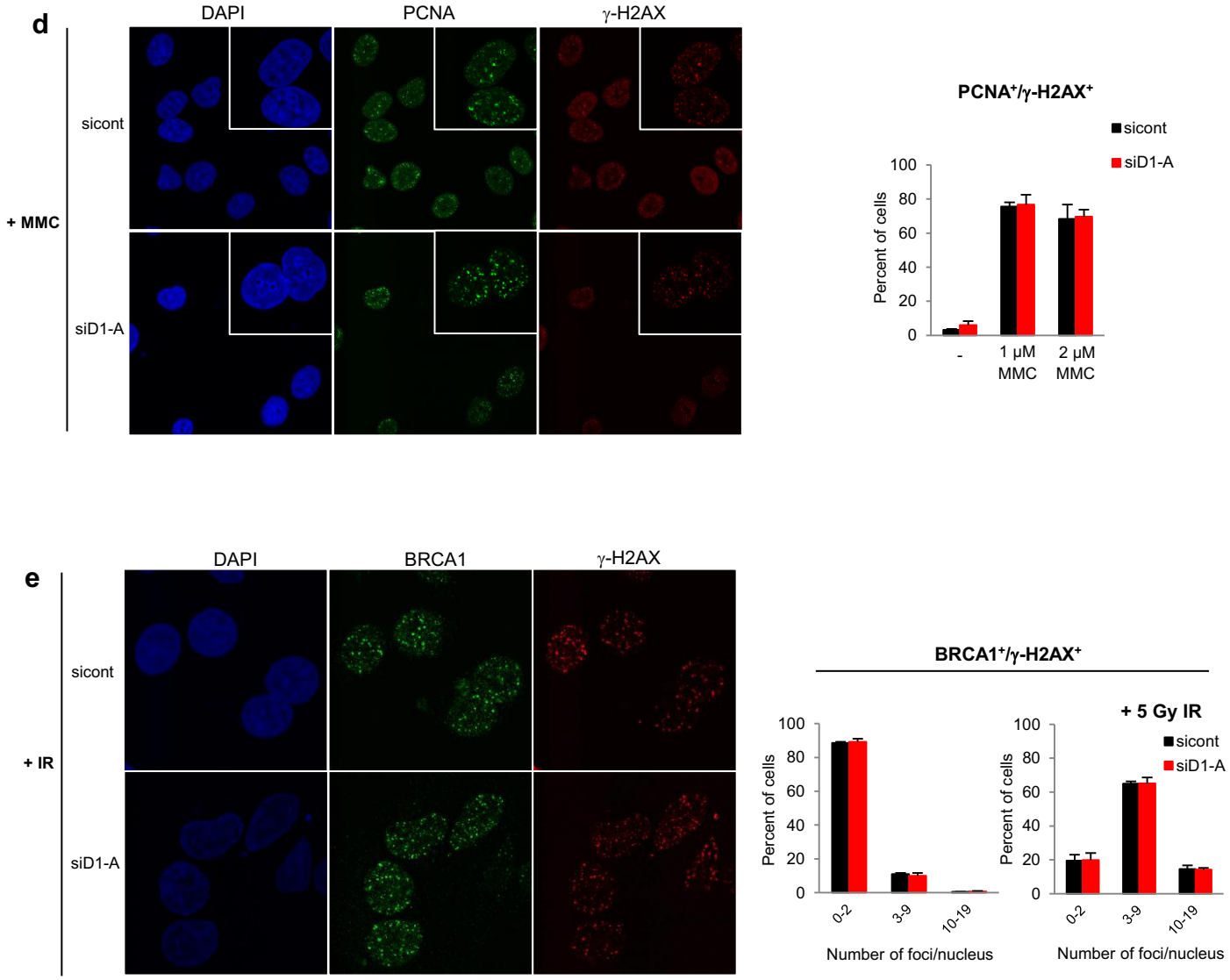

Supplementary Figure 17 l Normal recruitment of BRCA2, FANCD2, FANCI, PCNA and BRCA1 to DNA damage foci following cyclin D1-depletion

HeLa cells were transfected with control siRNA (sicont) or with an anti-cyclin D1 siRNA (siD1-A). Cells were irradiated (+IR) or treated with mitomycin C (+MMC) as indicated, and stained with the indicated antibodies. Left panels show representative immunofluorescent images. Quantification of the numbers of specific foci is shown in right panels, error bars represent standard deviation. Shown are foci for BRCA2 (**a**), FANCD2 (**b**), FANCI (**c**), PCNA (**d**) and BRCA1 (**e**).

Supplementary Figure 18

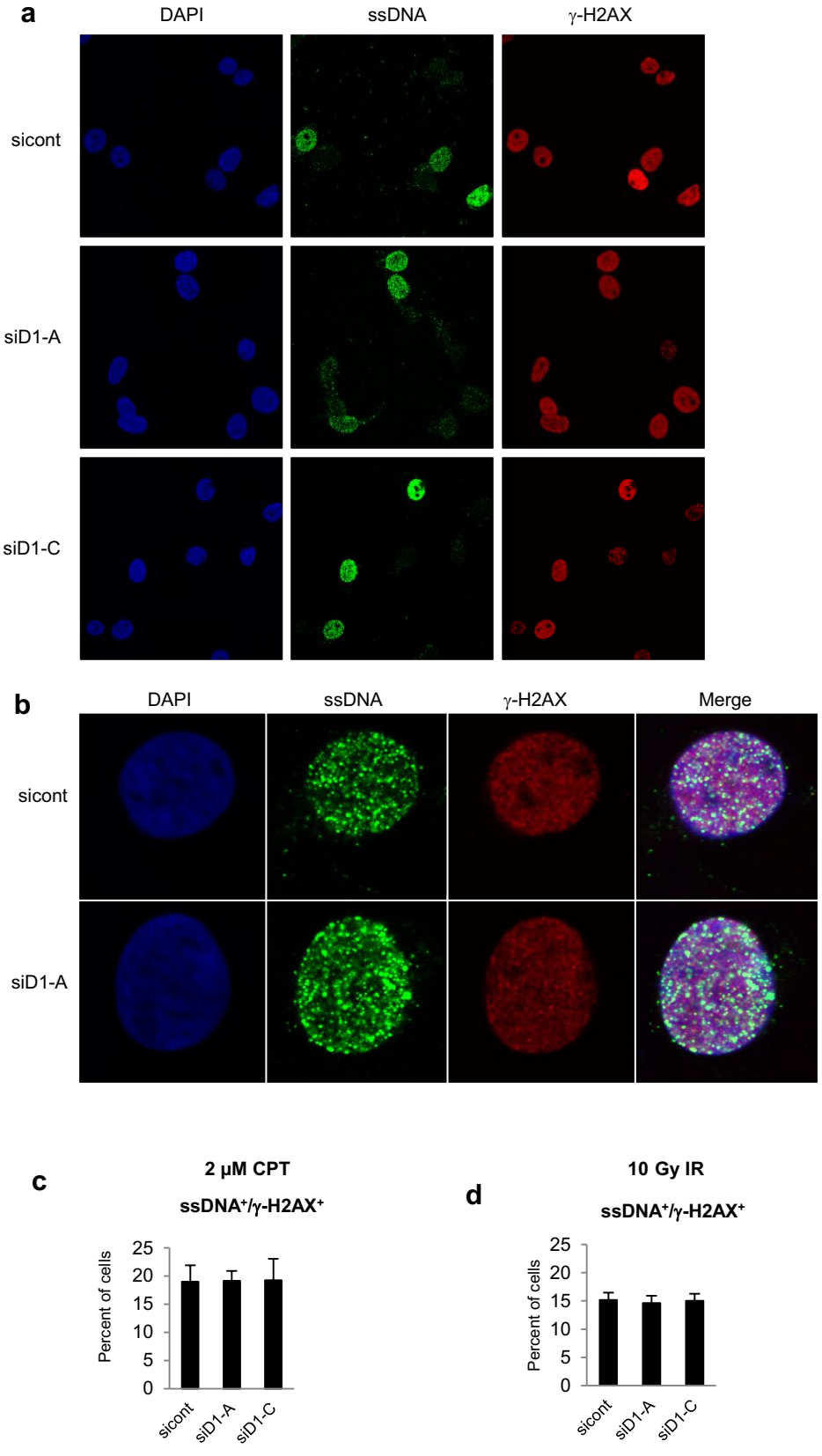

Supplementary Figure 18 (continued)

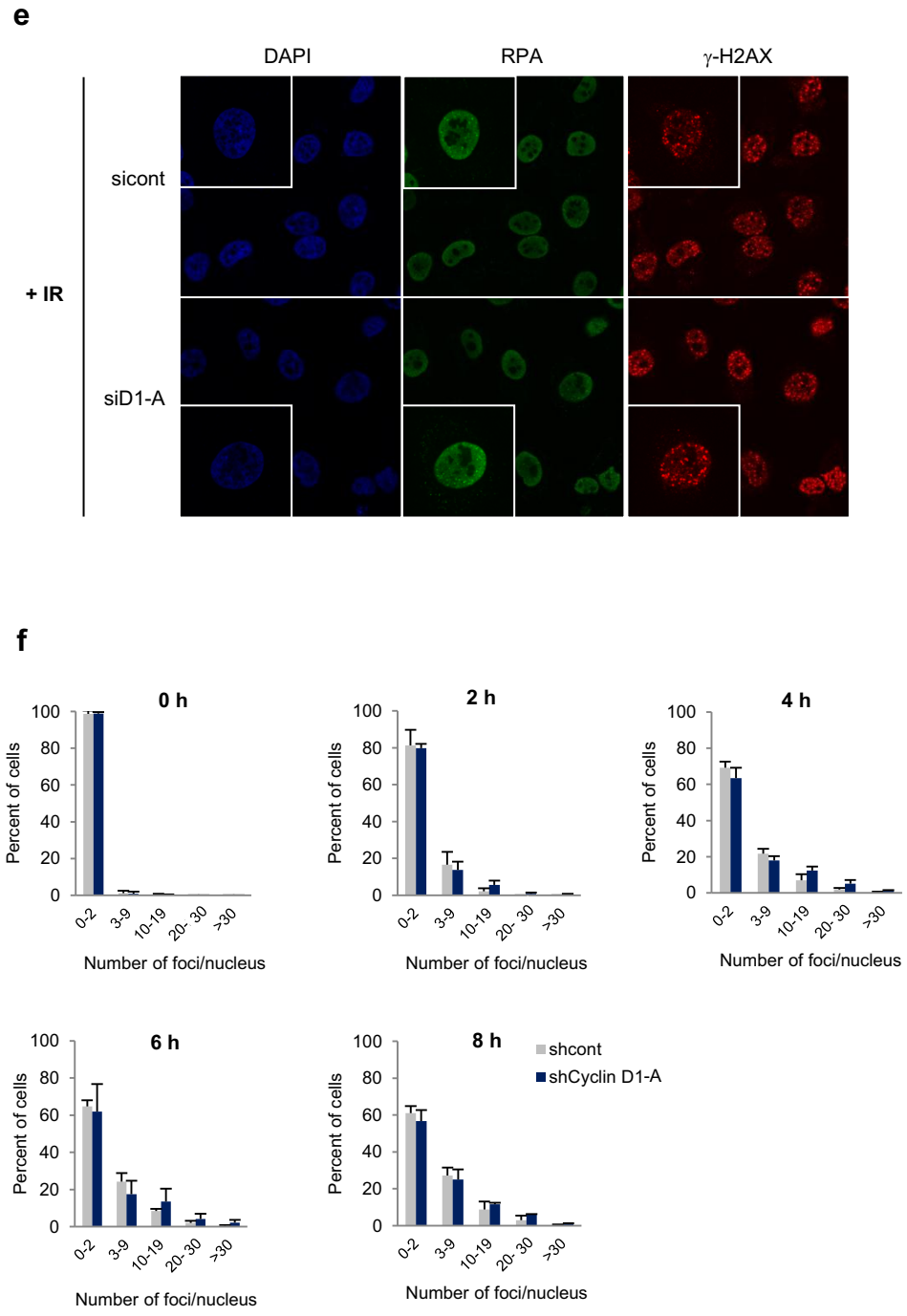

Supplementary Figure 18 l Unperturbed DNA end resection following depletion of cyclin D1

a-**d**, To detect single-stranded DNA (ssDNA) by microscopy, cells tranfected with anti-cyclin D1 siRNAs (siD1-A, -C) of control siRNA (sicont) were cultured for 24h in medium supplemented with 10 μM BrdU prior to a 1 hour treatment with 2 μM camptothecin (CPT) or 10 Gy radiation (IR). Cells were pre-extracted with Triton-X solution (see Methods), fixed in formaldehyde and co-immunostained with anti-γ-H2AX and anti-BrdU antibodies. Shown are representative immunofluorescent images (**a**), and higher magnification in **b**. The percentages of cells containing ssDNA after CPT and IR treatment are shown in **c** and **d**, respectively.

e-f, As another measure of DNA end resection we analyzed recruitment of single stranded DNA binding protein RPA34 in cyclin D1-depleted cells (siD1-A). HeLa cells were irradiated (IR) and analyzed by immunofluorescence (**e**). **f**, Percentage of irradiated cells displaying the indicated number of foci per cell at the indicated time-points after radiation. Error bars, standard deviation.

Supplementary Figure 19

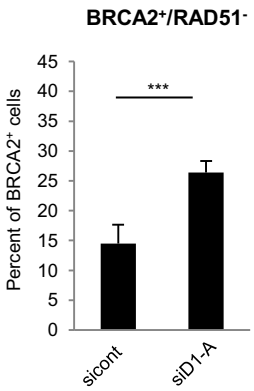

Supplementary Figure 19 l Reduced co-localization of BRCA2 and RAD51 following knock-down of cyclin D1

HeLa cells were transfected with control siRNA (sicont) or with an anti-cyclin D1 siRNA (siD1-A) and irradiated. At 2 hours after irradiation, cells were stained with anti-BRCA2 and -RAD51 antibodies to visualize BRCA2 and RAD51 which normally co-localize within DNA damage foci[5]. Shown is percent of BRCA2-positive foci which failed to recruit RAD51 ($BRCA2^+/RAD51^-$). Note that the number of BRCA2-positive foci was unchanged in cells depleted of cyclin D1 (Supplementary Fig. 18a), however, the subsequent recruitment of RAD51 to these foci was defective in cyclin D1 knock-down cells. ***, $p \leq 0.005$. Error bars, standard deviation. This experiment is a repetition of analysis shown in Fig. 3**m** in the main text using another anti-cyclin D1 siRNA sequence.

Supplementary Figure 20

a

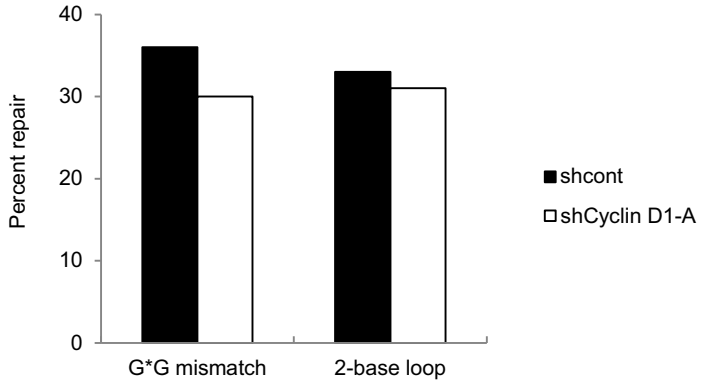

b

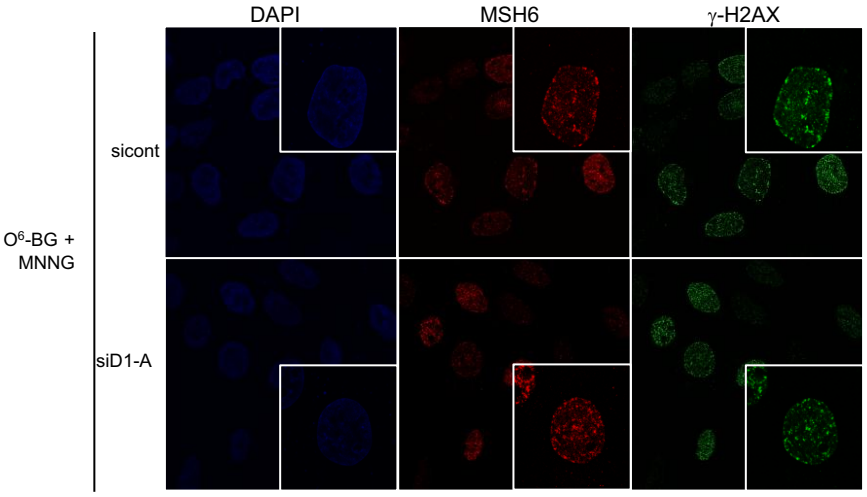

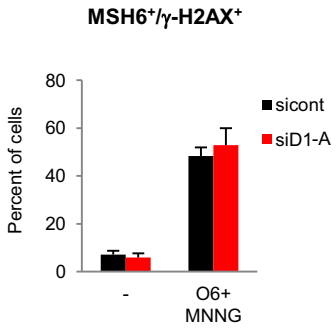

Supplementary Figure 20 l Proficient DNA mismatch repair in cells depleted of cyclin D1

a, Repair of DNA mismatches. Cytosolic extracts prepared from HeLa cells expressing cyclin D1 shRNA (shCyclin D1-A) or control shRNA (shcont) were assayed for the ability to repair heteroduplex substrates containing either a G•G mispair or a 2-base loop mismatch.

b, Normal recruitment of MSH6 protein to DNA damage foci. HeLa cells transfected with anti-cyclin D1 siRNA (siD1-A) or control siRNA (sicont) were treated with O^6-benzylguanine (O^6-BG) and N-methyl-N'-nitro-N-nitrosoguanidine (MNNG) to create DNA mismatches. The recruitment of MSH6 to DNA damage foci was analyzed by immunofluorescence (left panel). Right panel: quantification of the number of MSH6-containing DNA damage foci. Error bars represent standard deviation.

Supplementary Figure 21

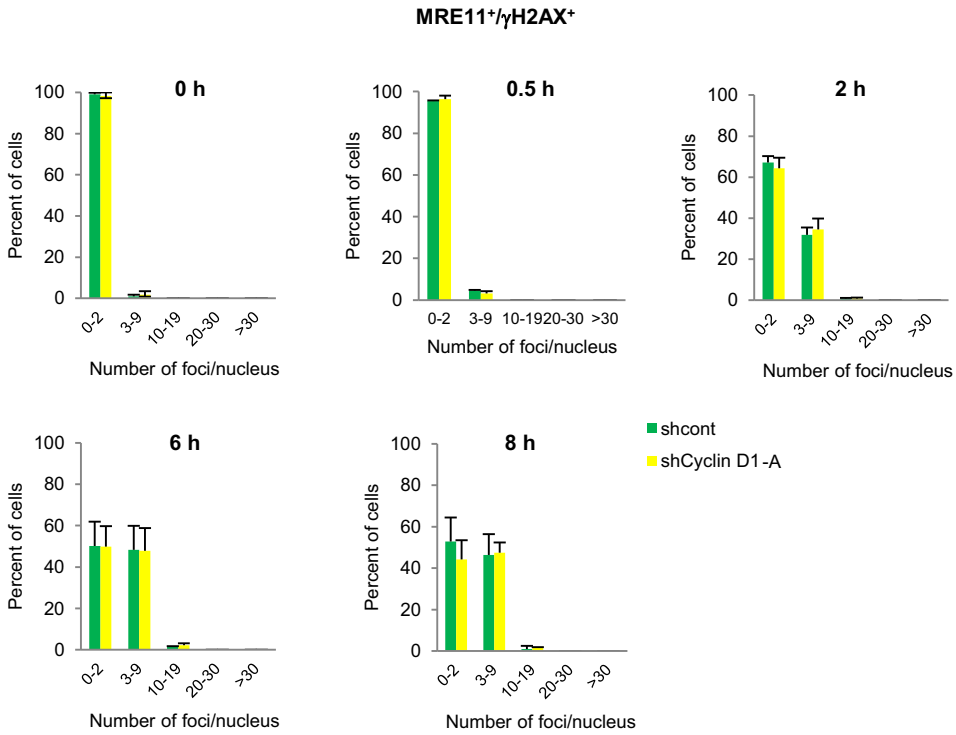

Supplementary Figure 21 I Normal recruitment of MRE11 to DNA damage foci following depletion of cyclin D1

HeLa cells were irradiated and analyzed at the indicated time-points. Shown is percentage of irradiated cells displaying the indicated number of MRE11 foci per cell, in cells expressing control shRNA (shcont) or anti-cyclin D1 shRNA (shCyclin D1-A). Error bars represent standard deviation.

Supplementary Figure 22

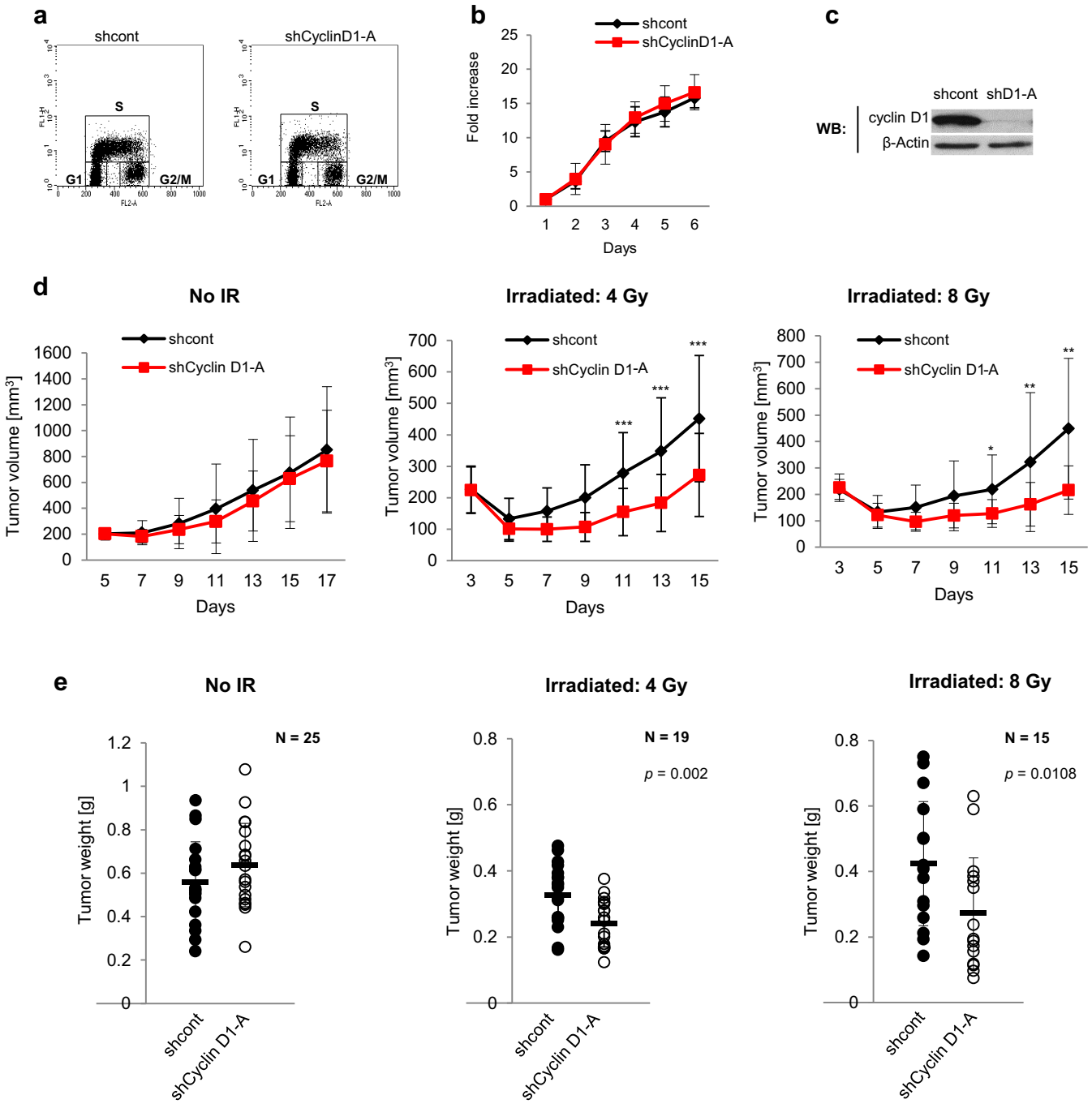

Supplementary Figure 22 l Increased sensitivity of lung cancer H2009 tumors to radiation following reduction of cyclin D1 levels

a, Unperturbed cell cycle distribution of *in vitro* cultured H2009 cells after cyclin D1 knock-down (shCyclin D1-A). Cells were pulse-labeled with bromodeoxyuridine (BrdU), then stained with anti-BrdU antibodies and with propidium iodide followed by FACS analysis. The percentages of cells in particular phases of cell cycle are shown in Supplementary Fig. 4d. For results using two another anti-cyclin D1 shRNA sequences, please see Supplementary Fig. 25a.

b, Unperturbed *in vitro* growth of H2009 cells after cyclin D1 knock-down. Equal numbers of cells were plated on day 0, and the number of cells was determined at the indicated time-points. Error bars, standard deviation. For results using two another anti-cyclin D1 shRNA sequences, please see Supplementary Fig. 25b.

c, Western blot (WB) analysis of cyclin D1 levels in H2009 cells following cyclin D1 knock-down, analyzed before injecting the cells (please see Supplementary Fig. 26 for cyclin D1 levels in tumors).

d, H2009 cells expressing control shRNA (shcont) or anti-cyclin D1 shRNA (shCyclin D1-A) were injected into nude mice and tumor volume was monitored at the indicated time-points.

Left panel, in the absence of irradiation (No IR), tumors with reduced cyclin D1 levels displayed unperturbed growth *in vivo* (this is the same graph as the one shown in Fig. 4a, left panel in the main text). Middle and right panels, at day 3 after tumor cell injection, mice received 4 Gy or 8 Gy of radiation, as indicated. Note that this resulted

in impaired growth of tumors with depleted cyclin D1 levels. Error bars, standard deviation. ***, $p \leq 0.005$.; **, $p \leq 0.01$; *, $p < 0.05$.

e, Weight of tumors at the end of the observation period. Each circle represents an individual tumor; horizontal bars denote mean values. In the absence of radiation, tumors with reduced cyclin D1 levels displayed unperturbed growth *in vivo* (left panel) (this graph is also shown in Fig. 4b, left panel in the main text). In contrast, upon irradiation with 4 Gy (middle panel), or with 8 Gy (right panel), tumors with reduced cyclin D1 levels showed decreased weight, as compared to control tumors (expressing normal levels of cyclin D1). Shown are the numbers of mice analyzed per group (N) and the *p*-values.

Supplementary Figure 23

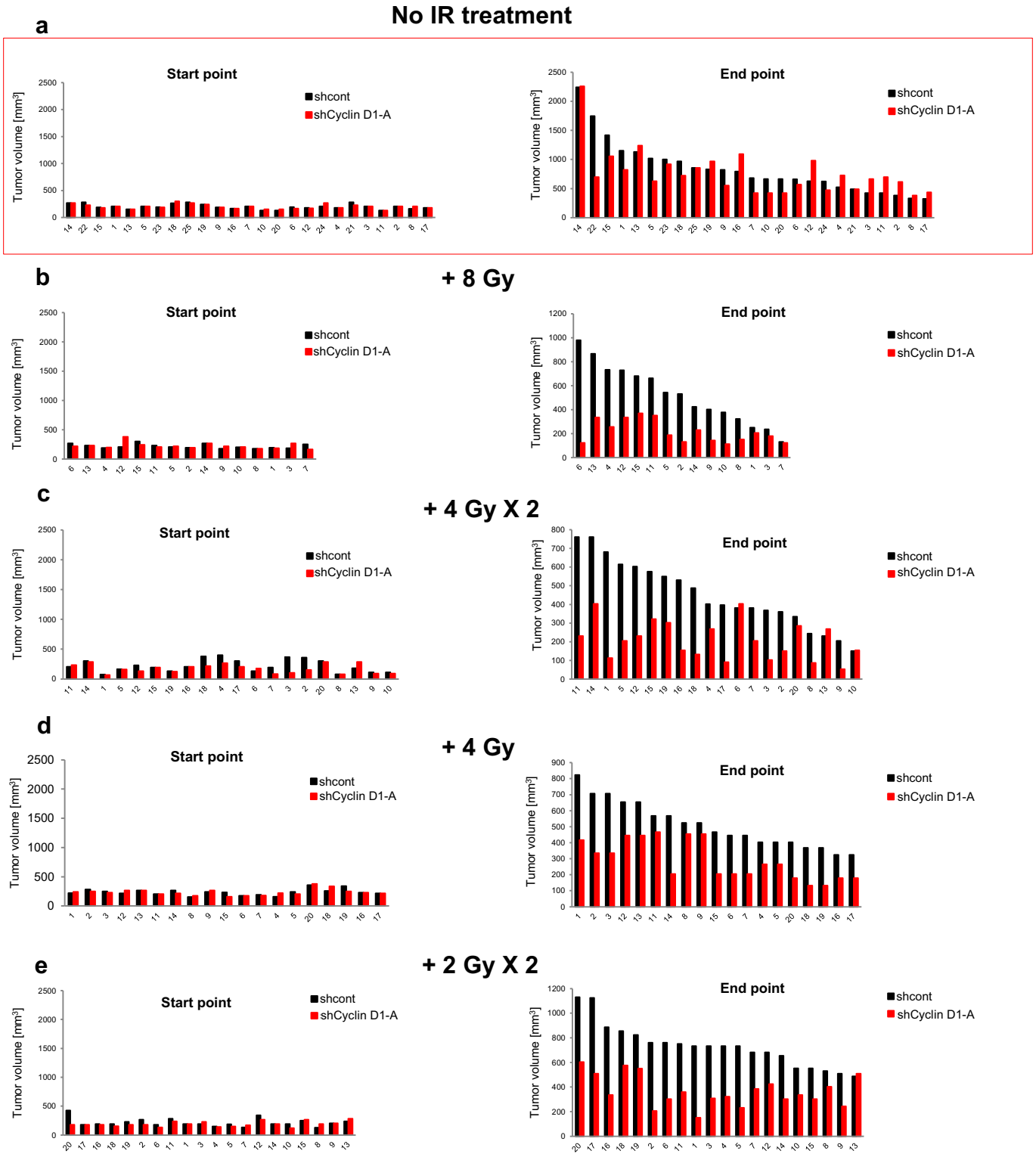

Supplementary Figure 23 I Volumes of individual H2009 tumors mouse-by-mouse

This figure shows volumes of H2009 tumors mouse-by-mouse (mean values and standard deviations are shown in Fig. 4 in the main text and in Supplementary Fig. 22). In our experiments shown in Fig. 4 and in Supplementary Fig. 22, H2009 cells were transduced with viruses encoding control shRNA (shcont), or anti-cyclin D1 shRNA (shCyclin D1-A), and injected subcutaneously into immunocompromised mice. Each recipient mouse was injected on one side with cyclin D1-depleted tumor cells and on the contralateral side with control tumor cells. In this figure, the tumor volumes are shown for each recipient mouse as a set of black/red bars. Black bar denotes the volume of a control tumor within a given mouse, the adjacent red bar - the volume of cyclin D1-depleted tumor within the same mouse. A number below each set of black/red bars denotes the identifying number of a particular recipient mouse.

In **a-e**, left panels depict tumor volumes at the beginning of observation period ("Start point", please see Methods for details). Please note that there was no difference between the volume of control and cyclin D1-depleted tumors at the beginning of the observation period. Right panels show tumor volumes at the end of observation period ("End point").

a, This panel shows volume of tumors which did not receive radiation (No IR treatment). In the absence of radiation, at the end of the observation period there was no difference between tumor size of control vs. cyclin D1-depleted tumors.

b-**e**, Tumors received the indicated doses of irradiation. Note that at the end of observation period, cyclin D1-depleted tumors were almost always (69/74 mice) smaller

than the contralateral control tumors within the same mouse. The mean tumor volumes of cyclin D1-depleted tumors were also smaller, and the differences were statistically significant (please see Fig. 4 and Supplementary Fig. 22).

Supplementary Figure 24

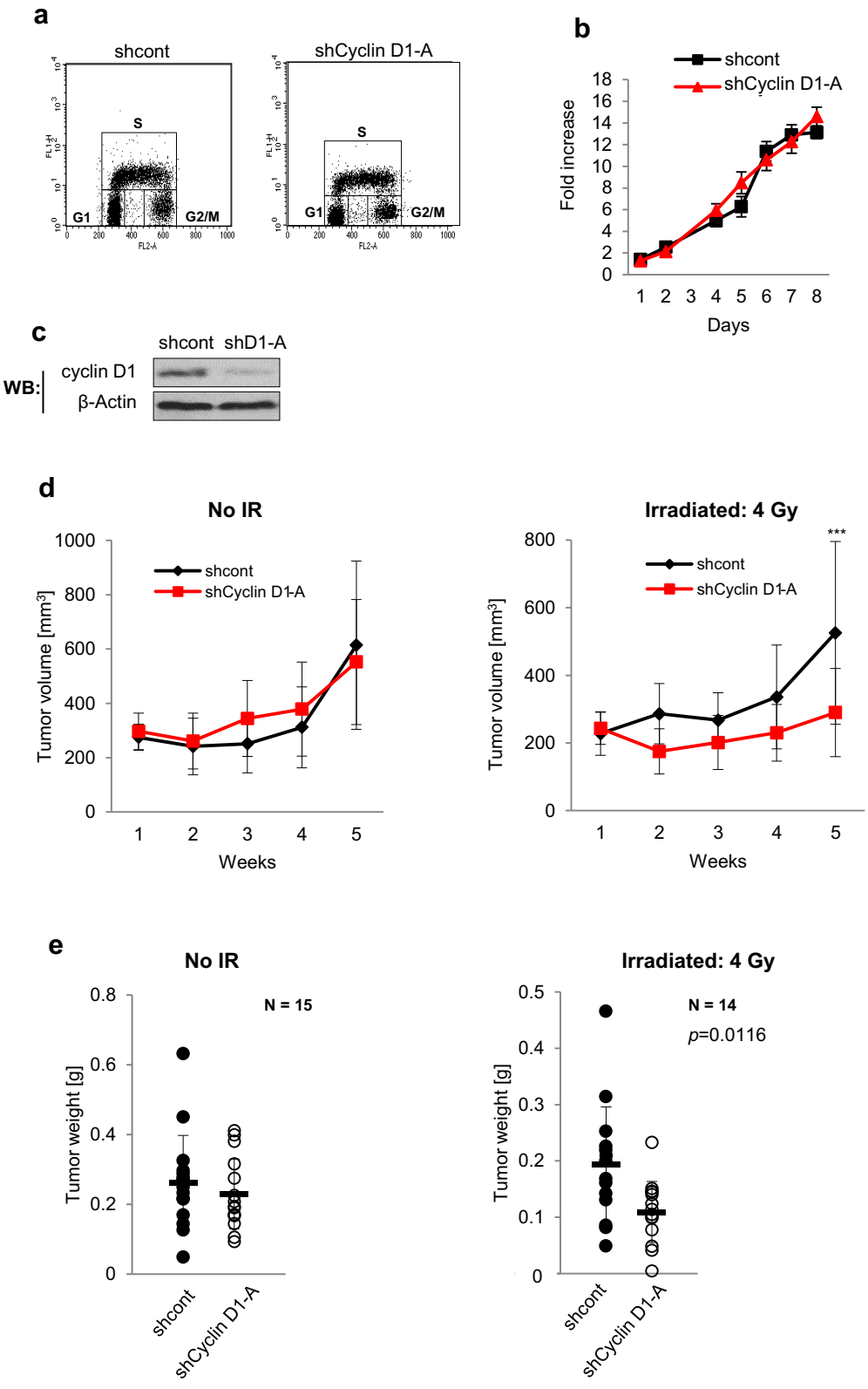

Supplementary Figure 24 l Increased sensitivity of cervical carcinoma HeLa tumors to radiation following reduction of cyclin D1 levels

a, Cell cycle profiles of *in vitro* cultured HeLa cells expressing control shRNA (shcont) or anti-cyclin D1 shRNA (shCyclin D1-A). Cells were pulse-labeled with BrdU and stained with anti-BrdU antibodies and with propidium iodide followed by FACS analysis. For histograms showing percentages of cells in particular cell cycle phases, please see Supplementary Fig. 4c.

b, *In vitro* growth curves of HeLa cells expressing control shRNA (shcont) or cyclin D1 shRNA (shCyclin D1-A). Equal numbers of cells were plated on day 0, and the number of cells was determined at the indicated time-points. Error bars, standard deviation.

c, The efficiency of cyclin D1 knock-down was gauged by western blotting (WB). Please see Supplementary Fig. 27 for the levels of cyclin D1 in tumors.

d, HeLa cells expressing control or anti-cyclin D1 shRNA (shCyclin D1-A) were injected into nude mice and tumor volume was monitored at the indicated time-points. Left panel, in the absence of irradiation, tumors with reduced cyclin D1 levels displayed unperturbed growth *in vivo.* Right panel, at day 10 after tumor cell injection, mice received 4Gy of ionizing radiation. Note that this resulted in impaired growth of tumors with reduced cyclin D1 levels. Error bars represent standard deviation. ***, $p \leq 0.005$

e, Weight of tumors at the end of the observation period. Each circle represents an individual tumor; horizontal bars denote mean values. Left panel, in the absence of radiation, tumors with reduced cyclin D1 levels displayed unperturbed growth *in vivo*. Right panel, in contrast, upon irradiation, tumors with reduced cyclin D1 levels showed

decreased weight, as compared to control tumors (expressing normal levels of cyclin D1). Shown are the numbers of mice analyzed per group (N) and the *p*-values.

Supplementary Figure 25

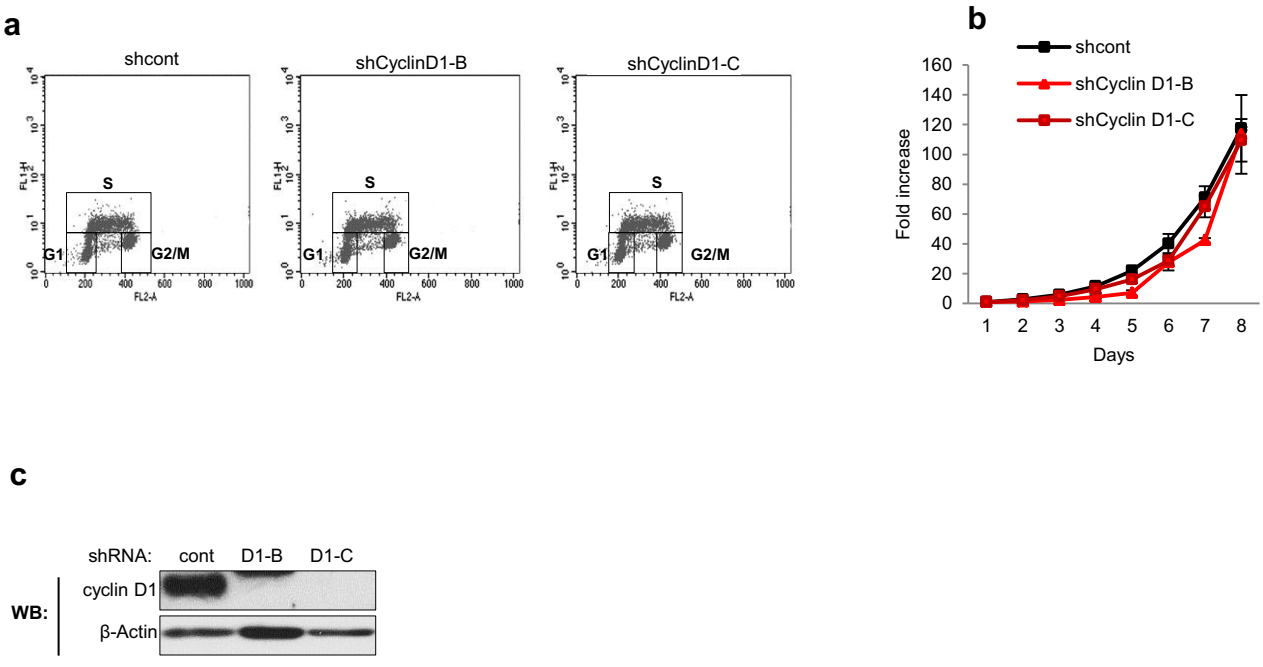

Supplementary Figure 25 (continued)

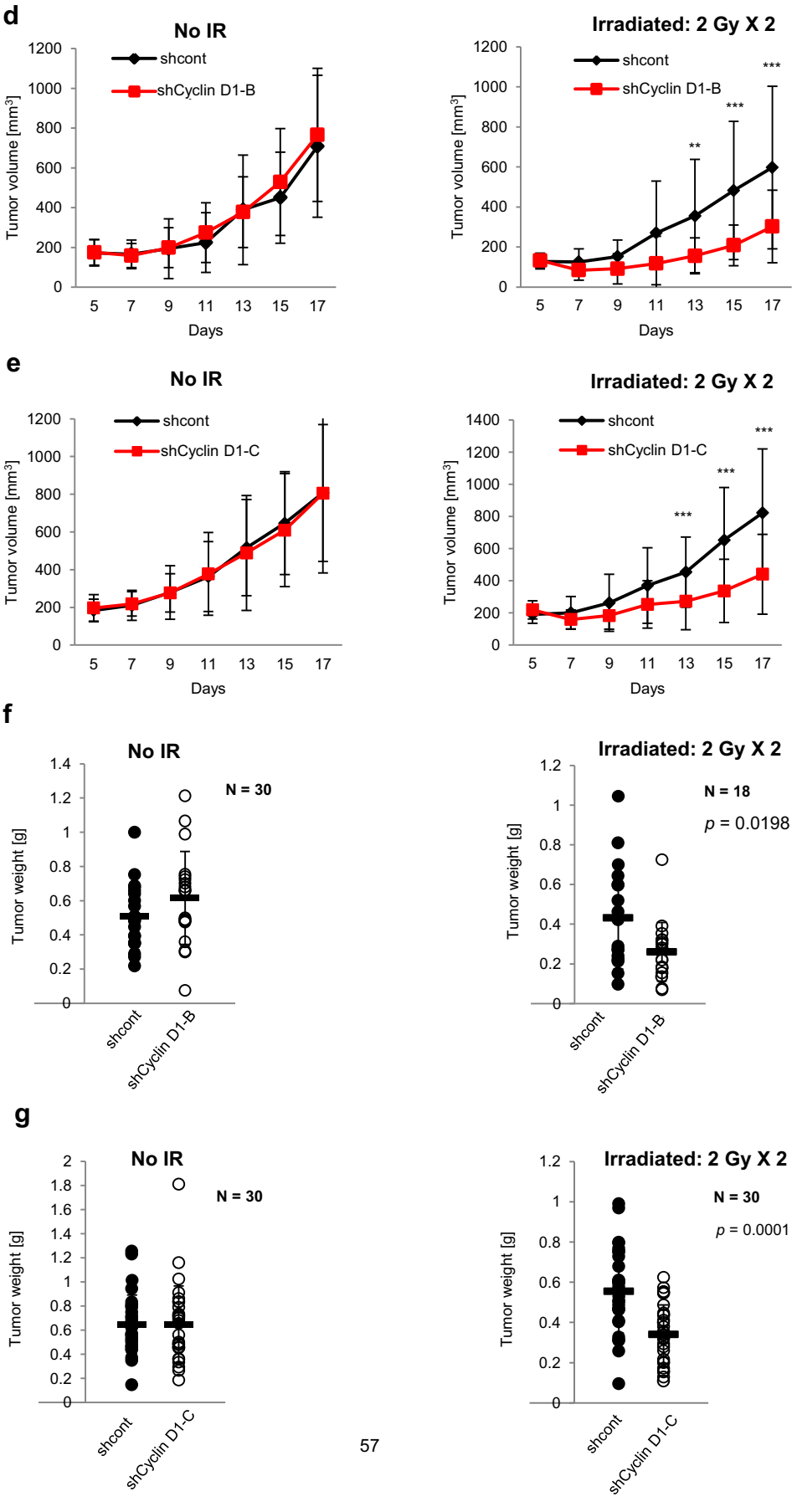

Supplementary Figure 25 l Increased sensitivity of lung cancer H2009 tumors to radiation following reduction of cyclin D1 levels

a, Cell cycle profiles of *in vitro* cultured H2009 cells expressing control shRNA (shcont), and two independent anti-cyclin D1 shRNAs (shCyclin D1-B and shCyclin D1-C). Cells were pulse-labeled with BrdU and stained with anti-BrdU antibodies and with propidium iodide followed by FACS analysis. For histograms showing percentages of cells in particular cell cycle phases, see Supplementary Fig 4d. This experiment is a repetition of analysis shown in Supplementary Fig. 22a using two additional independent anti-cyclin D1 shRNA sequences.

b, Unperturbed *in vitro* growth of H2009 cells after cyclin D1 knock-down. Equal number of cells was plated on day 0, and the number of cells was determined at the indicated time-points. Error bars, standard deviation. This experiment is a repetition of analysis shown in Supplementary Fig. 22b using two additional independent anti-cyclin D1 shRNA sequences.

c, The efficiency of cyclin D1 knock-down was assessed by western blotting (WB).

d and **e**, H2009 cells expressing control or anti-cyclin D1 shRNA were injected into nude mice and tumor volume was monitored at the indicated time-points. Left panels, in the absence of irradiation, tumors with reduced cyclin D1 levels displayed unperturbed growth *in vivo*. Right panels, at day 5 and 10 after tumor cell injection, mice received 2 Gy of radiation. Note that this resulted in impaired growth of tumors with reduced cyclin D1 levels. Error bars, standard deviation. ***, $p \leq 0.005$; **, $p \leq 0.01$. This experiment is a repetition of analysis shown in Fig. 4a in the main text using two additional

independent anti-cyclin D1 shRNA sequences (panel **d** shows results obtained with the second shRNA sequence (shCyclin D1-B), panel **e** results with the third one (shCyclin D1-C).

f and **g**, Weight of tumors at the end of the observation period. Each circle represents an individual tumor; horizontal bars denote mean values. Left panels, in the absence of radiation, tumors with reduced cyclin D1 levels displayed unperturbed growth *in vivo.* Right panels, in contrast, upon irradiation tumors with reduced cyclin D1 levels showed decreased weight, as compared to control tumors (expressing normal levels of cyclin D1). Shown are the numbers of mice analyzed per group (N) and the *p*-values. This experiment is a repetition of analysis shown in Fig. 4b in the main text using two additional independent anti-cyclin D1 shRNA sequences (panel **f** shows results obtained with the second shRNA sequence (shCyclin D1-B), panel **g** results with the third one (shCyclin D1-C).

Supplementary Figure 26

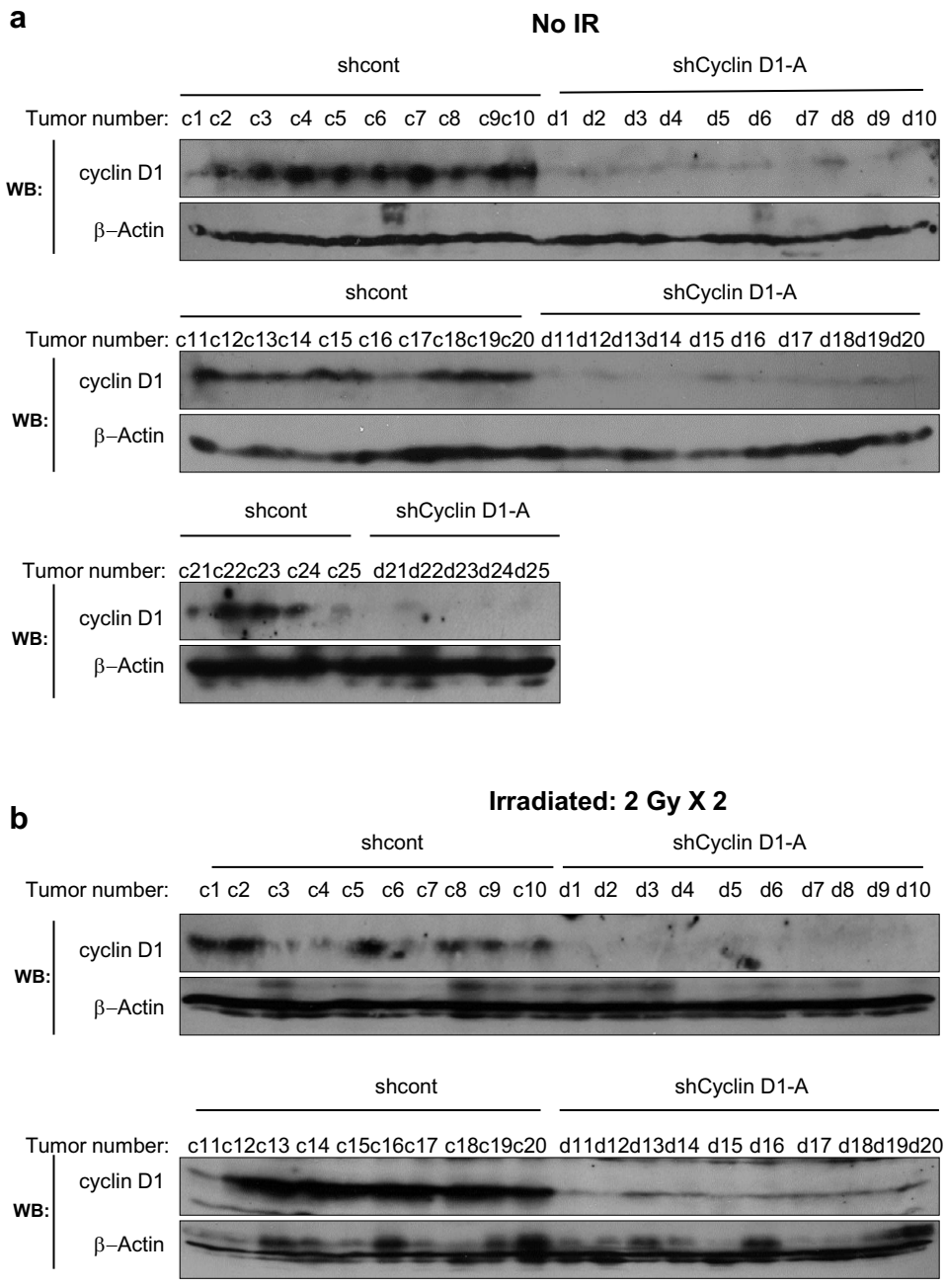

Supplementary Figure 26 (Continued)

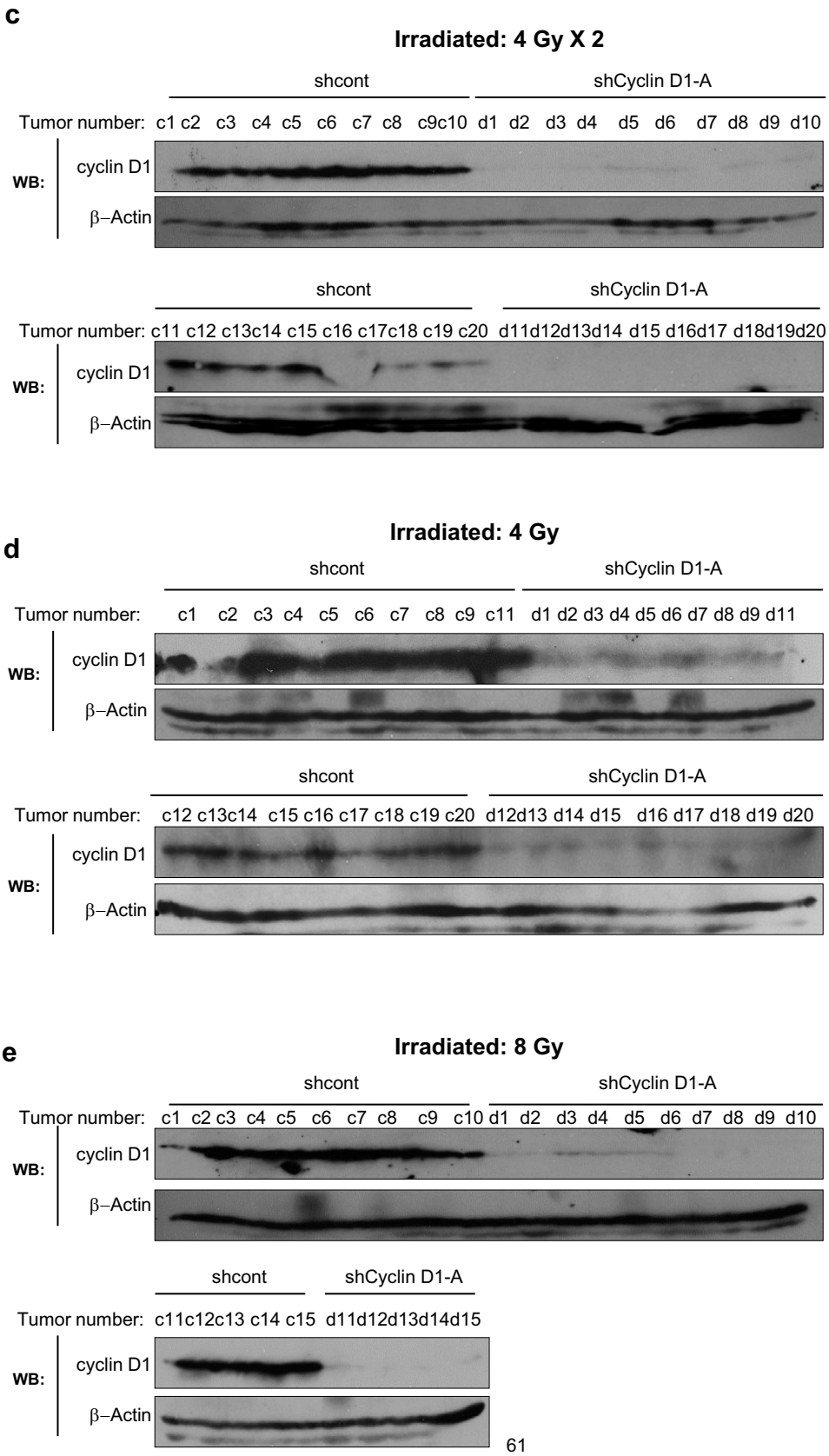

Supplementary Figure 26 l Cyclin D1 protein levels in lung cancer H2009 tumors

a, Cyclin D1 levels in control H2009 tumors (c1-c25) expressing control shRNA (shcont), and in cyclin D1 knock-down tumors (d1-d25) expressing anti-cyclin D1 shRNA (shCyclin D1-A). Tumors were harvested from a group of mice that was not exposed to radiation (No IR) (see Fig. 4a, b, left panels in the main text). β-Actin was used a loading control. WB, western blotting.

b, Cyclin D1 levels in control H2009 tumors (c1-c20) expressing control shRNA (shcont), and in cyclin D1 knock-down tumors (d1-d20) expressing anti-cyclin D1 shRNA (shCyclin D1-A). Tumors were harvested on day 17 from a group of mice that was treated with 2 Gy of radiation, twice (2 Gy X 2) (see Fig. 4a, b, middle panels in the main text).

c, Cyclin D1 levels in control H2009 tumors (c1-c20) expressing control shRNA (shcont), and in cyclin D1 knock-down tumors (d1-d20) expressing anti-cyclin D1 shRNA (shCyclin D1-A). Tumors were harvested on day 17 from a group of mice that has been treated with 4 Gy of radiation, twice (4 Gy X 2) (see Fig. 4a, b, right panels in the main text).

d, Cyclin D1 levels in control H2009 tumors (c1-c20) expressing control shRNA (shcont), and in cyclin D1 knock-down tumors (d1-d20) expressing anti-cyclin D1 shRNA (shCyclin D1-A). Tumors were harvested on day 15 from a group of mice that was treated once with 4 Gy of radiation (4 Gy) (see Supplementary Fig. 22d**,** e middle panels).

e, Cyclin D1 levels in control H2009 tumors (c1-c15) expressing control shRNA (shcont), and cyclin D1 knock-down tumors (d1-d15) expressing anti-cyclin D1 shRNA (shCyclin D1-A). Tumors were harvested on day 15 from a group of mice that was treated once with 8 Gy of radiation (8 Gy) (see Supplementary Fig. 22d, e, right panels).

Supplementary Figure 27

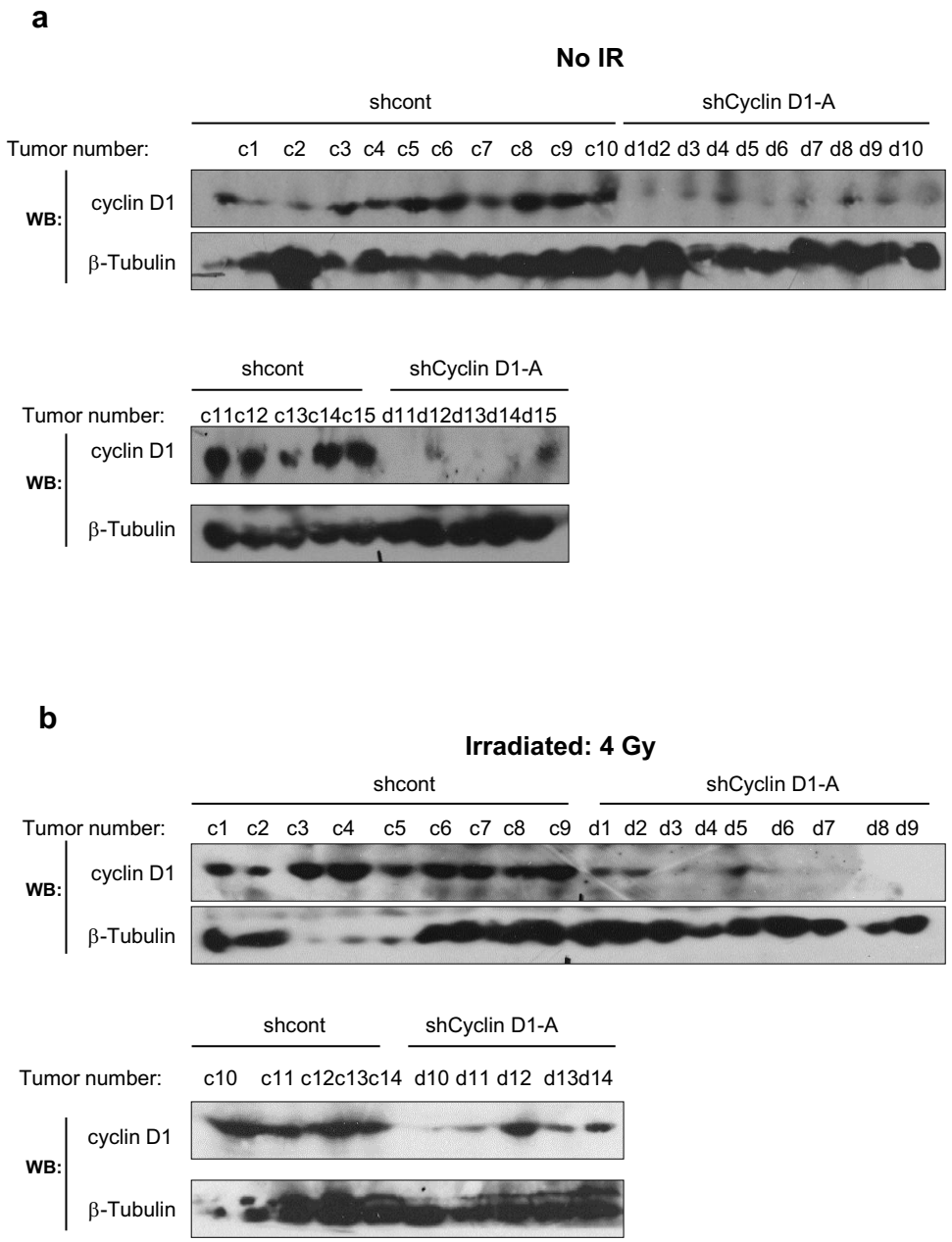

Supplementary Figure 27 I Cyclin D1 protein levels in cervical carcinoma HeLa tumors

a, Cyclin D1 levels in control HeLa tumors (c1-c15) expressing control shRNA (shcont), and in cyclin D1 knock-down tumors (d1-d15) expressing anti-cyclin D1 shRNA (shCyclin D1-A). Tumors were harvested after 5 weeks from a group of mice that was not exposed to radiation (No IR) (see Supplementary Fig. 24d, e, left panels). β-Tubulin was used as a loading control. WB, western blotting.

b, Cyclin D1 levels in control HeLa tumors (c1-c14) expressing control shRNA (shcont), and in cyclin D1 knock-down tumors (d1-d14) expressing anti-cyclin D1 shRNA (shCyclin D1-A). Tumors were harvested after 5 weeks from a group of mice that was treated with 4 Gy of radiation (4 Gy) (see Supplementary Fig. 24d, e, right panels).

Supplementary methods and discussion

Sample preparation for mass spectrometry

A pooled sample that contained at least 900 ng of tagged cyclin D1 (or the corresponding amount of material prepared from “mock” purified samples) was TCA precipitated, and digested for 5-6 hrs at 37°C in a reaction mixture consisting of 50 mM ammonium bicarbonate, pH 8, 10% Acetonitrile (ACN) and 400 ng modified trypsin (Promega). The digestion mixture was quenched with 50% ACN, 5% formic acid (FA), and lyophilized to dryness. Dried peptides were then desalted using Empore C18 solid phase extraction disks (3M) as previously described [6]. Samples were resuspended in 5% ACN, 5% FA prior to analysis by liquid chromatography and tandem mass spectrometry (see below).

Liquid chromatography and tandem mass spectrometry (LC-MS/MS) LC-MS/MS analyses were performed on an LTQ mass spectrometer (Thermo Fisher) equipped with an Agilent 1100 high-performance liquid chromatography (HPLC) pump (Agilent Technologies) and a Famos autosampler (LC Packings). Peptide mixtures were introduced into the mass spectrometer via a fused silica microcapillary column (internal diameter = 125 um), ending in an in-house pulled needle tip (internal diameter ~ 5 um). Columns were packed to a length of 18 cm with a C18 reversed-phase resin (Magic C18AQ, Michrom Bioresources). Sample solution containing approximately 300 ng of tagged cyclin D1 (or the corresponding amount from “mock” purified samples) were loaded onto the column. Peptides were eluted into the electrospray ionization source of the mass spectrometer via a linear gradient of 4 to 35% buffer B [2.5% water and 0.1% formic acid in acetonitrile (v/v)] in buffer A [2.5% acetonitrile and 0.1% formic acid in

water (v/v)] over 40 minutes followed by a high organic wash (100% buffer B, 6 minutes) and a column reconditioning wash (100% buffer A, at least 20 minutes). The LTQ was operated in a data-dependent mode: up to ten MS/MS spectra were acquired per data-dependent cycle from each master spectrum (mass range = 380 –1800 m/z).

We realize that, as with any large-scale analysis of complex protein mixtures, it is possible that the analysis platform used in this study may have missed low-abundance or weakly-associated cyclin D1 interactors. We tried to address this potential limitation by collecting multiple technical replicate analyses of each sample, as described above. Previously, we found this to be a highly efficient means to improve the depth of coverage of rare species in a complex mixture, improving sensitivity by 33% to 200%, depending on the number of replicates collected, and the complexity of the sample[7, 8] Other alternative strategies would include the use of high-resolution mass spectrometers and longer chromatographic gradients. While both of these approaches would likely improve identification rates, these improvements are more modest than those seen from technical replicates[9,10]. In addition to compensating for lower-resolution mass spectra and shorter gradients, replicate analyses used in this study provided a basis for statistically distinguishing true interactors from a non-specific background that can be typical of double affinity purifications, as described below.

While in our experiments we analyzed only exponentially growing cancer cells, it will be of interest in the future to use quantitative mass spectrometry to compare the sets of cyclin D1-binding proteins between non-irradiated versus irradiated cells. This approach may reveal novel interactors which become detectable upon radiation treatment.

Data processing All MS/MS spectra were searched with both SEQUEST[11] and Mascot[12] search engines against a composite sequence database consisting of the minimally-redundant human sequences stored at the International Protein Index[13] (version 3.37), common contaminant protein sequences, and reversed (decoy) versions of these sequences[14]. For both SEQUEST and Mascot, searches were performed using monoisotopic precursor and fragment masses, precursor mass tolerance of ±2 Da, static carbamidometylation of cysteines (+57.021464), variable oxidation of methionines (+15.99491), and up to two missed cleavage sites per peptide. SEQUEST searches were performed using partial tryptic enzyme specificity and default fragment ion mass tolerance. Mascot searches were performed using complete tryptic enzyme specificity and fragment mass tolerance of ±0.88 Da. In-house software was then used to design filtering criteria delivering precision rates (true positives divided by total positives) of 90%, 95%, and 99% guided by matches to decoy proteins as previously described[14]. Peptides selected by criteria delivering less than 99% precision were included only if they were assigned to at least one other peptide selected by criteria delivering 99% precision. All proteins deemed to be high confidence interactors with cyclin D1 were identified by at least two unique peptides (see below).

Selection of high-confidence cyclin D1 interacting proteins In order to identify high-confidence cyclin D1 interacting proteins, we compared the number of raw spectral counts observed for cyclin D1 pull-downs within each cell line with the number of raw spectral counts observed for all mock pull-downs, across all cell lines. For example, 78

MS/MS spectra mapping to the tumor Ki67 were acquired across three MCF-7 cyclin D1 pull-down analyses (EXP). These three replicates were compared to 22 mock replicates from all five cell lines (CTRL), in which 15 MS/MS spectra mapped to this protein. These two sets (EXP and CTRL) were used to calculate the probability that the two sets are drawn the same population (Mann-Whitney U-test, implemented in Matlab) ($p \leq 0.002$ in this case). The two sets were also used to calculate the fraction of the total spectra considered that are attributable to just the cyclin D1 analyses: (EXP/(EXP+CTRL) ("fractional difference", 0.975 in this case). These measurements were also made in reverse, i.e., comparing the two MS/MS spectra identified across six MCF-7 mock pull down analyses to the 435 MS/MS spectra assigned to this protein across 19 cyclin D1 pull downs. The *p*-values and fractions were 0.004 and 0.005, respectively, for this example. For the reasons previously described[7], spectral counts were not normalized, since normalization would introduce unacceptable biases.

We selected high-confidence cyclin D1-interacting proteins from each cell line that fulfilled all of the following criteria: (1) p value ≤ 0.005 (determined as described above); (2) at least 2 independent peptides in a given cell line; (3) the number of spectra ≥ (number of sequencing rounds x 1.3) -- for instance, 3 sequencing rounds of cyclin D1-containing samples were performed for colon cancer HT-29 cells, therefore the required number of spectra was ≥ 3.9); (4) the fractional difference (as defined above) ≥ 0.93. In total, 133 unique proteins from all cell lines fulfilled these criteria as being high-confidence cyclin D1-interacting proteins (Supplementary Table 3). In a similar fashion, 22 proteins included in Supplementary Table 3 that were selected when the same criteria were applied to the mock pull-downs. Identifying "mock-specific"

proteins is entirely expected from this sort of comparative analysis. These bead-interacting proteins may be out-competed by proteins that bind to the cyclin-D1 bait both on the beads, and in the mass spectrometer. Since most of the bead capacity and mass spectrometry analysis time is occupied by specific interactors in the cyclin D1 pull-down experiments, many proteins that appear in the mock condition would not be expected to be seen.

Fifteen randomly chosen high-confidence cyclin D1 interacting proteins from Granta 519 cells were selected for verification by western blotting. We were able to confirm physical interaction with cyclin D1 in all 15 cases (Supplementary Fig. 1e), thereby validating our selection criteria for high confidence interactors.

Please note, that in Figure 1a (depicting all high confidence interactors) we wanted to highlight true “cancer-specific interactors”. Therefore, if a given protein was found as a high confidence interactor in one cell line (for example in HT-29 cells), but it was also observed with one peptide (non-high confidence interactor) in another cell line (for example MCF7 cells), the protein was depicted as found in two cell lines, and a line was drawn between this protein and both HT-29 and MCF7 symbols in Figure 1a.

The proteomic data is shown in the form of five Supplementary Tables. **Table 1** lists all peptides identified in five human cancer cell lines. **Table 2** lists all proteins identified in five human cancer cell lines. **Table 3** lists high-confidence interactors identified in five human cancer cell lines. **Table 4** provides summary of proteins identified in each human cancer cell line. **Table 5** provides summary of proteomic data for proteins mentioned by name in the text.

Supplementary method reference

1. Toogood, P. L. et al. Discovery of a potent and selective inhibitor of cyclin-dependent kinase 4/6. J Med Chem 48, 2388-406 (2005).
2. Kozar, K. et al. Mouse development and cell proliferation in the absence of D-cyclins. Cell 118, 477-91 (2004).
3. Hinds, P. W., Dowdy, S. F., Eaton, E. N., Arnold, A. & Weinberg, R. A. Function of a human cyclin gene as an oncogene. Proc Natl Acad Sci U S A 91, 709-13 (1994).
4. Agami, R. & Bernards, R. Distinct initiation and maintenance mechanisms cooperate to induce G1 cell cycle arrest in response to DNA damage. Cell 102, 55-66 (2000).
5. Thorslund, T. & West, S. C. BRCA2: a universal recombinase regulator. Oncogene 26, 7720-30 (2007).
6. Rappsilber, J., Ishihama, Y. & Mann, M. Stop and go extraction tips for matrix-assisted laser desorption/ionization, nanoelectrospray, and LC/MS sample pretreatment in proteomics. Anal Chem 75, 663-70 (2003).
7. Bienvenu, F. et al. Transcriptional role of cyclin D1 in development revealed by a genetic-proteomic screen. Nature 463, 374-8 (2010).
8. Elias, J. E., Haas, W., Faherty, B. K. & Gygi, S. P. Comparative evaluation of mass spectrometry platforms used in large-scale proteomics investigations. Nat Methods 2, 667-75 (2005).
9. Haas, W. et al. Optimization and use of peptide mass measurement accuracy in shotgun proteomics. Mol Cell Proteomics 5, 1326-37 (2006).

10. Xu, P., Duong, D. M. & Peng, J. Systematical optimization of reverse-phase chromatography for shotgun proteomics. J Proteome Res 8, 3944-50 (2009).
11. Eng, J. K., McCormack, A. L. & Yates, J. R. An approach to correlate tandem mass spectral data of peptides with amino acid sequences in a protein database. J Am Soc Mass Spectrom 5, 976-989 (1994).
12. Perkins, D. N., Pappin, D. J., Creasy, D. M. & Cottrell, J. S. Probability-based protein identification by searching sequence databases using mass spectrometry data. Electrophoresis 20, 3551-67 (1999).
13. Kersey, P. J. et al. The International Protein Index: an integrated database for proteomics experiments. Proteomics 4, 1985-8 (2004).
14. Elias, J. E. & Gygi, S. P. Target-decoy search strategy for increased confidence in large-scale protein identifications by mass spectrometry. Nat Methods 4, 207-14 (2007).

A function for cyclin D1 in DNA repair uncovered by interactome analyses in human cancers

Siwanon Jirawatnotai[1,6], Yiduo Hu[1]*, Wojciech Michowski[1]*, Joshua E. Elias[2,9], Lisa Becks[1,7], Frederic Bienvenu[1,10], Agnieszka Zagozdzon[1], Tapasree Goswami[2], Yaoyu Wang[3], Alan B. Clark[4], Thomas A. Kunkel[4], Tanja van Harn[1], Bing Xia[5], Mick Correll[3], John Quackenbush[3,8], David M. Livingston[1], Steven P. Gygi[2] & Piotr Sicinski[1]

[1]Department of Cancer Biology, Dana-Farber Cancer Institute, and Department of Genetics, Harvard Medical School, Boston, Massachusetts 02115, USA
[2]Department of Cell Biology, Harvard Medical School, Boston, Massachusetts 02115, USA
[3]Center for Cancer Computational Biology, Dana-Farber Cancer Institute, Boston, Massachusetts 02115, USA
[4] Laboratory of Molecular Genetics and Laboratory of Structural Biology, National Institute of Environmental Health Sciences, National Institutes of Health, Department of Health and Human Services, Research Triangle Park, North Carolina 27709, USA
[5]Department of Radiation Oncology, The Cancer Institute of New Jersey, University of Medicine and Dentistry of New Jersey, Robert Wood Johnson Medical School, New Brunswick, New Jersey 08903, USA
[6]Institute of Molecular Biosciences, Mahidol University, Salaya, Nakhon Prathom, 73170 Thailand
[7]Department of Pharmacology, Massachusetts College of Pharmacy and Health Sciences, Boston, MA 02115, USA
[8]Department of Biostatistics and Computational Biology, Dana-Farber Cancer Institute, and Harvard School of Public Health, Boston, Massachusetts 02115, USA.
[9]Present address: Department of Chemical and Systems Biology, Stanford University School of Medicine, Stanford, California 94305, USA
[10]Present address: Institute of Functional Genomics, UMR 5203 CNRS – U 661 INSERM – Universite de Montpellier, 34094 Montpellier, France

*These authors contributed equally to this work

Correspondence and requests for materials should be addressed to P.S. (peter_sicinski@dfci.harvard.edu).

Cyclin D1 is a component of the core cell cycle machinery[1]. Abnormally high levels of cyclin D1 are detected in many human cancer types, including the majority of breast cancers[2]. To elucidate the molecular functions of cyclin D1 in human cancers, here we performed a proteomic screen for cyclin D1 protein partners in several types of human tumors. Analyses of cyclin D1 interactors revealed a network of DNA repair proteins, including RAD51, a recombinase that drives the homologous recombination process[3]. We found that cyclin D1 directly binds RAD51, and that cyclin D1-RAD51 interaction is induced by ionizing radiation. Like RAD51, cyclin D1 is recruited to DNA damage sites following radiation in a BRCA2-dependent fashion. Reduction of cyclin D1 levels in human cancer cells impaired recruitment of RAD51 to damaged DNA, impeded the homologous recombination-mediated DNA repair, and increased sensitivity of cells to radiation *in vitro* and *in vivo*, in solid tumors. This effect was seen in cancer cells lacking the retinoblastoma protein, which do not require D-cyclins for proliferation[4, 5], and it was found to be independent of cyclin D1-CDK kinase activity. These findings reveal an unexpected function of a core cell cycle protein in DNA repair and suggest that targeting cyclin D1 may be beneficial also in retinoblastoma-negative cancers which are currently thought to be oblivious to cyclin D1 inhibition.

In order to elucidate the molecular functions of cyclin D1 in human cancer cells, we set to identify cyclin D1-interacting proteins in four types of human tumors: mantle cell lymphoma (Granta 519 cells), breast cancer (MCF7 and ZR-75-1), squamous cell carcinoma (UMSCC-2), and colorectal cancer (HT-29). These cell lines overexpress cyclin D1 due to amplification or rearrangements within the *cyclin D1* gene, or mutations within the cyclin D1 degradation machinery[6-9]. Cyclin D1-containing complexes were purified from these cell lines using double immunoaffinity purification[10] (Supplementary Fig. 1a-d), and the identity of cyclin D1-interactors was determined by repeated rounds of liquid chromatography and high-throughput mass spectrometry (LC-MS/MS). A total of 132 unique proteins from 5 cancer cell lines were identified with high confidence, including several novel interactors (Fig. 1a, Supplementary Fig. 1e and Supplementary Tables 1-5). Some of these novel interactors were detected only in one particular tumor type; for example interaction of cyclin D1 with transcription factors Ikaros (IKZF1) and Aiolos (IKZF3) was seen only in mantle cell lymphomas (Fig. 1a). These cancer type-specific interactions of cyclin D1 correlated with the differential expression pattern of the interactors in particular types of tumors (Supplementary Fig. 2).

To gain insights into the molecular roles of cyclin D1 in human cancers, we constructed a biological process/molecular function enrichment heatmap of all cyclin D1 interactors we identified (Fig. 1b, Supplementary Table 6), and searched for common functions across all four tumor types. As anticipated, we detected significant enrichment for proteins involved in cell cycle control (Fig. 1b). Unexpectedly, we observed the DNA repair category amongst the most enriched functions of cyclin D1-

interactors (Fig. 1b, Supplementary Table 6), which included RAD51, BRCA2, FANCD2, FANCI, MSH6, and PCNA (Fig. 1c). We constructed a protein interaction network of all cyclin D1 interactors encountered across all human cancer types, using published databases of physical and functional interactions (Supplementary Fig. 3). Analyses of cyclin D1 network revealed a cluster of DNA repair proteins centered on RAD51, a key DNA recombinase mediating DNA repair via homologous recombination (HR)[3] (Supplementary Fig. 3). These observations raised a possibility that cyclin D1 may play a role in DNA damage repair in human cancer cells.

To investigate this possibility, we tested the requirement for cyclin D1 function following DNA damage. We depleted cyclin D1 by short hairpin RNA (shRNA) in cervical carcinoma HeLa and lung cancer H2009 cells, induced DNA damage by subjecting cells to ionizing radiation (IR), and gauged the ability of cells to overcome DNA damage by performing colony survival assays. We utilized these two retinoblastoma protein (pRB)-negative cell lines to rule out cell cycle effects of cyclin D1 knock-down, as pRB-negative cancer cells do not require D-cyclins for proliferation[4, 5]. Indeed, we confirmed that knock-down of cyclin D1 had no impact on proliferation of these cells (Supplementary Fig. 4). Strikingly, we found that depletion of cyclin D1 significantly increased the sensitivity of cancer cells to radiation (Fig. 2a, and Supplementary Fig. 5a, c). Reduction of cyclin D1 levels also sensitized cancer cells to DNA-damaging drugs such as camptothecin and etoposide (Fig. 2b). Moreover, fibroblasts lacking D-cyclins (*D1*$^{-/-}$*D2*$^{-/-}$*D3*$^{-/-}$ MEFs)[11] showed increased sensitivity to ionizing radiation, despite normal cell cycle progression of these cells (Supplementary

Fig. 5d, e). Importantly, re-expression of cyclin D1 in cyclin D-null fibroblasts restored radiation sensitivity (Supplementary Fig. 6).

The best-documented function of cyclin D1 is its ability to activate cyclin-dependent kinases CDK4 and CDK6[1]. To test whether the function of cyclin D1 in DNA damage repair depends on cyclin D1-CDK4/6 enzymatic activity, we treated HeLa cells with PD 0332991, a specific and potent inhibitor of cyclin D-CDK4/6 kinase[12]. We found that this treatment had no effect on sensitivity of cancer cells to IR, even at the highest concentration of the inhibitor tested (3 μM) (Supplementary Fig. 5b). Moreover, expression of cyclin D1 K112E point mutant which is unable to activate the CDKs[13,14], restored radiation susceptibility in cyclin D-null MEFs (Supplementary Fig. 6). Collectively, these observations suggested that cyclin D1 might play a CDK4/6 kinase-independent function in DNA repair.

To directly gauge the efficiency of DNA repair upon cyclin D1 depletion, we performed the so-called "comet assay"[15], which detects unrepaired DNA. We transfected anti-cyclin D1 siRNAs into pRB-negative HeLa cancer cells, verified that there was no effect of cyclin D1-depletion on proliferation of these cells (Supplementary Fig. 4a), and subjected cells to IR. We found that this insult induced comparable levels of DNA damage in control cells and in cells depleted of cyclin D1 (see middle panels of Fig. 2d and Supplementary Fig. 7a). However, at 16 hours post-radiation, more unrepaired DNA persisted in cells depleted of cyclin D1, as compared to control cells (right panels, Fig. 2d and Supplementary Fig. 7a, b).

We verified that this impaired rate of DNA repair in cells with reduced cyclin D1 levels was not a result of grossly compromised DNA damage-induced signaling. Thus, HeLa cells depleted of cyclin D1 displayed comparable phosphorylation of ATM, CHK1, CHK2 and CDC25A, and underwent G2/M arrest upon radiation with normal kinetics (Supplementary Fig. 8a, b, and data not shown), indicating that DNA-damage checkpoints are functional in these pRB-negative cancer cells upon cyclin D1 knock-down. Collectively, these findings suggested that cyclin D1 may play a direct role in DNA repair.

Since among cyclin D1 interactors we observed a network of DNA repair proteins including RAD51, a key DNA recombinase that drives the HR process[3,16] (Supplementary Fig. 3), we investigated a possible functional connection between cyclin D1 and HR-dependent DNA repair. Using a well-described HR repair reporter, the DR-eGFP system[17], we found that down-regulation of cyclin D1 levels by three independent small interfering RNAs (siRNAs) in HeLa and H2009 cancer cells significantly reduced the HR rate (Fig. 2e and Supplementary Fig. 9a, e, f). As expected, re-expression of siRNA-resistant cyclin D1 rescued this effect (Fig. 2f and Supplementary Fig. 9c). Importantly, none of anti-cyclin D1 siRNAs had any effect on cell cycle progression of these pRB-negative cancer cells, as expected[4, 5] (Supplementary Fig. 9b, d, g). These results suggested that cyclin D1 may be required for an efficient HR DNA repair process. Consistent with this thinking, we found that knock-down of cyclin D1 sensitized cancer cells to treatment with poly (ADP-ribose) polymerase (PARP)-inhibitors (Fig. 2c), in concordance with the reports that deficiency in HR renders cells hypersensitive to these agents[18].

To investigate in more detail a possible function of cyclin D1 in HR, we focused on cyclin D1 interaction with RAD51, detected in our proteomic screen. We established, using purified recombinant proteins, that cyclin D1 directly binds to RAD51, and mapped the domains of the two proteins which mediate this interaction (Fig. 3a-c). We found that the N-terminus of cyclin D1 and the C-terminus of RAD51 are required for cyclin D1-RAD51 binding (Fig. 3c and Supplementary Fig. 10). Expression of cyclin D1 mutant which is deficient in RAD51 binding failed to restore normal HR rate in cyclin D1-depleted cells (Fig. 2g), underscoring the significance of the interaction between the two proteins. We also verified physical binding of the endogenous cyclin D1 and RAD51 proteins, by immunoprecipitation – western blotting, in an extended panel of human cancer cell lines (Fig. 3d and Supplementary Fig. 11a). The interaction between cyclin D1 and RAD51 was strongly induced by radiation treatment over a period of 6 hrs, and it intensified with increased dose of radiation (Fig 3e, upper panel and Supplementary Fig. 11b, c). As previously reported, radiation resulted in a decrease of total levels of cyclin D1, without any major changes in RAD51 levels[19, 20] (Fig. 3e, lower panel and Supplementary Fig. 11c). The strong induction of cyclin D1-RAD51 interaction after radiation, in the face of reduced total cyclin D1 levels, indicates that an increased number of remaining cyclin D1 molecules is recruited to RAD51 complex to facilitate a repair process.

To investigate whether cyclin D1 is recruited to the sites of damaged DNA, where RAD51 localizes after radiation, we utilized a system in which a unique I-SceI recognition site has been stably integrated into the genome of HeLa cancer cells[17]. Transfection of a plasmid encoding I-SceI endonuclease induces a double-stranded

DNA break at a defined site within the genomic DNA. Using this system, one can monitor recruitment of DNA damage repair proteins to the site of DNA damage, using targeted chromatin immunoprecipitation (ChIP), followed by PCR with primers adjacent to DNA damage site[21-23]. As expected, we observed recruitment of RAD51 to the DNA damage site (Fig. 3h, Supplementary 12a, left panels), but not to several control DNA regions within the genome (Supplementary Fig. 12b). Importantly, targeted anti-cyclin D1 ChIP revealed that cyclin D1 was also recruited to the site of DNA damage following induction of a double-stranded break (Fig. 3i, left panel). As was the case with RAD51, the recruitment of cyclin D1 to DNA was specific to the site of the double-stranded break, since we did not detect recruitment of cyclin D1 to several other control regions in the genome (Supplementary Fig. 12d). Moreover, recruitment of cyclin D1 to the double-stranded DNA break disappeared once cyclin D1 had been knocked-down by an anti-cyclin D1 siRNA (Fig. 3i, right panel). Importantly, ChIP of cyclin D1 followed by re-ChIP with anti-RAD51 antibody revealed that cyclin D1 and RAD51 co-localize on the sites of double-stranded DNA breaks (Fig. 3j). Cyclin D1 recruitment to the damaged DNA was also detected by co-immunofluorescent staining with γ-H2AX at the stripes of damaged DNA induced by a laser beam (Supplementary Fig. 13).

To investigate whether cyclin D1 facilitates HR process by regulating RAD51, we studied the recruitment of RAD51 to damaged DNA, a step that is required for RAD51 to perform its DNA recombinase function[24]. We found that knock-down of cyclin D1 using three independent siRNAs strongly reduced the recruitment of RAD51 to I-SceI-induced DNA breaks (Fig. 3h and Supplementary Fig. 12a, right panels), to laser-induced DNA-damage stripes (Supplementary Fig. 14), and to radiation-induced DNA damage foci

(Fig. 3k and Supplementary Figs 15, 16). We verified that the overall levels of RAD51 and of several other DNA damage-response proteins were not affected by cyclin D1 knock-down (Supplementary Fig. 8c). Collectively, these findings indicate that cyclin D1 helps to recruit RAD51 to DNA damage sites through a direct physical interaction between cyclin D1 and RAD51.

We next asked how cyclin D1 is recruited to sites of DNA damage. Among cyclin D1 interactors we noted the presence of BRCA2 (Fig. 1a, c, and Supplementary Tables 1-5), an essential HR protein which is recruited to DNA damage sites prior to RAD51 loading[24]. We established using purified recombinant cyclin D1 protein and BRCA2 protein fragments[25] that cyclin D1 directly interacts with BRCA2 (Fig. 3f), and we verified physical interaction of the endogenous proteins by immunoprecipitation-western blotting (Fig. 3g). Importantly, we found that knock-down of BRCA2 abolished recruitment of cyclin D1 to DNA damage sites (Fig. 3l, left panel). On the other hand, depletion of cyclin D1 had no effect on BRCA2 recruitment (Supplementary Fig. 17a), consistent with the notion that BRCA2 acts upstream of cyclin D1. Likewise, depletion of cyclin D1 had no impact on DNA end resection, a rate-limiting step prior to BRCA2 loading, as evidenced by unperturbed generation of single-stranded DNA (Supplementary Fig. 18a-d) and normal loading of a single-stranded DNA binding protein RPA34 following DNA damage (Supplementary Fig. 18e, f). In contrast, depletion of cyclin D1 inhibited downstream events, namely recruitment of RAD51, and it led to decreased co-localization of RAD51 and BRCA2 on DNA damage sites (Fig. 3m and Supplementary Fig. 19).

Collectively, these results are consistent with the model that cyclin D1 is recruited to DNA damage sites through BRCA2; cyclin D1 then helps to recruit RAD51 through a direct cyclin D1-RAD51 interaction. Depletion of cyclin D1 reduces RAD51 recruitment and reduces RAD51-BRCA2 co-localization on DNA damage sites, leading to impaired HR rate. While expression of wild-type cyclin D1 in cells depleted of cyclin D1 restored normal HR rate, expression of cyclin D1 mutant deficient in RAD51 binding was ineffective in this function. Our findings are in agreement with a recent report that forced targeting of cyclin D1 to DNA resulted in increased co-recruitment of RAD51[26].

Importantly, we verified that cyclin D1 is not required for recruitment of other DNA damage proteins detected as cyclin D1-interacting proteins in our screen. Specifically, we established that recruitment of FANCD2, FANCI, PCNA and MSH6, as well as BRCA1 and MRE11 to DNA damage sites was unperturbed in cyclin D1-depleted cells (Supplementary Figs 17, 20b and 21).

Since among cyclin D1-interacting proteins we detected MSH6, which plays a role in DNA mismatch repair[27], we tested the impact of cyclin D1 knockdown on this DNA repair process. We observed that cyclin D1-depleted cells were fully proficient in mismatch repair (Supplementary Fig. 20a), consistent with the observed normal recruitment of MSH6 to DNA damage sites (Supplementary Fig. 20b). These findings underscore a specific requirement for cyclin D1 in HR, but not in DNA mismatch repair. The functional significance of the interaction between cyclin D1, MSH6, and several other proteins identified by us in cyclin D1-containing complexes (Fig. 1a, c) is unknown at present. It is likely that many of these proteins do not represent direct cyclin D1 interactors, but are components of multi-protein cyclin D1-containing complexes.

Cyclin D1 is required for proliferation of pRB-positive cancer cells, and it was reported that decrease of total cyclin D1 levels observed upon radiation contributes to cell cycle arrest of these cells[19]. Conversely, forced overexpression of cyclin D1 upon radiation in pRB-positive cells may overcome cell cycle checkpoints, and may lead to unscheduled DNA synthesis and apoptosis[20,28]. Our results reveal that after radiation the remaining, DNA-bound pool of cyclin D1 plays a positive role in DNA repair.

Our observations that cyclin D1 plays a role in DNA repair suggested that depletion of cyclin D1 could sensitize human cancers to radiation, by limiting DNA damage repair. To test this notion in an *in vivo* setting, we knocked down cyclin D1 in three pRB-negative cancer cell lines: HeLa, H2009 and in prostate cancer DU145 cells. Cells were then injected subcutaneously into nude mice, which resulted in formation of tumors. As expected, depletion of cyclin D1 did not affect proliferation of cancer cells *in vitro* (Supplementary Figs 4c, d and 22a-c), and had no impact on the rate of tumor growth *in vivo* (Fig. 4a, b, left panels, and Supplementary Fig. 23a). In clear contrast, upon irradiation, tumors with reduced cyclin D1 levels displayed significantly retarded growth as compared to control tumors, revealing increased sensitivity to ionizing radiation (Fig. 4a, b, middle and right panels, Supplementary Fig. 23b-e). We observed this effect with four different doses of radiation (Fig. 4a, b and Supplementary Fig. 22d, e), in all three cell lines (Supplementary Fig. 24 and data not shown), and using three independent anti-cyclin D1 shRNAs (Fig. 4a, b and Supplementary Fig. 25). Hence, while cyclin D1 is dispensable for proliferation of pRB-negative tumor cells, it plays an important role in DNA repair, which becomes evident once cells undergo DNA damage.

Cyclin D1 represents a major oncoprotein which is believed to drive proliferation of pRB-positive cancers[2]. The *cyclin D1* gene corresponds to the second most frequently amplified region within the human cancer genome[29]. Our proteomic screen revealed unexpectedly that in addition to its well-established role in cell proliferation, cyclin D1 plays an important function in human cancer cells in DNA repair via the HR. According to the current notion, cyclin D1-CDK4/6 is needed in human cancer cells to functionally inactivate the retinoblastoma protein[1]. Consequently, it is assumed that targeting cyclin D1 function has a therapeutic value exclusively in cancers which retain the expression of the wild-type retinoblastoma protein[12]. Indeed, there is an overwhelming body of evidence that cancer cells which lose pRB expression no longer require cyclin D1 for cell cycle progression[4, 5]. In contrast to this thinking, our results indicate that cyclin D1 plays a function in DNA repair which is independent of pRB, and this function becomes rate limiting in pRB-negative tumor cells once these cells accumulate damaged DNA. Our results suggest that targeting cyclin D1 in combination with radiation treatment may have potential therapeutic value also in a large pool of pRB-negative cancers.

METHODS SUMMARY

Nuclear extracts were prepared from cancer cell lines, and cyclin D1-containing complexes were purified using HA-FLAG double-affinity immunopurifications as described[10]. Mass spectrometry analyses were performed using at least 300ng of cyclin D1 per run, with at least 3 repeats per cell line. Comet assays were performed

according to manufacturer protocol (Trevigen, Inc.), with 1 Gy of ionizing radiation. For HR assay in HeLa and H2009 cells, DR-GFP system was used[17]. To knock-down cyclin D1, anti-cyclin D1 siRNAs (or control siRNAs) were transfected twice 24 hrs prior to induction of DNA damage. For analyses of DNA damage foci, cells were treated with IR (using Cs^{137}), 1 or 2 μM mitomycin C, or 25 μM O^6-Benzylguanine and 10 μM N-Methyl-N-nitrosoguanidine. UV-A laser was used to generate DNA damage stripes. RAD51 and cyclin D1 ChIP were performed using anti-RAD51 antibody (H-92), or anti-cyclin D1 antibody (H-295) from Santa Cruz Biotechnologies. For ChIP-re-ChIP, HA-tagged cyclin D1 was ChIP with anti-HA antibody (12CA5, Covance), eluted with HA peptide, and re-ChIP with anti-RAD51 antibody or with IgG for control. For *in vitro* binding assays, cDNAs were cloned into pGEX-5x-3 (GE Healthcare). Proteins were expressed in *E.coli* BL21, and purified using GSH-Sepharose. When required, GST was eliminated from purified protein by Factor Xa. Cancer cells used for *in vivo* tumor study were transduced with lentiviruses expressing anti-cyclin D1 or control shRNAs. Ten million tumor cells were injected subcutaneously into 6-week-old athymic *nu/nu* female mice. Tumors were target-irradiated using Cs^{137} as a source. Tumor size was assessed on indicated days. Tumor weight was determined at the end of experiments. Statistical significance of the differences was evaluated using paired two-tailed Student's *t*-test.

References

1. Sherr, C. J. & Roberts, J. M. Living with or without cyclins and cyclin-dependent kinases. Genes Dev 18, 2699-711 (2004).
2. Deshpande, A., Sicinski, P. & Hinds, P. W. Cyclins and cdks in development and cancer: a perspective. Oncogene 24, 2909-15 (2005).
3. Baumann, P. & West, S. C. Role of the human RAD51 protein in homologous recombination and double-stranded-break repair. Trends Biochem Sci 23, 247-51 (1998).
4. Bates, S. et al. Absence of cyclin D/cdk complexes in cells lacking functional retinoblastoma protein. Oncogene 9, 1633-40 (1994).
5. Lukas, J. et al. Retinoblastoma-protein-dependent cell-cycle inhibition by the tumour suppressor p16. Nature 375, 503-6 (1995).
6. Ek, S., Ortega, E. & Borrebaeck, C. A. Transcriptional profiling and assessment of cell lines as in vitro models for mantle cell lymphoma. Leuk Res 29, 205-13 (2005).
7. Lin, D. I. et al. Phosphorylation-Dependent Ubiquitination of Cyclin D1 by the SCF EBX4-aB Crystallin Complex. Molecular Cell 24, 355-366 (2006).
8. Hosokawa, Y. & Arnold, A. Mechanism of cyclin D1 (CCND1, PRAD1) overexpression in human cancer cells: analysis of allele-specific expression. Genes Chromosomes Cancer 22, 66-71 (1998).
9. Bartkova, J. et al. Abnormal patterns of D-type cyclin expression and G1 regulation in human head and neck cancer. Cancer Res 55, 949-56 (1995).

10. Nakatani, Y. & Ogryzko, V. Immunoaffinity purification of mammalian protein complexes. Methods Enzymol 370, 430-44 (2003).
11. Kozar, K. et al. Mouse development and cell proliferation in the absence of D-cyclins. Cell 118, 477-91 (2004).
12. Toogood, P. L. et al. Discovery of a potent and selective inhibitor of cyclin-dependent kinase 4/6. J Med Chem 48, 2388-406 (2005).
13. Hinds, P. W., Dowdy, S. F., Eaton, E. N., Arnold, A. & Weinberg, R. A. Function of a human cyclin gene as an oncogene. Proc Natl Acad Sci U S A 91, 709-13 (1994).
14. Landis, M. W., Pawlyk, B. S., Li, T., Sicinski, P. & Hinds, P. W. Cyclin D1-dependent kinase activity in murine development and mammary tumorigenesis. Cancer Cell 9, 13-22 (2006).
15. Ostling, O. & Johanson, K. J. Microelectrophoretic study of radiation-induced DNA damages in individual mammalian cells. Biochem Biophys Res Commun 123, 291-8 (1984).
16. Baumann, P., Benson, F. E. & West, S. C. Human Rad51 protein promotes ATP-dependent homologous pairing and strand transfer reactions in vitro. Cell 87, 757-66 (1996).
17. Pierce, A. J., Johnson, R. D., Thompson, L. H. & Jasin, M. XRCC3 promotes homology-directed repair of DNA damage in mammalian cells. Genes Dev 13, 2633-8 (1999).
18. Lord, C. J. & Ashworth, A. Targeted therapy for cancer using PARP inhibitors. Curr Opin Pharmacol 8, 363-9 (2008).

19. Agami, R. & Bernards, R. Distinct initiation and maintenance mechanisms cooperate to induce G1 cell cycle arrest in response to DNA damage. Cell 102, 55-66 (2000).

20. Pontano, L. L. et al. Genotoxic stress-induced cyclin D1 phosphorylation and proteolysis are required for genomic stability. Mol Cell Biol 28, 7245-58 (2008).

21. Sugawara, N., Wang, X. & Haber, J. E. In vivo roles of Rad52, Rad54, and Rad55 proteins in Rad51-mediated recombination. Mol Cell 12, 209-19 (2003).

22. Wolner, B., van Komen, S., Sung, P. & Peterson, C. L. Recruitment of the recombinational repair machinery to a DNA double-strand break in yeast. Mol Cell 12, 221-32 (2003).

23. Rodrigue, A. et al. Interplay between human DNA repair proteins at a unique double-strand break in vivo. Embo J 25, 222-31 (2006).

24. West, S. C. Molecular views of recombination proteins and their control. Nat Rev Mol Cell Biol 4, 435-45 (2003).

25. Lee, M., Daniels, M. J. & Venkitaraman, A. R. Phosphorylation of BRCA2 by the Polo-like kinase Plk1 is regulated by DNA damage and mitotic progression. Oncogene 23, 865-72 (2004).

26. Li, Z. et al. Alternative cyclin D1 splice forms differentially regulate the DNA damage response. Cancer Res 70, 8802-11 (2010).

27. Kunkel, T. A. & Erie, D. A. DNA mismatch repair. Annu Rev Biochem 74, 681-710 (2005).

28. Coco Martin, J. M., Balkenende, A., Verschoor, T., Lallemand, F. & Michalides, R. Cyclin D1 overexpression enhances radiation-induced apoptosis and radiosensitivity in a breast tumor cell line. Cancer Res 59, 1134-40 (1999).
29. Beroukhim, R. et al. The landscape of somatic copy-number alteration across human cancers. Nature 463, 899-905.

Acknowledgements

We thank the members of the Sicinski lab for help and advice, N. Li for help with initial experiments, S Panyim and Y. Geng for discussions and reading the manuscript, P. Nakatani for pOZ-F-HA construct, M. Jasin for DR-eGFP system, D. Bulavin and E. Apella for anti-S75/S123 CDC25A antibodies, A. Smogorzewska for anti-FANCI antibody, A. Venkitaraman and M. Lee for GST-BRCA2 fragments, E. Sicinska for help with designing tumor experiment, and DFCI Confocal and Light Microscopy Core Facility for assisting with confocal microscopy images. This work was supported by R01 CA083688, P01 CA080111 and P01 CA109901 grants from NIH (to P.S.). S.J. is supported by The Thailand Research Fund's MRG5280248. W.M. by Foundation for Polish Science, Y.W. through the CCCB and the Dana-Farber Strategic Plan Initiative, T.A.K. and A.B.C. by Project Z01 ES065089 (to T.A.K.) from the Division of Intramural Research of the NIH, NIEHS.

Author Contributions

S.J. and P.S. designed the study, analyzed the data and wrote the manuscript. S.J. performed most of the experiments with the help from collaborators. Y.H. and D.M.L. contributed to DNA repair analyses. W.M. contributed *in vitro* protein binding analyses J.E.E. and T.G. performed mass spectrometry; J.E.E. analyzed mass spec data with S.P.G. L.B., F.B. , A.Z. T.v.H helped with the experiments. Y.W. M.C and J.Q. performed computational analyses of interactors. A.B.C and T.A.K. contributed mismatch DNA repair analyses, B.X. helped with BRCA2 analyses.

Figure 1 | Analyses of cyclin D1 interactors identified in human cancers

a, A diagram depicting cyclin D1 interactors, grouped according to the cell line in which they were detected. A line between cyclin D1 and a circle with protein symbol indicates that this interactor was found among cyclin D1-associated proteins in a particular cell line. Thickness of the line corresponds to the abundance of peptides belonging to a given protein found in mass spectrometry. Circle colors denote interactors observed in all five (green circles), four (orange), three (red), two (blue), or only in one cell line (grey).

b, Biological process/molecular function enrichment heatmap of cyclin D1 interactors. The five columns correspond to five cell lines, each horizontal line denotes distinct biological process/molecular function. Red color depicts functions enriched among interactors in a particular cell line, green color – no enrichment. Left panel shows a complete map, right panel shows enlarged map of molecular functions/biological processes that are enriched across all 5 human cancer cell lines analyzed.

c, Cyclin D1 interactors classified according to a biological process.

Figure 2 | Impaired DNA repair upon reduction of cyclin D1 levels

a, Colony survival assay of HeLa cells expressing anti-cyclin D1 shRNA (shD1-A) or control shRNA (shcont). SF_{50} = 2.15 Gy for shcont and 1.07 Gy for shD1. For results using another two anti-cyclin D1 shRNA sequences, see Supplementary Fig. 5a.

b and **c**, Colony survival assays of H2009 cells expressing anti-cyclin D1 shRNAs (shD1-A or shD1-B), or control shRNA (shcont). Cells were exposed to the indicated doses of camptothecin (CPT), etoposide (ETO), or AZD2281 (Olaparib). SF_{50} values: camptothecin: shcont = 15.1 nM, shD1-A = 2.8 nM, shD1-B = 3.4 nM. Etoposide: shcont = 3.4 μM, shD1-A = 2.1 μM, shD1-B = 1.3 μM. Olaparib: shcont = 0.39 μM, shD1-A = 0.083 μM, shD1-B = 0.065 μM.

d, Results of comet assays to measure DNA repair in HeLa cells transfected with anti-cyclin D1 siRNA (siD1-A) or control siRNA (sicont) before (0 hrs) or at 4 and 16 hrs after IR. Shown are percentages of cells containing various comet tail length at the indicated time-points after IR; increased tail length is indicative of DNA damage. See Supplementary Fig. 7b for values obtained with another anti-cyclin D1 siRNA sequence.

e, HR assay in HeLa cells using a DR-eGFP-reporter system. sicont, control siRNA; siRAD51, anti-RAD51 siRNA; siD1-A, -B,-C, three independent anti-cyclin D1 siRNAs.

f, HR assay in HeLa cells expressing siRNA-resistant version of cyclin D1, transfected with anti-cyclin D1 siRNA (siD1-A + WTD1).

g, HR assay in HeLa cells expressing siRNA-resistant cyclin D1 mutant which is deficient in RAD51 binding, transfected with anti-cyclin D1 siRNA (siD1-A + mutD1).

Note that unlike wild-type cyclin D1 (see panel **f**), RAD51 binding-deficient cyclin D1 mutant fails to restore HR in cyclin D1-depleted cells.

In **a-g**, *, $p < 0.05$; **, $p < 0.01$; ***, $p < 0.005$; Error bars, standard deviation, n = 3-5.

Figure 3 | Functional interaction between cyclin D1 and RAD51

a, Direct binding between purified GST-cyclin D1 and purified recombinant RAD51 proteins. GST-Synapsin1, GST-Wave1 and GST served as negative controls for RAD51 binding. Upper panel: the indicated proteins were mixed, GST-containing proteins were precipitated using GSH-Sepharose, resolved on a PAGE gel and immunoblotted with an anti-RAD51 antibody (WB). Lower panel: GST-proteins used for binding reactions, were visualized by Ponceau S staining.

b, Reciprocal assay to the one shown in **a**, using GST-RAD51 and purified recombinant cyclin D1. GST-CDK4 served as a positive control for cyclin D1 binding, GST as a negative control. Cyclin D1 was visualized by anti-cyclin D1 western blot (WB). Lower panel: proteins used for binding reactions were resolved on a PAGE gel and probed with an anti-GST antibody.

c, *In vitro* binding assays using GST-RAD51 and purified, recombinant cyclin D1 deletion mutants. Upper left panel: the indicated proteins were mixed, GST-containing proteins were precipitated using GSH Sepharose, resolved on a PAGE gel and immunoblotted (WB) with an anti-cyclin D1 antibody. Upper right panel depicts input cyclin D1 deletion mutants used in binding reactions (for comparison, expression of full-length cyclin D1 is also shown in the last lane). Lower panel: GST-proteins used for binding reactions were resolved on a PAGE gel and probed with an anti-GST antibody.

d, Interaction between endogenous cyclin D1 and RAD51, detected in the indicated cell lines. Cyclin D1 was immunoprecipitated (IP) and western blots (WB) were probed with anti-RAD51 antibody. WCL, whole cell lysate.

e, Induction of cyclin D1 - RAD51 physical interaction at different time-points after irradiating HeLa cells. Top panel: cyclin D1 was immunoprecipitated (IP) and immunoblots (WB) were probed with anti-RAD51 antibody. Lower panel: total levels of cyclin D1 and RAD51 after IR were determined by western blotting. β-Actin served as loading control.

f, *In vitro* binding assays using the indicated GST-BRCA2 fragments[25] and purified recombinant cyclin D1. Upper panel: GST-BRCA2 fragments 1 to 9 and cyclin D1 were mixed, GST-containing proteins were precipitated using GSH Sepharose, resolved on a PAGE gel and immunoblotted (WB) with an anti-cyclin D1 antibody. Lower panel: The amount of GST-BRCA2 fragments used for binding reactions (Input) was visualized by Ponceau staining of the membrane.

g, Physical binding of endogenous cyclin D1 and BRCA2 (B2) in lung cancer H2009 cells demonstrated by immunoprecipitation (IP) – western blotting (WB). WCL, whole cell lysate

h, Left panel: Recruitment of RAD51 to I-SceI-induced double-stranded DNA break was gauged by anti-RAD51 ChIP followed by PCR with primers adjacent to DNA damage site. Bars show enrichment around DNA damage site before (light blue) and after induction of a DNA break (dark blue). For control, we used anti-E2F4 and non-immune IgG (IgG) ChIP (followed by PCR with the same set of primers adjacent to DNA damage

site) which did not show any enrichment after DNA damage. Right panel: the assay was repeated in cells transfected with anti-cyclin D1 siRNA. Note that cyclin D1 knock-down essentially abrogated RAD51 recruitment to DNA damage site. For results obtained with another anti-cyclin D1 siRNA sequence, see Supplementary Fig. 12a.

i, Recruitment of cyclin D1 to a double-stranded DNA break induced by I-SceI, tested as in **h**. Bars show enrichment around DNA damage site before (light green) and after induction of a DNA break (dark green). Right panel shows the same assay performed on cells transfected with anti-cyclin D1 siRNA. As expected, knock-down of cyclin D1 abrogated recruitment of cyclin D1 to damaged DNA.

j, Co-localization of cyclin D1 and RAD51 at DNA damage sites. Same assay as in **h** and **i**, except that anti-cyclin D1 ChIP was followed by anti-RAD51 re-ChIP and PCR with primers adjacent to double-stranded DNA break (DR-1). For control, we performed anti-cyclin D1 ChIP followed by re-ChIP with non-immune IgG (IgG). Upper panel: PCR products resolved on a gel. M, molecular weight markers. Lower panel: Bars show enrichment of cyclin D1 – RAD51 complex (cyclin D1 → RAD51) at DNA damage site before (light grey) and after induction of a DNA break (dark grey), as quantified by quantitative PCR.

k, Reduction of RAD51 recruitment to DNA damage foci following knock-down of cyclin D1. HeLa cells were transfected with two independent anti-cyclin D1 siRNAs (red and orange bars) or control siRNA (black bars), irradiated, and the percentage of cells displaying a given number of RAD51 foci per cell was determined at the indicated time-points after radiation.

l, Knock-down of BRCA2 abrogates recruitment of cyclin D1 to double-stranded DNA breaks. Left panel: Recruitment of cyclin D1 to a double-stranded DNA break induced by I-SceI was tested using anti-cyclin D1 ChIP as in **i**. Bars show enrichment around DNA damage site before (light green) and after induction of a DNA break (dark green). The assay was performed using cells transfected with two independent anti-BRCA2 siRNAs (siBRCA2-A, and -B), or with control siRNA (sicont), Right panel: For control, we monitored recruitment of RAD51 to a double-stranded DNA break, using anti-RAD51 ChIP (like in **h**). As expected, knock-down of BRCA2 abolished recruitment of RAD51 to a DNA break, consistent with the well-established role of BRCA2 in RAD51 recruitment[24].

m, Reduced co-localization of BRCA2 and RAD51 following knock-down of cyclin D1. HeLa cells were transfected with anti-cyclin D1 siRNA (siD1-C) or with control siRNA (sicont) and irradiated. At 2 hrs after irradiation, cells were co-stained with anti-BRCA2 and -RAD51 antibodies to visualize BRCA2 and RAD51 which normally co-localize within DNA damage foci[24]. Shown is percent of BRCA2-positive foci which failed to recruit RAD51 ($BRCA2^{+}/RAD51^{-}$). Note that the number of BRCA2-positive foci was unchanged in cells depleted of cyclin D1 (Supplementary Fig. 17a), however, the subsequent recruitment of RAD51 to these foci was defective in cyclin D1 knock-down cells. For results with another anti-cyclin D1 siRNA sequence, see Supplementary Fig. 19.

In **h-m**, ***, $p \leq 0.005$; **, $p \leq 0.01$; *, $p < 0.05$; Error bars, standard deviation, n=3-5.

Figure 4 | Increased radiation-sensitivity of tumors with reduced cyclin D1 levels.

a, H2009 cells expressing control or anti-cyclin D1 shRNA were injected into nude mice and tumor growth was monitored on the indicated days. Left panel: in the absence of irradiation, tumors with reduced cyclin D1 levels displayed unperturbed growth *in vivo*. Middle and right panels: at days 5 and 10, mice received 2 Gy or 4 Gy of radiation, respectively. Note that this resulted in impaired growth of tumors with reduced cyclin D1 levels. Error bars, standard deviation. ***, $p \leq 0.005$; **, $p \leq 0.01$. For tumor volumes mouse-by-mouse, see Supplementary Fig. 23. For results using two additional anti-cyclin D1 shRNA sequences, see Supplementary Fig. 25d, e.

b, Weight of tumors at the end of the observation period. Each circle represents an individual tumor, horizontal bars depict mean values. Left panel: in the absence of radiation, tumors with reduced cyclin D1 levels displayed unperturbed growth *in vivo*. In contrast, upon irradiation with 2 Gy twice (middle panel) or 4 Gy twice (right panel), tumors with reduced cyclin D1 levels showed decreased weight, as compared to control tumors (expressing normal levels of cyclin D1). Shown are the number of mice analyzed per group (N) and the p-values. For results using two additional anti-cyclin D1 shRNA sequences, see Supplementary Fig. 25f, g.

METHODS

Cells and cell lines

293, HeLa, MCF7, ZR-75-1 and HT-29 cells were purchased from American Type Culture Collection (ATCC). Granta 519, Z138C, NCEB-1 cells were a gift from Dr. G. Shapiro, Dana-Farber Cancer Institute, SP49 from Dr. J. Bartek, Institute of Cancer Biology and Centre for Genotoxic Stress Research, Danish Cancer Society, Denmark, H2009 and DU 145 from Dr. S. Kim, Novartis; UMSCC-2 were obtained from University of Michigan. Generation of *cyclin D1*$^{-/-}$*D2*$^{-/-}$*D3*$^{-/-}$ MEFs was described previously[11]. Wild-type cyclin D1 or cyclin D1K112E mutant[13] were expressed in *cyclin D1*$^{-/-}$*D2*$^{-/-}$*D3*$^{-/-}$ MEFs using pOZ-FH-N expression vector[10]. PD0332991 was obtained from Pfizer Inc.

Small interfering RNA (siRNA) and short-hairpin RNA (shRNA)

Cyclin D1-specific siRNA sequence A, (siD1-A, 5'-CCAAUAGGUGUAGGAAAUAGCGCTG-3') was from Integrated DNA Technologies. Cyclin D1-specific siRNA sequence B (siD1-B, 5'-AACACCAGCTCCTGTGCTGCG-3') and C (siD1-C, 5'-GCCCTCGGTGTCCTACTTCAA-3'), RAD51-specific siRNA (5'-AAGGGAATTAGTGAAGCCAAA-3'), and control siRNA (AllStars Negative control) were from Qiagen. BRCA2-specific siRNA-A (1949) and -B (2618) were described previously[30]. Cyclin D1-specific shRNA-A (5'-GCCAGGATGATAAGTTCCTTT-3'), C (5'-ATTGGAATAGCTTCTGGAAT-3') and non-target control shRNA (5'-CAACAAGATGAAGAGCACCAA-3') were from Sigma. Cyclin D1-specific shRNA-B (5'-CCACAGATGTGAAGTTCATTT-3') was from Dr. E. Sicinska, Dana-Farber Cancer Institute.

Expression of tandemly tagged cyclin D1, nuclear extraction and double-affinity immunopurification

Tandemly tagged cyclin D1 was obtained by cloning human cyclin D1 cDNA into Xho I and Not I sites of pOZ-FH-N expression vector[10]. The resulting N-terminally tagged cyclin D1 contained FLAG- and Hemagglutinin- (HA-) tags fused to its N-terminus. The construct was introduced into cancer cell lines, and stable cell lines were obtained as described[10]. We verified the expression of FLAG- and HA-tagged cyclin D1, and expression of the tagged and the endogenous cyclin D1 in nuclear and cytoplasmic extracts from these cell lines using western blotting. Nuclear extractions were performed as described[31], using 2 x10^7 cells expressing tagged cyclin D1 as a source of material. Nuclear extracts were then used for double-affinity immunopurification of cyclin D1-containing complexes, as described[10,32]. In parallel, we obtained nuclear extracts from cells expressing empty pOZ-FH-N vectors, which were used for control ("mock") purifications. From each purification, 5% of purified products were run on NuPAGE® 4-12% Bis-Tris Midi Gel (Invitrogen) and silver-stained. The rest of the material was subjected to mass spectrometry analyses as described below.

Mass spectrometry and proteomic analyses

For each cell line we immunopurified cyclin D1-associated protein complexes containing at least 900 ng of tagged cyclin D1, and the corresponding amount of "mock" purified material prepared from the same number of cells expressing empty vector. Purified cyclin D1-containing complexes from a given cell line were pooled and subjected to three independent mass spec runs (each using a sample containing approximately 300 ng of cyclin D1). In parallel, "mock" purified samples were subjected to three mass spec

runs. For Granta 519 cells, we immunopurified 2100 ng of cyclin D1, pooled, and subjected the material to seven mass spec runs (each using material containing approx. 300 ng of cyclin D1). In total, we performed 41 mass spec sequencing runs: for cyclin D1-containing samples - three from HT-29, UMSCC-2, ZR-75-1 and MCF7, seven from Granta 519; for "mock" purified samples - three from HT-29, UMSCC-2, ZR-75-1, six from MCF7, seven from Granta 519.

Liquid chromatography and tandem mass spectrometry (LC-MS/MS)

Sample preparation was as described previously[32]. LC-MS/MS analyses were performed on an LTQ mass spectrometer (Thermo Fisher) equipped with an Agilent 1100 high-performance liquid chromatography (HPLC) pump (Agilent Technologies) and a Famos autosampler (LC Packings). Peptide mixtures were introduced into the mass spectrometer via a fused silica microcapillary column (internal diameter = 125 μm), ending in an in-house pulled needle tip (internal diameter ~ 5 μm). Columns were packed to a length of 18 cm with a C18 reversed-phase resin (Magic C18AQ, Michrom Bioresources). Sample solution containing approximately 300 ng of tagged cyclin D1 (or mock) was loaded onto the column. Peptides were eluted into the electrospray ionization source of the mass spectrometer via a linear gradient of 4 to 35% buffer B [2.5% water and 0.1% formic acid in acetonitrile (v/v)] in buffer A [2.5% acetonitrile and 0.1% formic acid in water (v/v)] over 40 minutes followed by a high organic wash (100% buffer B, 6 minutes) and a column reconditioning wash (100% buffer A, at least 20 minutes). The LTQ was operated in a data-dependent mode: up to ten MS/MS spectra were acquired per data-dependent cycle from each master spectrum (mass range = 380 –1800 m/z).

(For extended protocol and method discussion, please see the Supplementary Material)

Data processing All MS/MS spectra were searched with both SEQUEST[33] and Mascot[34] search engines against a composite sequence database consisting of the minimally-redundant human sequences stored at the International Protein Index[35] (version 3.37), common contaminant protein sequences, and reversed (decoy) versions of these sequences[36]. In-house software was then used to design filtering criteria delivering precision rates (true positives divided by total positives) of 90%, 95%, and 99% guided by matches to decoy proteins as previously described[36]. Peptides selected by criteria delivering less than 99% precision were included only if they were assigned to at least one other peptide selected by criteria delivering 99% precision. (For extended description of this procedure, discussion, and selection of high-confidence cyclin D1 interacting proteins, please see the Supplementary Material).

Gene Ontology enrichment

Gene Ontology (GO) enrichment analysis (shown in Fig. 1b) was performed using the DAVID web server (http://david.abcc.ncifcrf.gov/)[37,38]. In order to obtain higher statistical power, for this analysis we selected interactors with p-values ≤ 0.01 (Mann-Whitney U-test, Matlab) from each cell line (see Supplementary Tables 2 and 6) (total of 1,508 unique proteins). GO terms with q-value < 0.2 were considered enriched. The fold-enrichment values were formulated into matrix and imported into MultiExperiment Viewer (MeV)[39] to generate the heat map.

Analyses of cyclin D1 interactor network

To construct the network, we used the same set of data as in GO enrichment analysis (see above), with $p \leq 0.01$ (Mann-Whitney U-test, Matlab). Cyclin D1 interactor network (shown in Supplementary Fig. 3) was then derived from human protein-protein interactions (hPPI) from STRING database[40] version 8.2 (confidence score ≥0.7). Cyclin D1 interactors that either did not have high-confidence interacting partners in STRING database, or formed small fragmented "islands" with only a few nodes (n<7) were not shown. The significance of connectivity was evaluated by bootstrapping using the whole hPPI as background for 1,000,000 iterations, and it was evaluated by the following formula:

P- val = (Number of times [edges of random network > edges of network]) ÷ Total number of iterations.

This network exhibits significantly higher degree of connectivity when compared with randomly selected protein data set of the same size ($p = 2.8 \times 10^{-5}$).

Colony survival assays

Cells were seeded 24 hrs before irradiation (2-8 Gy of IR, source: Cs^{137}) or drug treatment. For camptothecin or etoposide treatment, cells were cultured for 24 hrs in medium containing drug, washed with PBS, and the culture was continued in drug-free medium. For Olaparib treatment, cells were cultured in the medium containing the inhibitor throughout the experiment. Colonies were stained with crystal violet, and those with at least 25 cells were counted under a dissecting microscope. Experiments were performed 3 times per cell line. Data shown depict representative experiments. Camptothecin and etoposide were from Sigma, Olaparib from ChemieTek.

Comet assays

HeLa cells were transfected with anti-cyclin D1 siRNAs or control siRNA, 48 hrs before irradiation. Cells were treated with 1 Gy of IR, and harvested at 0 hr (before radiation), 4 hrs, or 16 hrs after treatment. Neutral comet assays with silver staining (CometAssay™ Silver) were performed according to the manufacturer protocol (Trevigen, Inc.). The quantitation of tail DNA was done using CometScore^{TM} Version 1.5. Data was analyzed using unpaired two-tailed *t*-test.

Homologous recombination assays

HeLa and H2009 cells containing DR-eGFP reporter system were established, and DNA damage was induced by transfection of an I-SceI expression plasmid as described[17]. To knock-down cyclin D1, anti-cyclin D1 siRNAs (or control siRNAs) were transfected twice 24 hrs prior to DNA damage induction. The efficiency of homologous recombination was determined by FACS, 48 hrs after DNA damage.

DNA mismatch repair assays

The *in vitro* DNA mismatch repair assays using M13 heteroduplexes containing a G•G mispair at position 88 and a 3' nick or a 2-base loop mismatch at positions 90 and 91 and a 5' nick were performed as previously described[41]**.**

Radiation-, drug- and laser-induced DNA damage

For quantification of DNA damage foci, cells were exposed to the indicated dose of ionizing radiation, using Cs^{137} as a source. For analyses of FANCD2, FANCI, and PCNA foci, cells were treated with 1 or 2 μM mitomycin C for 24 hrs prior to the staining. For analyses of MSH6 foci, cells were cultured in medium containing 25 μM O^6-

Benzylguanine (O^6-BG, Sigma) for 2 hrs, then for 1 hr in medium containing O^6-BG and 10 μM N-methyl-N-nitro-N-nitrosoguanidine (MNNG, Fisher Scientific) before staining at 4 hrs later. Laser-induced DNA double stranded breaks were generated using a P.A.L.M. MicroBeam laser (UV-A) microdissection[42,43] in HeLa cells stably expressing C-terminally HA-tagged human cyclin D1 (pWZL Blast-cyclin D1-HA a gift from Mark Ewen, Dana-Farber Cancer Institute). Laser-stripes were generated in 70-100 cells per coverslip with the above-noted laser (λ=337 nm) using the 40x objective at 60%-75% power.

Immunofluorescence

Cells were fixed in 3% paraformaldehyde/2% sucrose solution, permeabilized with Triton X solution (0.5% Triton X-100, 20 mM Hepes pH 7.4, 50 mM NaCl, 3 mM MgCl, 300 mM sucrose) with an exception of PCNA-staining (methanol and 0.5% NP40 were used for fixing and permealizing, respectively), incubated with primary antibodies at 37°C for 1 hr, followed by 1 hr incubation with secondary antibodies. Staining for FANCD2, and FANCI was performed as described[44]. The following antibodies were used: HA (HA.11), Covance; γ-H2AX Ser139 (JBW301), Millipore or (Ab2893), Abcam; PCNA (PC-10), RAD51 (H-92), BRCA1 (D-9), MSH6 (N-20), Santa Cruz Biotechnologies; RPA34 (Ab1), Lab Vision; MRE11 (12D4), GeneTex Inc; FANCD2 (NB100-182), Novus Biologicals; RAD51 (14B4), Abcam. Anti-BRCA2 antibody was described previously[30]. Anti-FANCI antibody was a gift from Dr. A Smogorzewska, Rockefeller University. Secondary antibodies with Fluorophores Alexa 488 and Alexa 594 were from Invitrogen. To detect single-stranded DNA (ssDNA) by microscopy, HeLa cells were transfected with the indicated siRNAs. Two days later, cells were cultured for

24 h in medium supplemented with 10 μM BrdU followed by 1 hour treatment with 2 μM camptothecin or by 10 Gy radiation. Cells were then permeabilized (without any preceding DNA denaturation or nuclease treatment), fixed and incubated with anti-BrdU and γ-H2AX antibodies, followed by incubation with secondary antibodies.

Quantification of RAD51 DNA damage foci was performed using HeLa and H2009 cells. Recruitment of other proteins to DNA damage foci was analyzed using HeLa cells. Only foci of DNA repair proteins that co-localized with γ-H2AX foci were counted. For each time-point at least 180 cells were counted.

Laser-induced DNA damage was visualized with γ-H2AX antibody. Anti-HA antibody was then used to detect cyclin D1. Images were collected with a Leica SP5X confocal microscope equipped with a 405nm Argon (excitation at 488nm), and white light laser (excitation at 594nm), 63x 1.4NA objective using LAS-AF software. For quantitation of the intensity of RAD51 stripes, images were collected using a Yokogawa Spinning Disk confocal attached to a Nikon Ti (Nikon Instruments, Melville, NY) with Plan Apo 100x 1.4NA objective and a Hamamatsu OrcaER camera. Acquisition parameters, shutters, laser wavelength and focus were controlled by Andor iQ software (Andor Technology, South Windsor, CT). Images were analyzed using Metamorph software. Only stripes that co-stained with γ-H2AX and RAD51 antibodies were used for quantification. Stripe intensities were background subtracted using the non-damaged area from the same nucleus as the background. More than 100 cells were analyzed from each group.

Chromatin immunoprecipitation (ChIP)

Targeted ChIP was performed as described[23] with some modifications. Briefly, HeLa cells which contain stably integrated into their genome DR-eGFP reporter system (containing I-SceI endonuclease recognition site) were used. Cells were transfected with the I-SceI expression plasmid pCβASce (to induce site-specific DNA damage) or were transfected with an empty vector. 18 hrs after transfection, cells were fixed in 1% formaldehyde, washed in 5 mg/ml BSA/PBS buffer, collected and re-suspended in lysis buffer (1% SDS, 10 mM EDTA, 0.5 mM Tris-HCl pH 7.5, 0.25% Triton X-100, and proteinase inhibitors). The lysates were sonicated, cleared by centrifugation at 16,000 x g, diluted in 9 volumes of dilution buffer (1% Triton X-100, 2 mM EDTA, 150 mM NaCl, 20 mM Tris-HCl pH 7.5, and proteinase inhibitors), and incubated with antibodies overnight. RAD51 and cyclin D1 ChIP were performed using anti-RAD51 antibody (H-92), or anti-cyclin D1 antibody (H-295) (Santa Cruz Biotechnologies). Protein A beads were then added for 2 hrs incubation at 4°C. Beads were washed 6 times using a washing buffer (50 mM HEPES pH 7.5, 1 mM EDTA, 0.7% sodium deoxycholate, 1% NP40, 0.5 M LiCl, and proteinase inhibitors), and 2 times with TE buffer. DNA was eluted with an elution buffer (1% SDS, 0.1 M $NaHCO_3$), overnight at 65°C. For ChIP-re-ChIP, C-terminally HA-tagged cyclin D1 was stably expressed in HeLa cells which also contained stably integrated DR-eGFP reporter. Cyclin D1 was ChIP using anti-HA antibody (12CA5, from Covance), eluted with 400 μg/ml HA-peptide twice at room temperature, and re-ChIP with an anti-RAD51 antibody or with non-immune IgG (IgG) for control (Fig. 3j in the main text). PCR primers: DR-1 (adjacent to DNA break), forward 5'-GAGCAAGGGCGAGGAGCTGT-3',

reverse 5'-CCGTAGGTCAGGGTGGTCAC-3', Control DNA segments: GAPDH, forward 5'-GCTTGCCCTGTCCAGTTAAT-3', reverse 5'-TAGCTCAGCTGCACCCTTTA-3'; SOD promoter, forward 5'-ATTGCAGGGGAAGAAAAGGT-3', reverse 5'-CCCAAGATGGATGCTTTTGT-3'; TFF-1 intragenic, forward 5'-AATACCTGAGGACCCCAACC-3', reverse 5'-TCTTCACTCTCCTCGCATTG-3'; CDC25A promoter, forward 5'-AGCCTAGCTGCCATTCGGTTG-3', reverse 5'-AGCAGAAAACCAAGCCGACCTA-3'.

Production of recombinant proteins and binding assays

GST-human cyclin D1, RAD51, CDK4 and deletion mutants were expressed using pGEX-5x-3 (GE Healthcare). GST-fragments of BRCA2[25] were kindly provided by Dr. A. Venkitaraman, University of Cambridge: GST-BRCA2-1 (corresponding to BRCA2 amino acid aa1-454); BRCA2-2 (aa420-906); BRCA2-3 (aa885-1362); BRCA2-4 (aa1338-1781); BRCA2-5 (aa1744-2115); BRCA2-6 (aa2106-2472); BRCA2-7 (aa2438-2824); BRCA2-8 (aa2780-3197); BRCA2-9 (aa3189-3418). GST-human Synapsin 1 (aa1-455) and GST-rat Wave 1 (aa449-701) were from Dr. J. Odajima, Dana-Farber Cancer Institute. Protein expression was carried out in *E. coli* BL21 Rosetta strain (Novagen) according to manufacturer protocol. *In vitro* binding was performed as described[45] with modifications. Briefly, 1 µg of each GST fusion protein was incubated (30 min, 37˚C) with 5 µl of GSH Sepharose in 200 µl binding buffer (20 mM Hepes pH 7.5, 150 mM KCl, 10% glycerol, 0.1% NP40, 1 mM EDTA, 5 mM $MgCl_2$, 1 mM DTT, 0.5 mM PMSF). 100 ng of tested proteins were added and incubated for another 30 min at 37˚C, followed by 1 h incubation at 4˚C. To identify RAD51-interacting region of cyclin D1, 10 pmoles of each cyclin D1 deletion mutant were mixed

with GST-RAD51. After the binding, beads were washed and bound proteins were separated using 12% SDS-PAGE gels and analyzed by western blotting using specific antibodies. For *in vivo* binding assays, full-length cyclin D1 and its fragments were expressed using p3xFLAG-CMV-10 (Sigma). HA tag was added to the full-length RAD51 coding sequence using PCR amplification. PCR product was cloned into the p3xFLAG-CMV-10 vector (from which 3X FLAG has been removed). Plasmids were transfected into 293 cells, cells were lysed in ELB lysis buffer (0.5% NP40, 160 mM NaCl, 50 mM HEPES, pH 7.4, 50 mM EDTA, proteinase inhibitors), HA-RAD51 was immunoprecipitated using anti-HA antibody, and FLAG-cyclin D1 fragments were detected by western blotting using anti-FLAG antibody (M2, Sigma).

Co-immunoprecipitation of endogenous cyclin D1-interactor complexes

Cell lysates were prepared in ELB buffer. Ten µg of mouse anti-cyclin D1 (Ab1, Lab Vision), rabbit anti-RAD51 antibody (H-92, Santa Cruz Biotechnologies), or 4 µg of rabbit BRCA2 antibody[30] were incubated with 10 mg of lysate. Protein G beads were then added, incubated at 4C/2hrs, and immunoprecipitated products were detected by western blotting. Other cyclin D1-interacting proteins were detected by antibodies listed below. In case when specific antibodies were not available (TRIM28, TK1) V5-tagged versions of the proteins were expressed and western blots were probed with anti-V5 antibody (Invitrogen).

***In vivo* tumor experiments**

HeLa, H2009 or DU 145 cells were transduced with lentiviruses expressing anti-cyclin D1 or control shRNA, and selected in puromycin for 7 days. Ten million tumor cells mixed with matrigel (BD Biosciences) were injected subcutaneously into 6-weeks-old

athymic *nu/nu* female mice (Charles River Labs). Tumors were irradiated at the indicated time-points using Cs^{137} as a source (the rest of the animal was shielded from radiation). Tumor growth was assessed every other day (H2009) or twice weekly (HeLa, DU145), and tumor volumes were calculated according to the formula:

Tumor volume [mm^3] = (1/6) X π X (tumor length) x (tumor width) ^{2}

Tumor weights were determined at the end of experiments. Statistical significance of the differences was evaluated using paired two-tailed *t*-test.

Antibodies

In addition to antibodies mentioned above, the following antibodies were used: cyclin D1 (Ab1 or Ab3), CDK1 (A17.1), CDK3 (Ab1), $p18^{INK4c}$ (Ab3) - all from Lab Vision, ZFP106 (A301-527A) and RIF1 (BL2003) from Bethyl Laboratories, phospho-ATM S1981 (10H11.E12), phospho-CHK2 S33/35, phospho-CHK2 T68, phospho-CHK1 S317, CHK2 and CHK1 from Cell Signaling Technology, ATM (2C1) from GeneTex, Inc., CDK2 (M2), CDK4 (C-22), CDK5 (DC-17), PCNA (C-20), Ikaros (H-100), Aiolos (O-21) and MLF2 (C-14), GST (Z-5) from Santa Cruz Biotechnologies, RB1 (554136), and $p27^{Kip1}$ (Clone 57) from BD Biosciences, β-Actin (AC-15) from Sigma, BRCA2 (Ab-1) from Calbiochem, KEAP1 (ab31973), CDC25A (DSC-120 + DSC-121) and phospho-CDC25A S75 (ab47279) from Abcam, anti-phospho-CDC25A S123 antibody was a gift from Drs. D. Bulavin and E. Apella, Anti-NUMA1 antibody from Dr. D. Campton, Dartmouth Medical School.

Method references

30. Xia, B. et al. Control of BRCA2 cellular and clinical functions by a nuclear partner, PALB2. Mol Cell 22, 719-29 (2006).

31. Dignam, J. D., Martin, P. L., Shastry, B. S. & Roeder, R. G. Eukaryotic gene transcription with purified components. Methods Enzymol 101, 582-98 (1983).

32. Bienvenu, F. et al. Transcriptional role of cyclin D1 in development revealed by a genetic-proteomic screen. Nature 463, 374-8 (2010).

33. Eng, J. K., McCormack, A. L. & Yates, J. R. An approach to correlate tandem mass spectral data of peptides with amino acid sequences in a protein database. J Am Soc Mass Spectrom 5, 976-989 (1994).

34. Perkins, D. N., Pappin, D. J., Creasy, D. M. & Cottrell, J. S. Probability-based protein identification by searching sequence databases using mass spectrometry data. Electrophoresis 20, 3551-67 (1999).

35. Kersey, P. J. et al. The International Protein Index: an integrated database for proteomics experiments. Proteomics 4, 1985-8 (2004).

36. Elias, J. E. & Gygi, S. P. Target-decoy search strategy for increased confidence in large-scale protein identifications by mass spectrometry. Nat Methods 4, 207-14 (2007).

37. Dennis, G., Jr. et al. DAVID: Database for Annotation, Visualization, and Integrated Discovery. Genome Biol 4, P3 (2003).

38. Huang da, W., Sherman, B. T. & Lempicki, R. A. Systematic and integrative analysis of large gene lists using DAVID bioinformatics resources. Nat Protoc 4, 44-57 (2009).

39. Saeed, A. I. et al. TM4 microarray software suite. Methods Enzymol 411, 134-93 (2006).

40. Jensen, L. J. et al. STRING 8--a global view on proteins and their functional interactions in 630 organisms. Nucleic Acids Res 37, D412-6ps1 (2009).

41. Thomas, D. C., Roberts, J. D. & Kunkel, T. A. Heteroduplex repair in extracts of human HeLa cells. J Biol Chem 266, 3744-51 (1991).

42. Greenberg, R. A. et al. Multifactorial contributions to an acute DNA damage response by BRCA1/BARD1-containing complexes. Genes Dev 20, 34-46 (2006).

43. Sobhian, B. et al. RAP80 targets BRCA1 to specific ubiquitin structures at DNA damage sites. Science 316, 1198-202 (2007).

44. Smogorzewska, A. et al. Identification of the FANCI protein, a monoubiquitinated FANCD2 paralog required for DNA repair. Cell 129, 289-301 (2007).

45. Esashi, F. et al. CDK-dependent phosphorylation of BRCA2 as a regulatory mechanism for recombinational repair. Nature 434, 598-604 (2005).

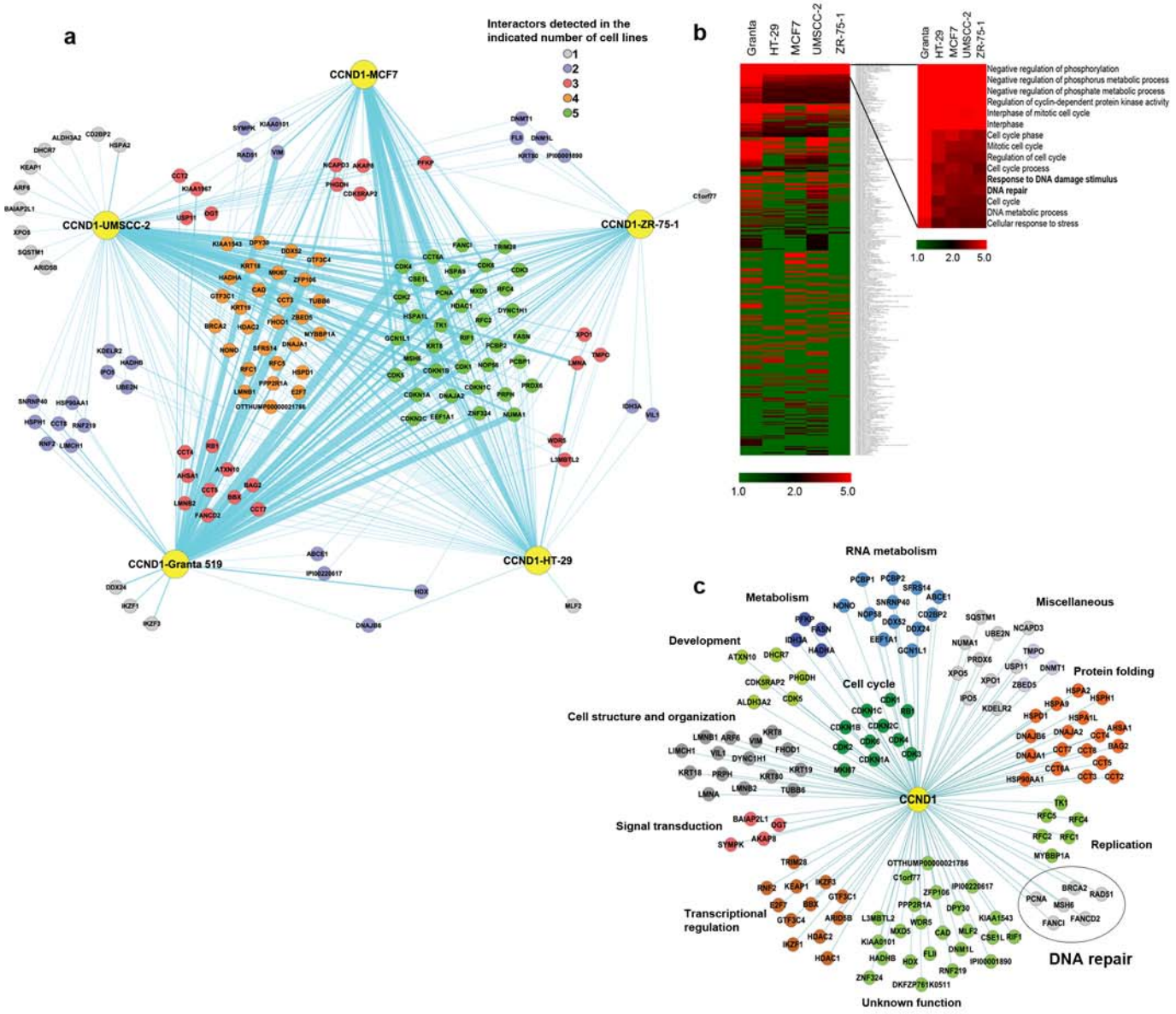
a
Interactors detected in the indicated number of cell lines
1
2
3
4
5
CCND1-MCF7
CCND1-UMSCC-2
CCND1-ZR-75-1
CCND1-Granta 519
CCND1-HT-29
b
Granta
HT-29
MCF7
UMSCC-2
ZR-75-1
Negative regulation of phosphorylation
Negative regulation of phosphorus metabolic process
Negative regulation of phosphate metabolic process
Regulation of cyclin-dependent protein kinase activity
Interphase of mitotic cell cycle
Interphase
Cell cycle phase
Mitotic cell cycle
Regulation of cell cycle
Cell cycle process
Response to DNA damage stimulus
DNA repair
Cell cycle
DNA metabolic process
Cellular response to stress
1.0
2.0
5.0
c
RNA metabolism
Metabolism
Miscellaneous
Development
Protein folding
Cell cycle
Cell structure and organization
CCND1
Signal transduction
Replication
Transcriptional regulation
DNA repair
Unknown function

Figure 1

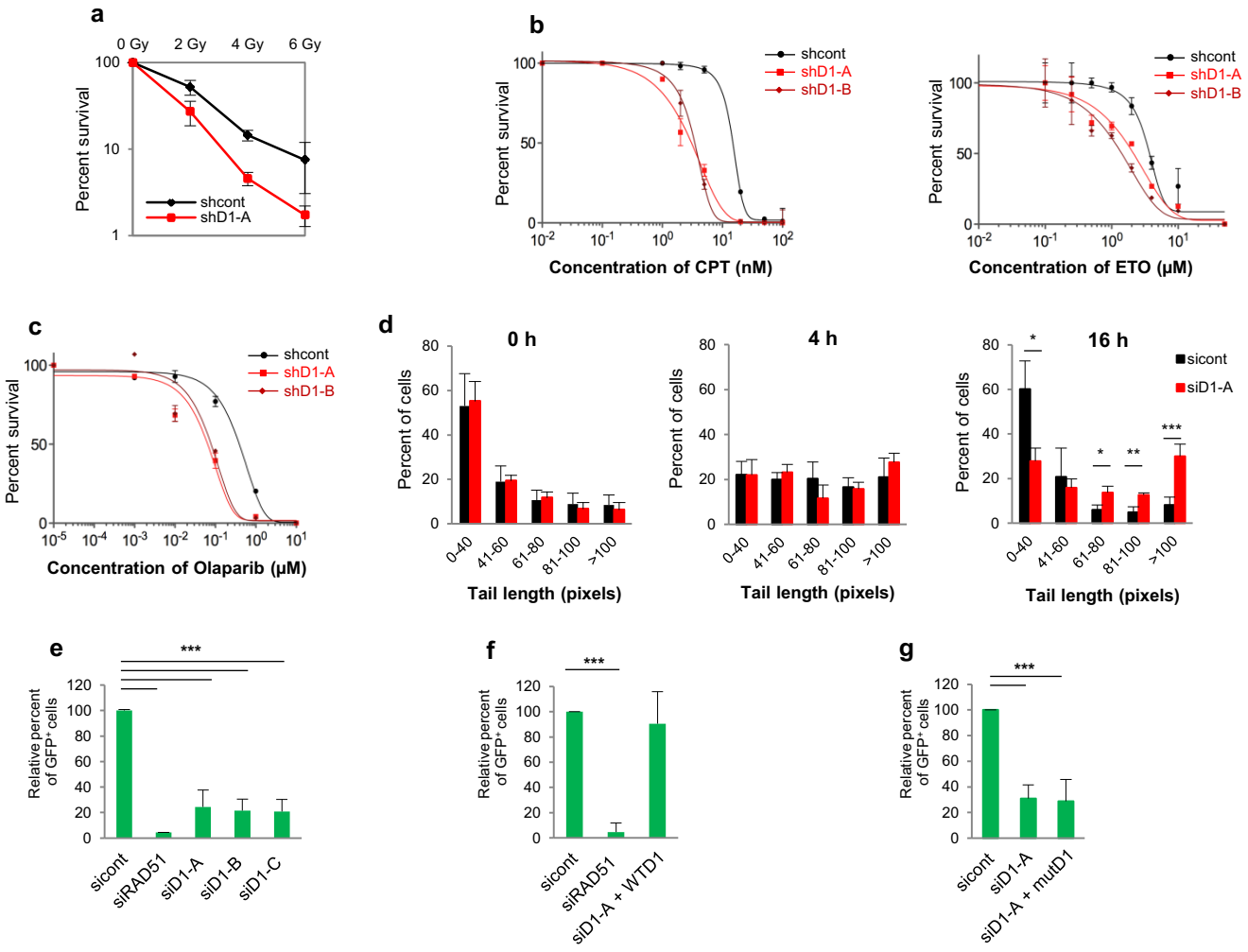
a
0 Gy
2 Gy
4 Gy
6 Gy
Percent survival
shcont
shD1-A
b
shcont
shD1-A
shD1-B
Percent survival
Concentration of CPT (nM)
Concentration of ETO (μM)
c
Concentration of Olaparib (μM)
d
0 h
4 h
16 h
sicont
siD1-A
Percent of cells
Tail length (pixels)
0-40
41-60
61-80
81-100
>100
e
f
g
Relative percent of GFP+ cells
sicont
siRAD51
siD1-A
siD1-B
siD1-C
siD1-A + WTD1
siD1-A + mutD1

Figure 2

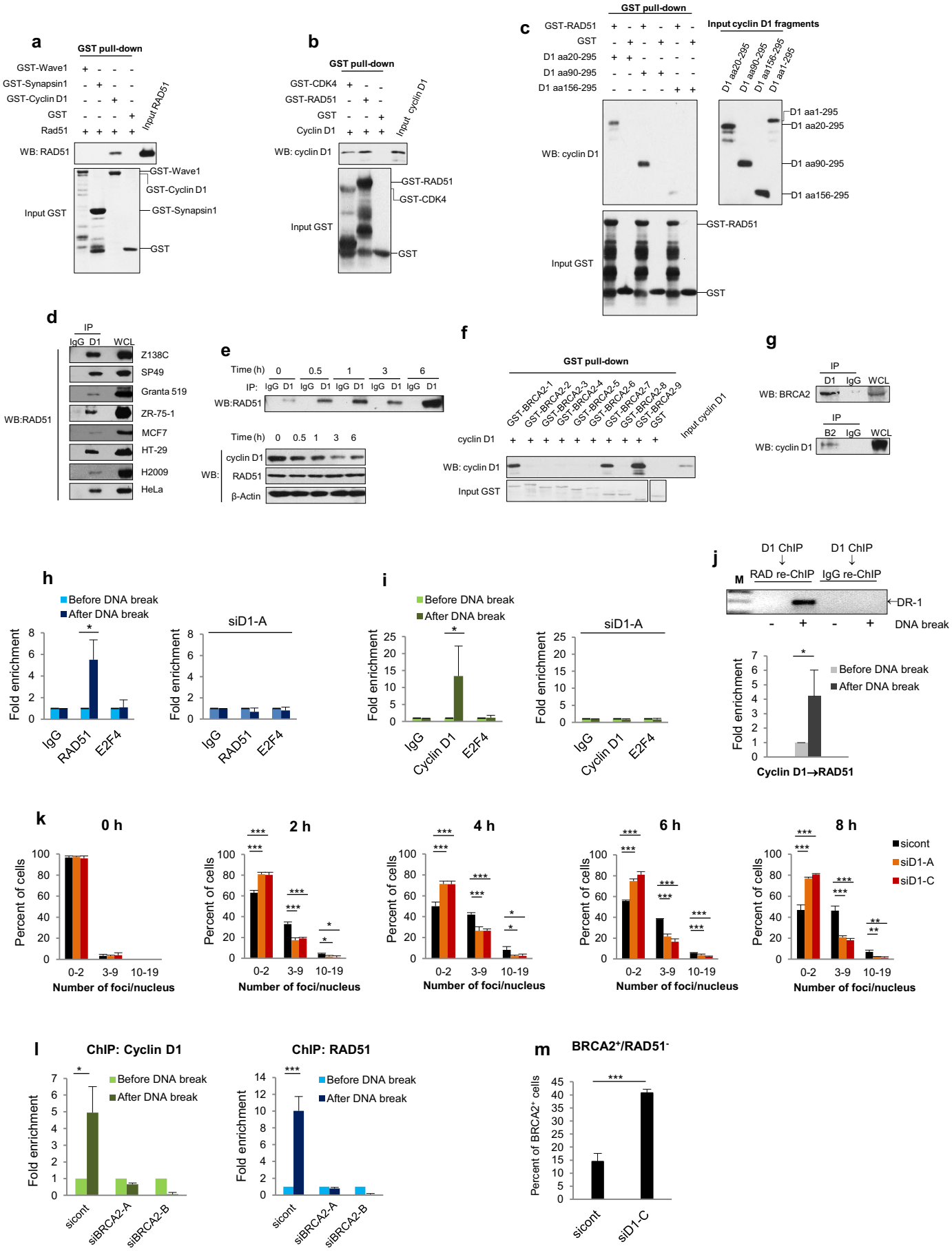
a
GST pull-down
GST-Wave1
GST-Synapsin1
GST-Cyclin D1
GST
Rad51
Input RAD51
WB: RAD51
Input GST
GST-Wave1
GST-Cyclin D1
GST-Synapsin1
GST
b
GST pull-down
GST-CDK4
GST-RAD51
GST
Cyclin D1
Input cyclin D1
WB: cyclin D1
Input GST
GST-RAD51
GST-CDK4
GST
c
GST pull-down
Input cyclin D1 fragments
GST-RAD51
GST
D1 aa20-295
D1 aa90-295
D1 aa156-295
D1 aa1-295
D1 aa20-295
D1 aa90-295
D1 aa156-295
WB: cyclin D1
Input GST
GST-RAD51
GST
d
IP
IgG D1 WCL
WB:RAD51
Z138C
SP49
Granta 519
ZR-75-1
MCF7
HT-29
H2009
HeLa
e
Time (h) 0 0.5 1 3 6
IP: IgG D1 IgG D1 IgG D1 IgG D1 IgG D1
WB:RAD51
Time (h) 0 0.5 1 3 6
WB:
cyclin D1
RAD51
β-Actin
f
GST pull-down
GST-BRCA2-1
GST-BRCA2-2
GST-BRCA2-3
GST-BRCA2-4
GST-BRCA2-5
GST-BRCA2-6
GST-BRCA2-7
GST-BRCA2-8
GST-BRCA2-9
GST
Input cyclin D1
cyclin D1
WB: cyclin D1
Input GST
g
IP
D1 IgG WCL
WB: BRCA2
IP
B2 IgG WCL
WB: cyclin D1
h
Before DNA break
After DNA break
Fold enrichment
IgG
RAD51
E2F4
siD1-A
i
Before DNA break
After DNA break
Fold enrichment
IgG
Cyclin D1
E2F4
siD1-A
j
D1 ChIP
RAD re-ChIP
D1 ChIP
IgG re-ChIP
M
DR-1
DNA break
Before DNA break
After DNA break
Fold enrichment
Cyclin D1→RAD51
k
0 h
2 h
4 h
6 h
8 h
Percent of cells
Number of foci/nucleus
0-2
3-9
10-19
sicont
siD1-A
siD1-C
l
ChIP: Cyclin D1
ChIP: RAD51
Before DNA break
After DNA break
Fold enrichment
sicont
siBRCA2-A
siBRCA2-B
m
BRCA2+/RAD51-
Percent of BRCA2+ cells
sicont
siD1-C

Figure 3

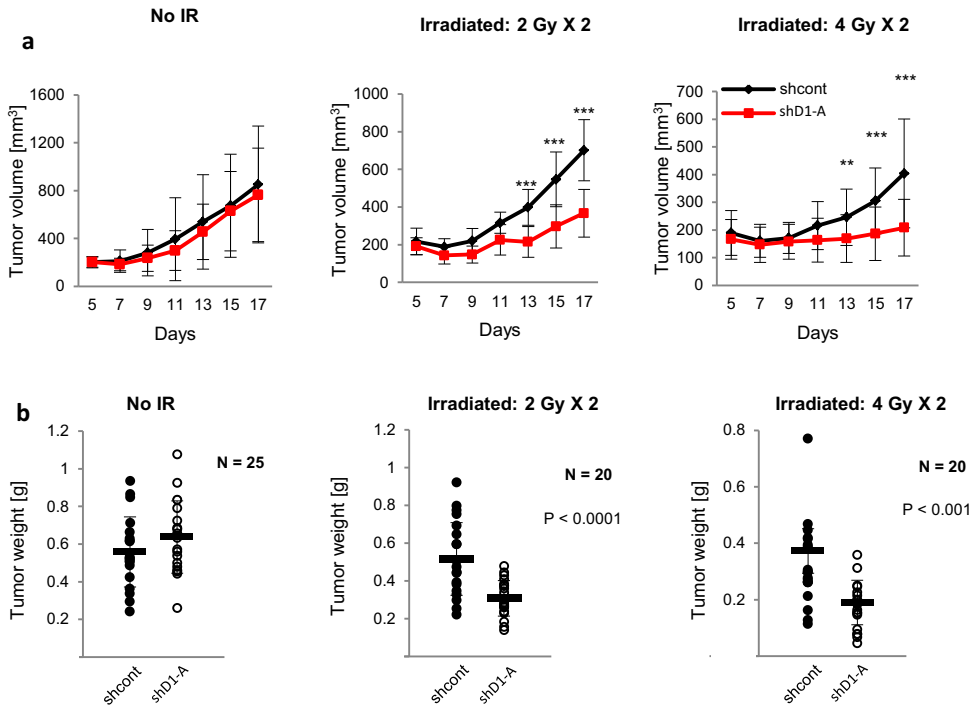
a
No IR
Irradiated: 2 Gy X 2
Irradiated: 4 Gy X 2
Tumor volume [mm3]
Days
shcont
shD1-A
***
**
b
N = 25
N = 20
P < 0.0001
P < 0.001
Tumor weight [g]
shcont
shD1-A

Figure 4